Diplomarbeit

Impact of Auditory Nerve Parameters on Threshold and Spike Initiation Site for Cochlear Implant Users: A Modeling Study

zur Erlangung des akademischen Grades

Diplom-Ingenieurin

im Rahmen des Studiums

Biomedical Engineering

ausgeführt von

Eva Sophia Aitenbichler, BSc

11915396

am Institut für Analysis und Scientific Computing
der Fakultät für Mathematik und Geoinformation
der Technischen Universität Wien

unter der Betreuung von
Ao.Univ.-Prof.i.R. Privatdoz. Dipl.-Ing. Dr.sc.med. Dr.techn. Dr.rer.nat.
Frank Rattay

Wien, 2025

Kurzfassung

Cochlea-Implantate stellen das Hörvermögen wieder her, indem sie geschädigte oder verlorene Haarzellen in der Cochlea überbrücken und Hörnervfasern direkt über Elektroden-Arrays stimulieren. Während das Grundprinzip einfach klingt, stellt die komplexe Geometrie der Hörnervfasern eine große Herausforderung bei der Auswahl optimaler Elektrodenpositionen und Stromstärken dar. Ziel dieser Arbeit ist es, die Parameter zu identifizieren, die den größten Einfluss auf die Auslösung und Ausbreitung von Aktionspotentialen haben.

Für diese Masterarbeit wurden zwei Multikompartment-Modelle einer Hörnervfaser in Matlab R2023b entwickelt. Das erste Modell stellt eine Simulation einer gesunden Hörnervfaser dar und wird genutzt, um zu analysieren, welche Parameter sich wie auf die Nervenleitgeschwindigkeit, präsomatische Verzögerung und geometrische Aktionspotentialausbreitung auswirken. Diese Erkenntnisse wurden für das zweite Modell berücksichtigt, das eine pathologische Hörnervfaser mit Haarzellenverlust simuliert. Die Stimulation erfolgt durch eine extrazelluläre Punktelektrode, deren Einfluss an verschiedenen Positionen untersucht wird.

Die Ergebnisse zeigen, dass Faktoren wie Myelinisierung der Hörnervfaser, Faserdurchmesser, Geometrie der Ranvier'schen Schnürringe und Ionenkanaldichte die Nervenleitgeschwindigkeit und präsomatische Verzögerung beeinflussen. Die kritischsten Parameter für eine zuverlässige Auslösung und Ausbreitung von Aktionspotentialen sind Somadurchmesser und Länge der präsomatischen Region. Die extrazelluläre Stimulation führt zusätzliche Faktoren ein, die Ausbreitung und Initiierung von Aktionspotentialen beeinflussen - die Elektrodenposition und die Stärke des Elektrodenstroms.

Diese Arbeit veranschaulicht, wie wichtig es ist, die Variabilität der Hörnervfasergeometrie bei verschiedenen Patienten zu berücksichtigen. Während einige Parameter nur einen marginalen Einfluss auf die Auslösung von Aktionspotentialen haben und eher die Nervenleitgeschwindigkeit beeinflussen, führen Unterschiede von Somadurchmesser und präsomatischer Länge im μm Bereich in extremen Fällen zum Versagen der Aktionspotentialausbreitung und haben Auswirkungen auf die Stromstärke in Abhängigkeit von der Elektrodenposition. Es ist essenziell, diese Faktoren bei der Auswahl der Stimulationsparameter und der Elektrodenposition bei der Entwicklung von Cochlea-Implantaten zu berücksichtigen.

Abstract

Cochlear implants restore hearing by bypassing damaged or lost hair cells in the cochlea and directly stimulating the auditory nerve fiber via electrode-arrays. While the basic principle is straightforward, the complex geometry of the auditory nerve fiber poses significant challenges in selecting the optimal electrode positions and current magnitudes. The aim of this thesis is to identify key parameters that influence action potential propagation and initiation.

For this thesis, two multi-compartment models of the auditory nerve fiber have been developed in Matlab R2023b. The first is a simulation of a healthy auditory nerve fiber to analyze which parameters have an impact on conduction velocity, presomatic delay and action potential propagation. Insights have been applied to the second model which simulates a pathological case with hair cell loss. Stimulation is provided by an extracellular point electrode and its effects are investigated across different positions.

Results have shown that factors like myelination state, fiber diameter, node of Ranvier geometry and ion channel density influence conduction velocity and presomatic delay. The most critical parameters for reliable action potential initiation and propagation have been found to be the soma diameter and the length of the presomatic region. Extracellular stimulation introduces an additional factor influencing propagation and initiation of action potentials - the electrode position and electrode current magnitude.

This thesis highlights the importance of accounting for variability in auditory nerve fiber geometry between patients. While some parameters have only a marginal influence on action potential initiation, differences in soma diameter and presomatic length in the μm range in extreme cases lead to the failure of action potential propagation and have an impact on current magnitude depending on the electrode position. It is crucial to consider these factors when selecting stimulation parameters and electrode position in cochlear implant design.

Acknowledgements

I would like to express my sincere gratitude to Dr. Rattay for the opportunity to write my thesis in this fascinating research area. His guidance and support throughout the process are greatly appreciated. I also wish to thank my family and friends for their continued support.

Table of Contents

Acronyms

AIS	Axon Initial Segment
ANF	Auditory Nerve Fiber
AP	Action Potential
BFM	Briaire and Frijns Multi-Compartment Model
BM	Basilar Membrane
CI	Cochlear Implant
HCN	Hyperpolarization-Activated Cation
HHM	Hodgkin-Huxley Model
IHC	Inner Hair Cell
KLT	Low-Threshold Potassium
MET	Mechanoelectrical Transduction Ion Channel
NoR	Node of Ranvier
OHC	Outer Hair Cell
RF	Radio Frequency
RM	Rattay et al. Multi-Compartment Model
SGN	Spiral Ganglion Neuron
SM	Scala Media
SMM	Smit et al. Multi-Compartment Model
ST	Scala Tympani
SV	Scala Vestibuli
TM	Tectorial Membrane

1 Introduction

This chapter provides a short introduction to the topic. A more detailed description is given in the following chapters.

1.1 Motivation and Problem

The auditory nerve fiber (ANF) is responsible for signal transmission from the cochlea to the first auditory processing center in the brainstem (Rattay and Danner, 2014). Crucial for successful signal conduction is the function of the inner hair cells (IHCs). The IHCs are sensory cells located on the organ of Corti in the cochlea. In the healthy case, they convert sound waves into electrical nerve impulses (Sheikh et al., 2022). Deafness and severe hearing loss are often caused by damage or destruction of these sensory hair cells, preventing the conversion of sound waves into electrical signals. The aim of cochlear implants (CIs) is to bypass the damaged hair cells by direct stimulation of the ANF with electrical impulses delivered through an electrode array inserted into the cochlea (Eshraghi et al., 2012). To ensure that CIs work properly, correct electrode array placement is important. Less-than-ideal electrode array placement may require higher stimulating currents which in turn have an impact on spatial selectivity of ANF activation for a given frequency (Limb and Roy, 2014).

1.2 Aim

The aim of this thesis is to analyze the impact of auditory nerve parameters on action potential (AP) initiation and propagation in the ANF. As an approach, two multi-compartment models based on the Hodgkin-Huxley Model (HHM) and previous models of the ANF (Hodgkin and Huxley, 1952a; Rattay et al., 2001; Bachmaier et al., 2019) have been developed in this study. The first is a model of a healthy ANF, where APs are initiated using intracellular stimulation. This model is used to investigate the influence of nerve fiber geometry and to identify key factors affecting signal conduction. Insights gained from this model are then applied to the second model, which represents an ANF with hair cell loss. In this case, an external point electrode stimulates the ANF. Electrode position and geometry of the ANF have a big impact on AP initiation and conduction, which will be investigated in this thesis.

2 Theoretical Background

2.1 Anatomical and Physiological Basics

This chapter focuses on the anatomical and physiological basics that are necessary for understanding the core concepts of this thesis. It provides an overview of the auditory process with particular focus on the cochlea, signal transmission from the IHCs to the ANF and propagation of signals from the cochlea to the auditory cortex of the brain.

2.1.1 Anatomy of the Human Ear and Basics of Hearing

Sound is the vibration of molecules in the air or other media that propagates through space. The human hearing organ *auris* allows the perception of these vibrations in the range of $16Hz$ to $20kHz$. The *auris* is structurally and functionally divided into the *auris externa* (outer ear), *auris media* (middle ear) and *auris interna* (inner ear) (Sheikh et al., 2022; Schiebler and Korf, 2007).

The *auris externa* consists of the pinna, auditory canal and eardrum. The main task of the pinna is to collect and localize sound vibrations and funnel them into the auditory canal. The auditory canal ends at the last part of the outer ear: the eardrum, also referred to as the *tympanic membrane*. The *tympanic membrane* separates the outer and middle ear. The three auditory ossicles *malleus*, *incus*, and *stapes* are part of the middle ear, where they conduct the vibrations of the *tympanic membrane* to the oval window of the inner ear (Moore, 2012).

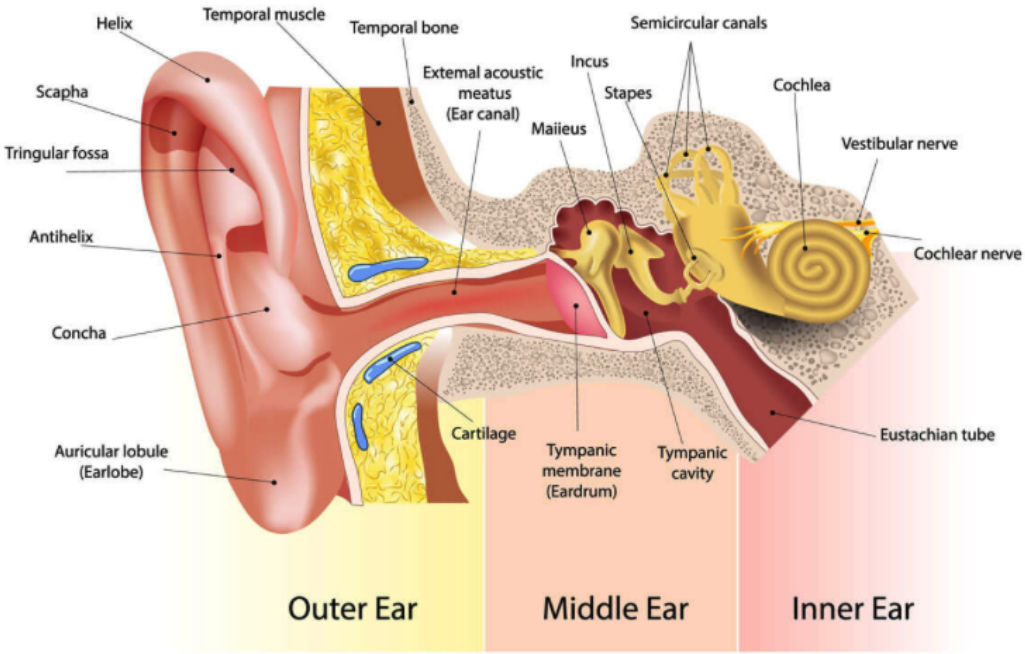

Figure 1: Schematic drawing of the outer, middle and inner ear with their respective components (Dewsnup, 2022).

The most important structure in the inner ear is the cochlea, a spiral-shaped canal. It contains three main sections: the *Scala Vestibuli (SV)*, the *Scala Media (SM)* and the *Scala Tympani (ST)*. The *SV* and *ST* are the perilymph-filled outer chambers of the cochlea that meet at the *helicotrema*, the apex of the cochlea (Sheikh et al., 2022). Perilymph is in its composition similar to cerebral spinal fluid. It is crucial for sound transmission within the cochlea and bathes multiple structures necessary for signal transduction (Peter et al., 2022).

The oval window lies at the base of the *SV* and is set in motion by movement of the *stapes* (Moore, 2012). This initiates a pressure wave in the *SV* that travels through the *helicotrema* to the *ST*. The *ST* terminates at the round window, a membrane that moves in response to the motion of the oval window for pressure release (Sheikh et al., 2022; Moore, 2012).

The *SM* lies between the *SV* and the *ST* and is filled with endolymph, which is rich in potassium and low in sodium (Vlajkovic and Thorne, 2022). The *SV* and *SM* are separated by Reissner's membrane, while the *ST* and *SM* are separated by the basilar membrane (BM). The BM contains the organ of Corti, which houses the sensory hair cells responsible for signal transduction (Sheikh et al., 2022).

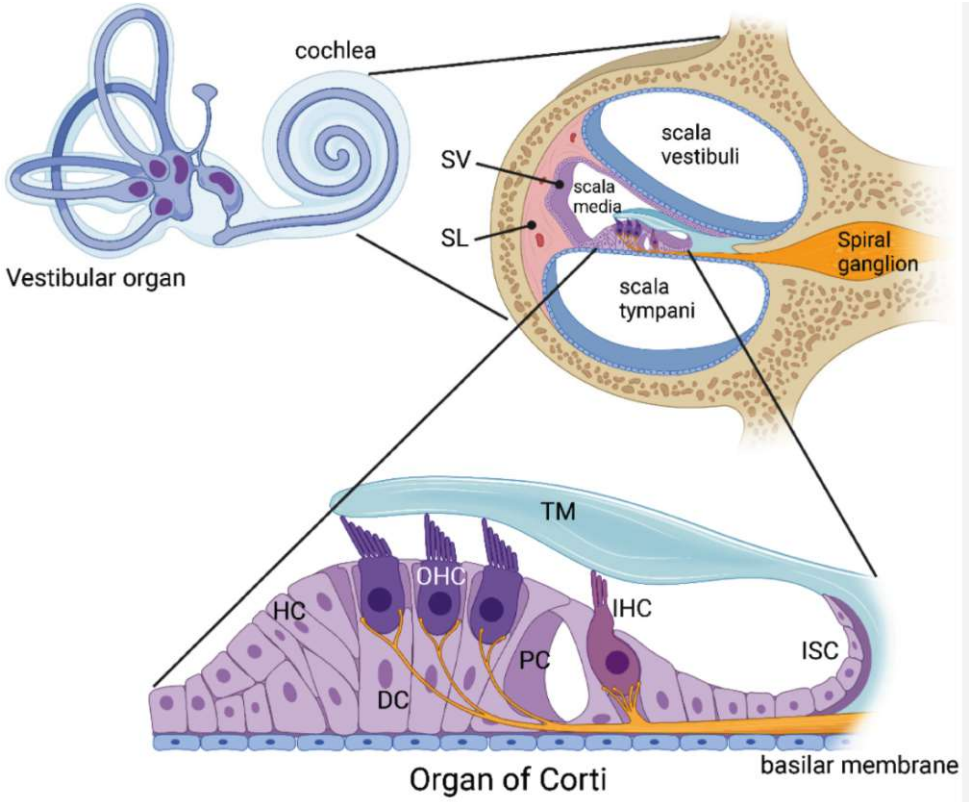

Figure 2: Anatomy of the three main sections of the cochlea: *ST*, *SM*, and *SV*. Emphasis is put on the organ of Corti, which houses the outer hair cells (OHCs) and IHCs as well as the tectorial membrane (TM). Supporting cells like the Deiters' cells (DC), Hensen's cells (HC) and pillar cells (PC) surround the sensory hair cells. The medial border of the organ of Corti is formed by inner sulcus cells (ISC) (Vlajkovic and Thorne, 2022).

Two types of hair cells can be distinguished: the IHCs and OHCs. The TM lies above the hair cells and is in contact with the tips of the OHCs' stereocilia. The IHCs have only weak or no connections with the TM (Sheikh et al., 2022). Pressure changes in the SV and ST produce a traveling wave on the BM that peaks more basally for stimuli of higher frequencies and more apically for stimuli of lower frequencies. Stimulus frequency is mapped to the place of stimulation in the cochlea (Pickles, 2015).

The hair cells are organized according to their function. There are about 3500 IHCs in the human cochlea which are arranged in a single row along the BM. Their primary task is to convert sound waves into electrical nerve impulses which are transmitted to the brain. The about 12 000 OHCs are arranged in three parallel rows. Their strong connection to the TM via their longest stereociliae allows them to amplify sound waves (Sheikh et al., 2022).

The stereocilia of hair cells are arranged in ranks of increasing height and are interconnected by fine extracellular filaments called tip links. Deflection of the bundle, caused by movement of the BM relative to the TM, bends the stereocilia. Depending on the direction of bending, mechanoelectrical transduction (MET) ion channels either open or close. Deflection of the bundle toward the taller edge increases the probability of MET channel opening, whereas displacement in the opposite direction decreases it, leading to channel closure (Fettiplace and Hackney, 2006).

The open MET channels allow the influx of potassium ions from the potassium-rich endolymph, leading to depolarization of the hair cell. This depolarization triggers the opening of voltage-gated calcium channels at the base of the cell, allowing calcium to enter. The calcium influx promotes the release of neurotransmitters which bind to receptors on the postsynaptic membrane of the ANF, leading to its depolarization and the initiation of APs (Swenson, 2017).

Experiments show, that in the resting state of the hair cell about 30% of the MET channels are open (Hudspeth, 2014). This causes a baseline release of neurotransmitters generating spontaneous activity in the auditory nerve in the absence of a sound. Deflection of the stereocilia leads to the opening or closing of the MET channels, causing a higher or lower rate of APs in the ANF (Swenson, 2017).

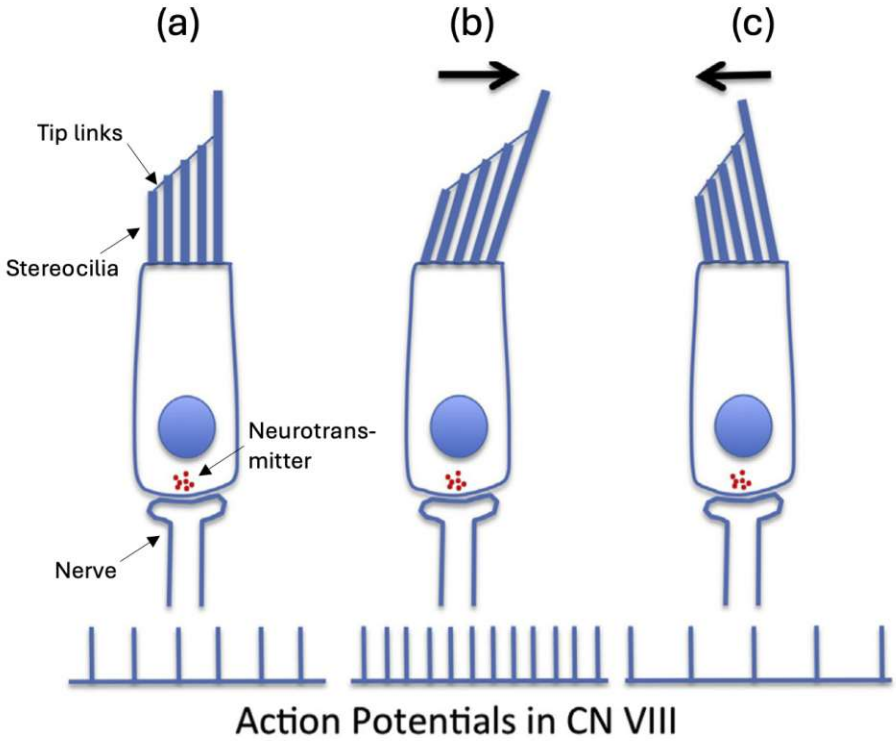

Figure 3: Effect of stereocilia deflection on transmitter release and AP frequency. In the resting position (a), a small number of ion channels are open, leading to a small release of transmitter, which generates a baseline frequency of APs. Deflection towards the tallest row (b) creates tension on the tip links, opening potassium channels, resulting in increased transmitter release and a higher frequency of APs. Deflection away from the tallest row (c) closes potassium channels, which inhibits transmitter release and lowers the frequency of APs (Swenson, 2017).

2.1.2 Anatomical and Functional Aspects of the Human Auditory Nerve

Transmission of information in the human body via electrochemical signals is carried out by neurons. Neurons consist of a cell body, known as the soma, and at least one extension called a neurite. Neurites can be either axons, which relay signals away from the soma, or dendrites, which carry signals toward the soma. Most axons and some long dendrites are covered by myelin sheaths. Myelin acts as an electrical insulator, but does not cover the entire neurite, leaving small gaps called nodes of Ranvier (NoR), where signal propagation is reinforced (Ashley and Lui, 2023).

Dendrites primarily receive incoming signals from other neurons, causing small electrical changes called graded potentials. These graded potentials travel to the axon initial segment (AIS), a specialized membrane region in the axon located directly after the soma, before the start of myelination, where APs are usually initiated. The AIS has a high density of voltage-gated ion channels. If the combined signals arriving at the AIS reach a certain threshold, an AP is elicited (Kole and Stuart, 2012). Due to the bipolar structure of Type-I ANFs, the AIS in SGNs functionally corresponds to the region near the hair cell synapse where APs are initiated following synaptic input from the IHCs.

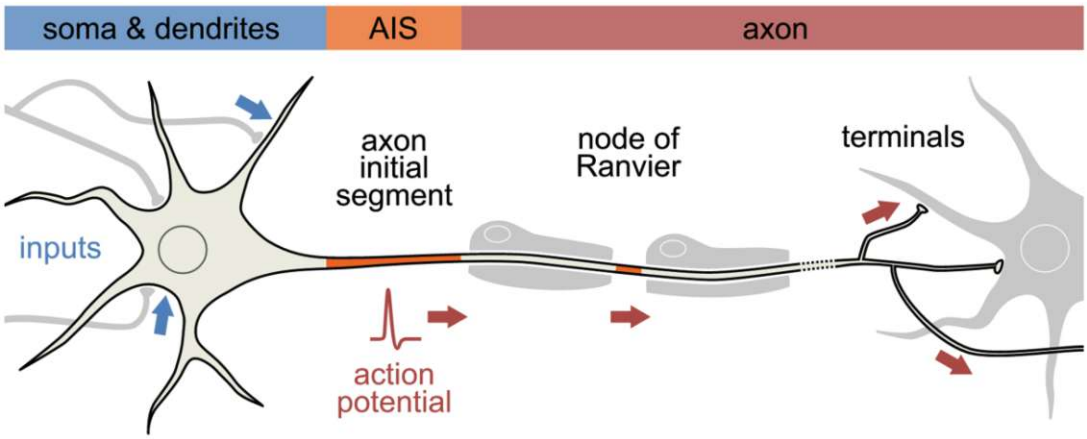

Figure 4: Typical structure of a neuron: Dendrites carry information as graded potentials to the soma. If the combined signals arriving at the AIS reach a certain threshold voltage, an AP is generated and propagates along the axon. Myelin sheaths cover segments of the axon membrane, leaving gaps called NoR, where the AP is regenerated, resulting in an increased conduction velocity (Leterrier, 2016).

Myelination increases the conduction velocity v of impulses along the fiber. Another important factor influencing conduction velocity is the diameter d of the fiber (Equations 1, 2). Larger fiber diameters result in lower internal resistance, allowing electrical signals to propagate more rapidly. For fibers with a diameter greater than 11μm, the coefficient 4.5 in equation 1 changes to 6 (Rattay, 1990).

$$v_{\text{myelinated}} = 4.5 \cdot d \tag{1}$$

$$v_{\text{unmyelinated}} = 1.1 \cdot \sqrt{\text{d}} \tag{2}$$

It is crucial to differentiate between afferent and efferent innervation of the cochlea. Afferent fibers, primarily spiral ganglion neurons (SGNs), transmit auditory information from the hair cells within the cochlea to the cochlear nucleus in the brainstem. In contrast, efferent fibers carry signals from the superior olivary complex back to the cochlea, regulating cochlear activity (Carricondo and Romero-Gómez, 2019). This thesis focuses exclusively on the afferent innervation of the cochlea, specifically the SGNs.

The afferent signals generated by the hair cells in the cochlea are conducted along the ANF by two types of SGNs, the Type-I and Type-II neurons (Rattay et al., 2013). Approximately 90-95% of the SGN are Type-I. These large bipolar neurons connect the IHCs with the cochlear nucleus in the brainstem. IHCs are innervated by 10-20 afferent Type-I dendrites, but each Type-I dendrite only connects to one IHC. The smaller Type-II neurons innervate the OHCs and only make up 5-10% of the SGNs. Each OHC receives only one contact from a Type-II fiber, but each Type-II neuron innervates approximately 15-20 OHCs. Type-I neurons are myelinated whereas Type-II neurons lack myelination (Carricondo and Romero-Gómez, 2019).

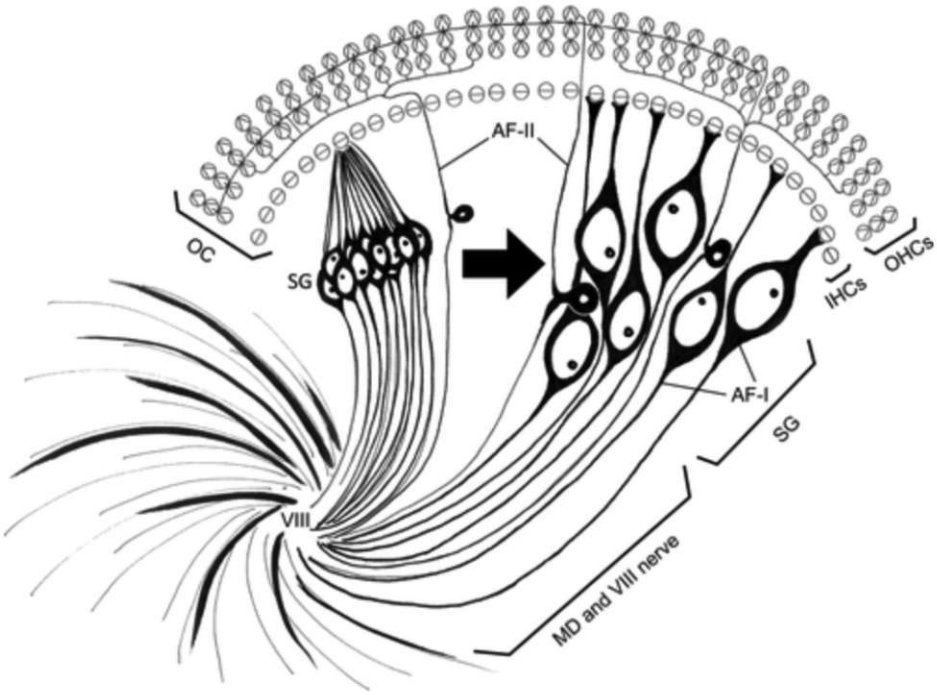

Figure 5: Afferent innervation of the cochlea. Each IHC is innervated by 10-20 larger Type-I spiral ganglion cells (left). Each Type-I dendrite only connects to one IHC. The OHCs are innervated by smaller Type-II dendrites, where each OHC receives contact from only one Type-II fiber and each Type-II neuron innervates 15-20 OHCs (Carricondo and Romero-Gómez, 2019).

Human ANFs of Type-I are bipolar cells, meaning that they possess two distinct processes, a peripheral dendrite connecting to the IHCs in the cochlea and a central axon relaying signals toward the cochlear nucleus in the brainstem (Nayagam et al., 2011). Rattay et al. (2013) report a total path length (peripheral process + soma region + central axon) of $32.35 \pm 1.45mm$.

ANFs are each tuned to a specific region of the cochlea, corresponding to the frequency range (apical - low frequency, basal - high frequency). The length of the peripheral and axonal processes of human Type-I ANFs therefore increases from base to apex (Spoendlin and Schrott, 1988; Potrusil et al., 2020). These findings have been confirmed by Potrusil et al. (2020), reporting that the longest and most variable linear lengths of dendritic processes can be found in apical fibers ($2.29 \pm 0.37mm$). Dendritic processes are most uniform in the middle turn ($1.44 \pm 0.11mm$) and intermediate in the basal turn ($1.89 \pm 0.11mm$). For the central axon, the longest central processes are also found in apical fibers ($8.15 \pm 0.31mm$) with the most uniform lengths. The basal fibers show the smallest mean length of central processes ($6.7 \pm 1.02mm$).

Determining the length of the NoR remains a challenge and is in modeling studies mostly based on animal data. Arancibia-Carcamo et al. (2017) report values for the NoR length of the rat optic nerve and cerebral cortical axons (optic nerve 0.5-2.2μm, cortex 0.43-3.7μm). In a study on the mouse cochlea, Panganiban et al. (2022) reported axonal node lengths ranging approximately from 1.5 to 2.8μm and ganglion node lengths from 2.8 to 4μm, with values varying by cochlear location and developmental stage. For modeling of the human cochlea, often values between 1 and 2.5μm are chosen (2.5 μm (Rattay et al., 2001), 1.5 μm (Rattay and Tanzer, 2022)). Also for the length of the internodal (myelinated) segments, data for human ANFs is scarce. For cat data, Arnesen et al. (1978) reported values between 250 and 300μm for the internodal length in the cochlear nerve trunk. The first three internodes in cats are about 150μm long, length gradually increases in the first part of the central axon up to 350μm (Rattay et al., 2001). For the pre- and postsomatic compartment, values of 100μm and 5μm were used in modeling studies (Rattay et al., 2001), although direct experimental evidence supporting these values remains rare.

Rattay et al. (2013) have reported that the diameter of both the peripheral and central parts of human Type-I ANFs varies by cochlear location. For the dendritic part, the diameters are $1.35 \pm 0.15\mu m$ in the basal region, $1.28 \pm 0.13\mu m$ in the middle region, and $1.32 \pm 0.17\mu m$ in the apical region. For the axonal part, the diameters are larger, with $2.67 \pm 0.29\mu m$ (basal), $2.63 \pm 0.29\mu m$ (middle) and $2.60 \pm 0.34\mu m$ (apical).

Despite ongoing efforts, determining an exact range for the diameter of Type-I somata in humans remains difficult. Based on cat data (cat Type I SGNs: basal $15.81 \pm 2.03\,\mu m$, middle $13.74 \pm 3.25\,\mu m$, apical $13.41 \pm 2.29\,\mu m$ (Potrusil et al., 2020)) and literature (12-20μm diameter for Type-I human ANF (Biacabe et al., 2001), 30μm Type-I human ANF (Spoendlin and Schrott, 1988)) most modeling studies choose values in that range or slightly above that range (27μm (Smit et al., 2008); 30 μm (Rattay et al., 2001); 20 μm (Rattay et al., 2013)). In most modeling studies, the soma is modeled as a sphere (Rattay et al., 2013; Smit et al., 2008).

In their ultrastructural study of the human spiral ganglion, Ota and Kimura (1980) have stated that the soma has an ovoid shape and is not myelinated but rather surrounded by a thin single layer of satellite glial cells providing structural and metabolic support rather than insulation like myelin. They have also shown, that a few thin layers of sheath or some loose layers of myelin can cover parts of the soma. Rattay et al. (2001) report that the pre- and postsomatic compartment of human ANFs are unmyelinated in contrast to other mammals.

It is important to note that - due to ethical constraints - most knowledge about the neural coding in the auditory nerve is derived from experiments conducted in cats. While the unmyelinated Type-II neurons exhibit similar physiological properties in both humans and cats, the more common myelinated Type-I neurons differ fundamentally between humans and other mammals (Rattay et al., 2013). In human ANFs, the peripheral dendritic processes are mostly unmyelinated or only thinly myelinated, while the central axons exhibit more consistent and thicker myelination, as reported in anatomical and modeling studies (Ota and Kimura, 1980; Rattay et al., 2001; Spoendlin and Schrott, 1988).

Anatomical and physiological differences between humans and cats in the ANF are of great interest in CI research, as they raise important questions about how reliably findings from cat models can be translated to humans. Rattay et al. (2013) highlighted fundamental differences between cat and human SGNs that have significant impact on conduction velocity. One major distinction is the extent of myelination. While in cats the majority of Type-I SGNs are myelinated including soma and axonal segments, only about 3.65% of human Type-I SGNs are myelinated. Most of Type-I soma in the human ANF lack myelin entirely or have a very thin myelin sheath with only a few layers. The pre- and postsynaptic compartments are unmyelinated in both cats and humans but the regions are notably longer in humans further increasing the presomatic delay. These key differences result in slower conduction velocity and increased variability in spike timing for humans. Further delays in signal transmission are introduced by longer and unmyelinated peripheral processes in humans. This leads to the need for stronger synaptic input to reliably trigger APs in humans. Nadol (1988) described the SGN organization as uniform and more densely packed in cats, while in humans it is more loosely organized with greater variability in neuron size and morphology contributing to less consistent conduction properties.

Despite ongoing efforts, the full extent of coding in the ANF remains unknown. To gain further insight into the molecular mechanisms involved in human auditory nerve processing, Liu et al. (2021) combined transmission electron microscopy, super-resolution structured illumination microscopy and RNA-scope analysis on human inner ear tissue. They identified hemi-nodal proteins (typically found near NoR) beneath the IHCs suggesting an early site of AP generation. Additionaly, they visualized voltage-gated ion channels in the SGN and AIS. Nav1.6, indicating the presence of voltage-gated sodium channels, was primarily found at the NoR.

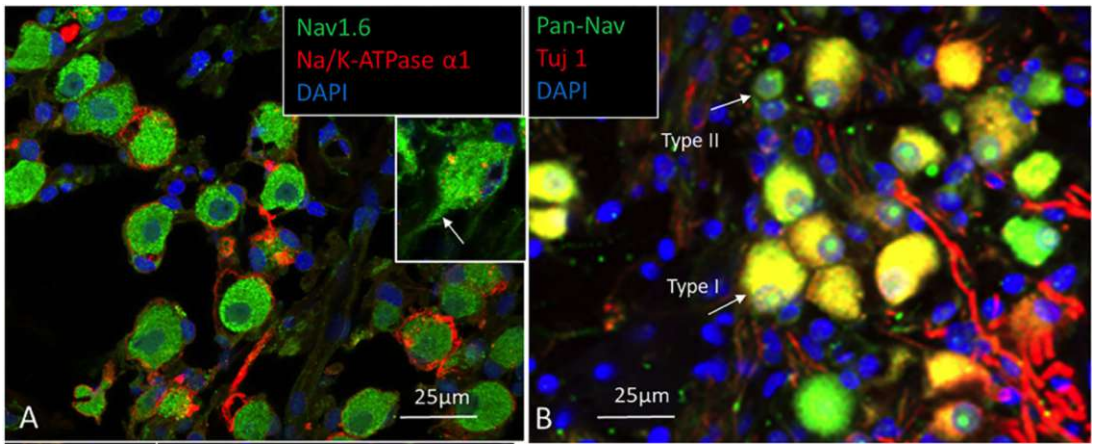

Figure 6: Human SGN with different colors to highlight specific proteins. Green marks sodium channel proteins (Nav 1.6 in (A) and all types in (B)) symbolizing functional sites on the neuron where APs are initiated, predominantly at the NoR. Blue visualizes cell nuclei (DAPI) demonstrating the location and number of cells present in a sample. Red stained are the nerve fibers (axon or dendrite) or surrounding structures. Panel (B) also visualizes the size difference between Type-I and Type-II spiral ganglion neurons (Adapted from (Liu et al., 2021)).

2.1.3 Action Potential Propagation in the Auditory Nerve

The paper titled *A quantitative description of membrane current and its application to conduction and excitation in nerve* by Hodgkin and Huxley (1952a) has laid the groundwork for modern neuroscience. With a set of nonlinear differential equations, Hodgkin and Huxley modeled the ionic mechanisms underlying APs. This work forms the foundation for our modern understanding of neuronal excitability and its core findings remain valid and influential many decades later. The Hodgkin–Huxley model will be further discussed in section 2.2.2.

At rest, the cell is in a polarized state, characterized by an intracellular potential approximately $70mV$ more negative than the extracellular fluid (Rattay, 1990). This resting membrane potential arises from differences in ionic concentrations across the membrane and the membrane's selective permeability to these ions (Chrysafides et al., 2024).

Crucial ions for explaining the resting potential include sodium (Na^+), potassium (K^+), chloride (Cl^-) and various negatively charged intracellular proteins. Higher concentrations of Na^+ and Cl^- outside and K^+ and negatively charged proteins inside the cell lead to a concentration gradient across the membrane. Ions move through specific membrane channels down their gradients. Based solely on the concentration gradient, K^+ moves out of the cell and Na^+ into the cell. The membrane is more permeable for K^+ ions. The gradient is maintained by sodium-potassium pumps using ATP as an energy source. During one cycle, 3 Na^+ ions are pumped out and 2 K^+ into the cell leading to one positive net charge leaving the cell (Rattay, 1990; Chrysafides et al., 2024).

As ions move across the membrane down their concentration gradients, an opposing electrical gradient develops due to the separation of charges. This electrical gradient increasingly resists further ion movement. Eventually, an electrochemical equilibrium is reached, in which the electrical and chemical driving forces are balanced, resulting in no net ion flux (Chrysafides et al., 2024).

For each ion, the electrochemical equilibrium potential (membrane voltage at which the electrical gradient exactly balances the chemical gradient) can be calculated using the Nernst equation (Equation 3), yielding approximately $+60mV$ for sodium and -90mV for potassium under typical physiological conditions (Chrysafides et al., 2024).

$$E_{\mathrm{m}} = \frac{RT}{zF} \ln\left(\frac{c_2}{c_1}\right) \tag{3}$$

where
E_{m} is the membrane potential $[V]$
R is the universal gas constant $[J \cdot mol^{-1} \cdot K^{-1}]$
T is the absolute temperature $[K]$
z is the charge number of the ion [+1 for Na^+ and K^+]
F is the Faraday constant $[C \cdot mol^{-1}]$
c_2 is the extracellular ion concentration $[mol \cdot m^{-3}]$
c_1 is the intracellular ion concentration $[mol \cdot m^{-3}]$

To account for the different concentrations of multiple ions, the Goldman equation (Equation 4) is used. Because of the high permeability of the membrane to potassium, the resulting resting potential of approximately -70mV is closer to the potassium equilibrium potential (Rattay, 1990).

$$E_m = \frac{RT}{F} \ln \left(\frac{P_{K^+}[K^+]_\mathrm{o} + P_{Na^+}[Na^+]_\mathrm{o} + P_{Cl^-}[Cl^-]_\mathrm{i}}{P_{K^+}[K^+]_\mathrm{i} + P_{Na^+}[Na^+]_\mathrm{i} + P_{Cl^-}[Cl^-]_\mathrm{o}} \right) \tag{4}$$

where
E_m is the membrane potential $[V]$
R is the universal gas constant $[J \cdot mol^{-1} \cdot K^{-1}]$
T is the absolute temperature $[K]$
F is the Faraday constant $[C \cdot mol^{-1}]$
P are the membrane permeabilities for ions $[m \cdot s^{-1}]$
$[K^+]_\mathrm{o}$, $[Na^+]_\mathrm{o}$, $[Cl^-]_\mathrm{o}$ are the extracellular concentrations $[mol \cdot m^{-3}]$,
$[K^+]_\mathrm{i}$, $[Na^+]_\mathrm{i}$, $[Cl^-]_\mathrm{i}$ are the intracellular concentrations $[mol \cdot m^{-3}]$.

If the membrane potential Vm rises above a critical threshold value between -50 and -40mV, voltage-gated Na^+ channels open, initiating the rapid depolarization phase of an AP. These channels have two gates, one fast activation gate m that opens almost immediately after depolarization and one slower inactivation gate h that closes shortly after, terminating the sodium influx. As a result, Na^+ ions enter the cell rapidly, driven by both concentration and electrical gradients. As depolarization proceeds and the membrane potential reaches its peak, most Na^+ channels become inactivated due to the closure of the h gate. Simultaneously, the depolarization triggers the opening of voltage-gated K^+ channels, which are controlled by a single slow activation gate n. Because of the high intracellular concentration of K^+, K^+ ions exit the cell, driving the repolarization phase. The delayed closing of K^+ channels leads to a hyperpolarization of the membrane before it returns to the resting potential. (Raghavan et al., 2019; Hille, 1940)

At the peak of the AP, all Na^+ channels are inactivated due to the closure of the h gate, while the m gate remains open. Recovery of the h gate takes a few milliseconds, resulting in a period during which no new AP can be triggered regardless of stimulus strength. This time frame is called the absolute refractory period. The absolute refractory period is followed by the relative refractory period, during which a stronger-than-normal stimulus can trigger an AP because some Na^+ channels have recovered as their h gates have reopened. However, the threshold for firing is higher due to ongoing K^+ efflux and hyperpolarization of the membrane (Raghavan et al., 2019).

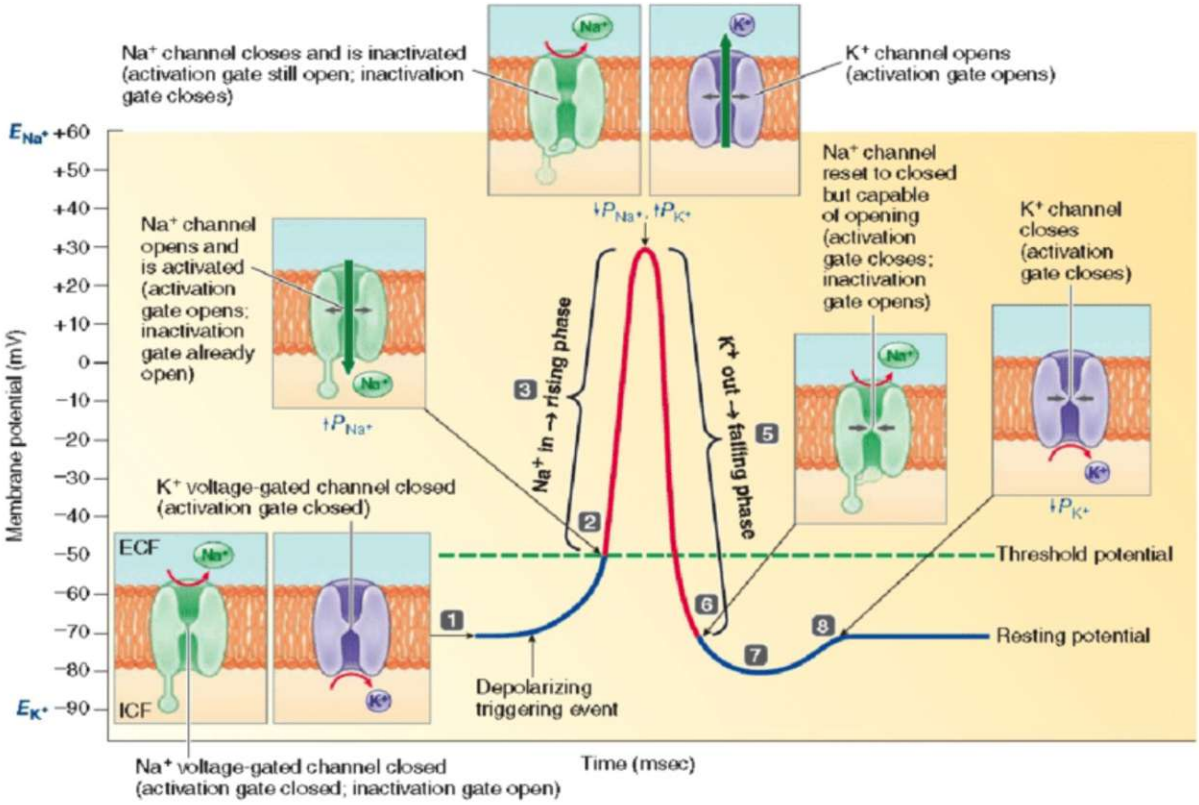

Figure 7: At rest, the activation gates m and n of Na^+ and K^+ channels are closed. The inactivation gate h of Na^+ channels is open. During depolarization, the m gate opens allowing the rapid influx of Na^+ ions. The n gate also opens, but much slower. At the peak of the AP, most h gates are closed. If h gates are closed, no new AP can be triggered (absolute refractory period). More n gates open allowing K^+ ions to leave the cell leading to a falling membrane potential. During hyperpolarization, n gates close, but h gates open theoretically allowing another AP (relative refractory period). The closure of n gates allows the membrane potential to return to the resting state (Asaad, 2019).

Neuron models often focus primarily on Na^+ and K^+ channels to simulate AP generation. Negm and Bruce (2014) suggest incorporating two additional ion channels for more accurate neuronal modeling of ANFs: low-threshold potassium (KLT) channels and hyperpolarization-activated cation (HCN) channels. KLT channels activate near the resting membrane potential, creating a fast outward potassium current that stabilizes the membrane potential and raises the threshold for spike initiation. This mechanism prevents the neuron from firing too easily or too frequently. Without KLT channels, models tend to overestimate firing rates and fail to reproduce the precise spike timing observed in ANF responses. HCN channels activate during hyperpolarization and produce a slow, inward mixed sodium and potassium current that depolarizes the cell. This current facilitates faster recovery of the membrane potential, thereby supporting rapid recovery from inhibition and sustained firing during ongoing sound stimuli.

2.2 Technical Basics

2.2.1 Equivalent Circuit of a Patch of Membrane

The first step in building a model of the human auditory nerve is to find equivalent circuits describing the behavior of the different compartments. As described in Section 2.1.3, the initiation and propagation of APs mainly depends on the voltage difference across the cell membrane.

The simplest equivalent circuit of a cell membrane is the parallel connection of a resistance and capacitance. Due to the thinness of the lipid bilayer, the membrane capacitance is relatively high and can be considered constant across compartments, regardless of whether they are passive (e.g., internodes covered with myelin) or active (e.g., NoR, unmyelinated). The membrane resistance represents the membrane's permeability to ions through ion channels, primarily reflecting the passive flow of ions through open channels. This resistance varies considerably depending on the gating state of ion channels. Approximating the resistance with a constant value is only valid in passive regions. In active membrane areas, conductance (inverse of resistance) is voltage-dependent due to the dynamics of ion channel gating. In equivalent circuit models, electrochemical gradients (no net movement of ions) are represented by batteries in series with the membrane resistances. These batteries drive ionic currents: sodium and leakage channels produce inward currents, while potassium and chloride channels generate outward currents (Rattay, 1990).

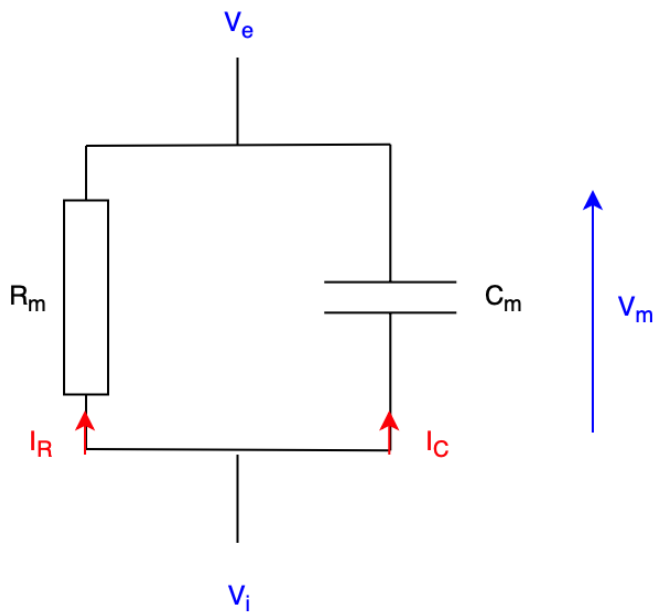

Figure 8: Equivalent circuit for the passive part of the membrane represented by a parallel connection of a resistance and a capacitance. The resistance represents the membrane's passive ionic permeability, while the capacitance represents the membrane's ability to separate and store electrical charge across the lipid bilayer (Adapted from (Rattay, 1990) drawn with *diagrams.net* (JGraph Ltd., 2023)).

It is important to note that in the equivalent circuit model of the active membrane (Figure 9), all ionic currents (sodium, potassium, and leak) are conventionally drawn with arrows pointing from the intracellular space to the extracellular space. Although physiologically sodium and leak currents flow from the extracellular to the intracellular space, this convention simplifies circuit analysis. Consequently, currents are assigned a negative sign in calculations if their actual direction opposes the chosen reference.

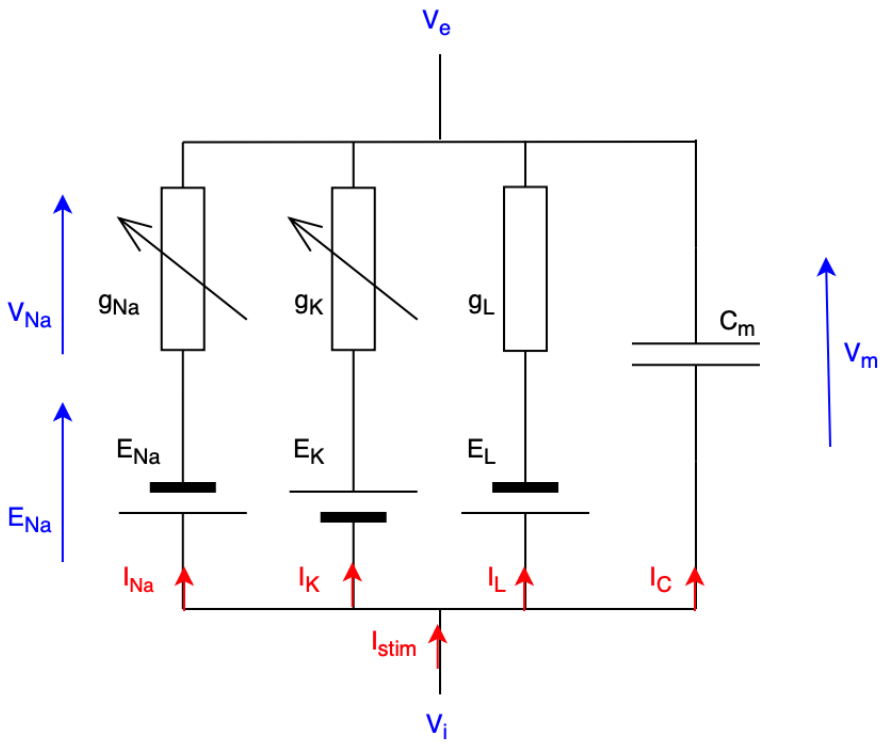

Figure 9: Equivalent circuit for the active part of the membrane, including voltage-dependent conductances representing sodium, potassium and leak channels, each modeled as a resistance in series with a battery representing the electrochemical equilibrium potential. The membrane capacitance accounts for the lipid bilayer's electrical properties (Adapted from (Rattay, 1990) drawn with *diagrams.net* (JGraph Ltd., 2023)).

2.2.2 The Hodgkin-Huxley Model

In their Nobel Prize-winning work (1952a, 1952b), Hodgkin and Huxley have developed the HHM which describes the ionic mechanisms underlying the initiation and propagation of APs in nerve cells. The original experiments, which investigated the relationship between membrane voltage and ionic currents, were carried out on a giant squid axon using intracellular stimulation with an electrode inserted directly into the axon. Their findings have resulted in a system of four coupled differential equations which will be discussed in further detail.

Unless otherwise indicated, the following equations and descriptions are based on Rattay (1990). To make the analysis independent of geometrical parameters, all currents are expressed as current densities per cm^2 of membrane (indicated by lower case letters), with c representing the capacitance per cm^2.

The circuit shown in Figure 9 is used to derive the HHM. A patch of membrane is modeled by a capacitor in parallel with three conductance-battery branches (sodium, potassium, leak). Kirchhoff's first law states, that the sum of currents at a node equals zero. In this thesis, currents entering the node are considered negative, while currents leaving the node are positive. Using these conventions for the intracellular node, this leads to the following equation:

$$i_{st} = c \cdot \frac{dV}{dt} + i_{Na} + i_K + i_L \tag{5}$$

To calculate the ionic currents, Kirchhoff's voltage law (sum of all voltages around a closed loop in a circuit must be zero) is used to determine the voltage drop for each ion channel. As each ionic current follows Ohm's law ($I = U \cdot G$), this leads to the following equations for the ionic currents:

$$i_{Na} = g_{Na}(t, V) \cdot (V - E_{Na}) \tag{6}$$

$$i_K = g_K(t, V) \cdot (V - E_K) \tag{7}$$

$$i_L = g_L \cdot (V - E_L) \tag{8}$$

As the conductance of sodium and potassium varies with time and voltage, Hodgkin and Huxley have introduced gating variables representing the probability of an open gate to model that process. As stated in previous chapters, sodium conductance is controlled by the activation gate m and inactivation gate h. Potassium is only controlled by the activation gate n. Experimental data show that the sodium channels contain three identical, rapidly responding m gates and one single, slower responding h gate. Potassium channels only have 4 individual n gates. These considerations can be incorporated in Equations 6 and 7 with g_{Na} and g_K symbolizing the maximum conductance.

$$i_{Na} = g_{Na} \cdot m^3 h \cdot (V - E_{Na}) \tag{9}$$

$$i_K = g_K \cdot n^4 \cdot (V - E_K) \tag{10}$$

Equations 6, 7, and 8 are substituted into Equation 11 and rearranged, resulting in the first equation of the HHM (Equation 15).

$$i_{st} = c \cdot \frac{dV}{dt} + g_{Na} \cdot m^3 h \cdot (V - E_{Na}) + g_K \cdot n^4 \cdot (V - E_K) + g_L \cdot (V - E_L) \tag{11}$$

$$\frac{dV}{dt} = \frac{1}{c} \cdot [-g_{Na} \cdot m^3 h \cdot (V - E_{Na}) - g_K \cdot n^4 \cdot (V - E_K) - g_L \cdot (V - E_L) + i_{st}] \tag{12}$$

In the final step, the gating variables m, h and n have to be modeled. A gating process can be described by a single variable that depends on time and voltage. The variable y describes statistically the gating behavior of a high number of channels of one special type in a small patch of membrane. As this is a probabilistic approach, y=0 means that all gates are closed and y=1 that all gates are open. The variable β represents the closing rate, α the opening rate. Using these considerations, a simple gating process can be modeled using the following equation:

$$\frac{dy}{dt} = \alpha(1 - y) - \beta y \tag{13}$$

To account for temperatures that differ from the original experimental conditions (T = 6.3°C), the right sides of the gating variable equations in the HHM are multiplied by a temperature correction factor k (Equation 14). This correction ensures, that the voltage-dependent kinetics of ion channels accurately reflect the faster or slower gating dynamics observed at different temperatures. At higher temperatures, the AP propagation is impeded due to the reduced amplitude and duration starting at temperatures above 31°C. This phenomenon is known as heat block. (Rattay, 1990; Hodgkin and Katz, 1949)

$$k = 3^{\frac{T-6.3}{10}} \tag{14}$$

Together with Equation 13, these considerations lead to the Hodgkin-Huxley equations. For completeness, the first equation is included as well.

$$\frac{dV}{dt} = \frac{1}{c} \cdot [-g_{Na} \cdot m^3 h \cdot (V - E_{Na}) - g_K \cdot n^4 \cdot (V - E_K) - g_L \cdot (V - E_L) + i_{st}] \tag{15}$$

$$\frac{dm}{dt} = [-(\alpha_m + \beta_m) \cdot m + \alpha_m] \cdot k \tag{16}$$

$$\frac{dn}{dt} = [-(\alpha_n + \beta_n) \cdot n + \alpha_n] \cdot k \tag{17}$$

$$\frac{dh}{dt} = [-(\alpha_h + \beta_h) \cdot h + \alpha_h] \cdot k \tag{18}$$

The values for the rate constants α and β have been determined experimentally.

$$
\begin{aligned}
\alpha_m &= \frac{2.5 - 0.1 \cdot V}{e^{2.5-0.1\cdot V} - 1} & \beta_m &= 4 \cdot e^{-\frac{V}{18}} \\
\alpha_n &= \frac{1 - 0.1 \cdot V}{10 \cdot (e^{1-0.1\cdot V} - 1)} & \beta_n &= 0.125 \cdot e^{-\frac{V}{80}} \\
\alpha_h &= 0.07 \cdot e^{-\frac{V}{20}} & \beta_h &= \frac{1}{e^{3-0.1\cdot V} + 1}
\end{aligned}
\tag{19}
$$

The HHM has one peculiarity. As the inside potential is negative compared to the outside in the polarized state, it is expected that a positive (anodal) current will lead to depolarization which elicits an AP if strong enough and a negative (cathodic) current will hyperpolarize the membrane. In contrast to all other models, the HHM also allows the generation of an AP by stimulation with the cathodic current. There is an extensively discussed similar mechanism for the extracellular stimulation (anodic break excitation) which will be discussed in Section 2.3.1. The intracellular case has received comparatively little attention (Rattay, 1990).

In anodal stimulation, the applied positive current makes the inside less negative (depolarizes), effectively bringing the membrane voltage closer to the threshold where sodium channels open and the AP is triggered. Thus, in intracellular anodic stimulation, the AP is directly caused by making the cell interior more positive. When a cathodic current is applied, the negative current initially makes the inside more negative (hyperpolarizes) which usually prevents an AP. After hyperpolarization, the membrane voltage returns to the resting state. Due to the differing activation and inactivation kinetics of ion channels, this repolarization can overshoot the resting potential. If this overshoot reaches the threshold potential, an AP is elicited (Rattay, 1990).

2.2.3 Cochlear Implants

Deafness and severe loss in hearing are often caused by damage or destruction of the sensory hair cells (IHCs, OHCs - function discussed in Section 2.1.1). The aim of CIs is to bypass the damaged hair cells by directly stimulating the ANF with electrical impulses delivered through an electrode array inserted into the *ST* via the round window (Eshraghi et al., 2012).

Figure 10 shows the main components of a modern CI implant. The external processor behind the ear, which includes an ear hook and battery case, uses a microphone to capture sound. The sound is first converted into a digital signal, which is then processed and encoded into a radio frequency (RF) signal. This RF signal is transmitted to an implanted internal receiver via inductively coupled coils. The receiver, held in place by a magnet aligned with the external headpiece, is connected to a hermetically sealed stimulator containing active electronics. Within the stimulator, power is extracted from the RF signal, the encoded information is decoded, and electrical pulses are generated. These pulses travel through wires inserted into the cochlea, where electrodes stimulate the ANFs. The site of stimulation corresponds to the frequency content of the sound. The auditory nerve then transmits this information to the brain, where it is perceived as sound (Zeng et al., 2008).

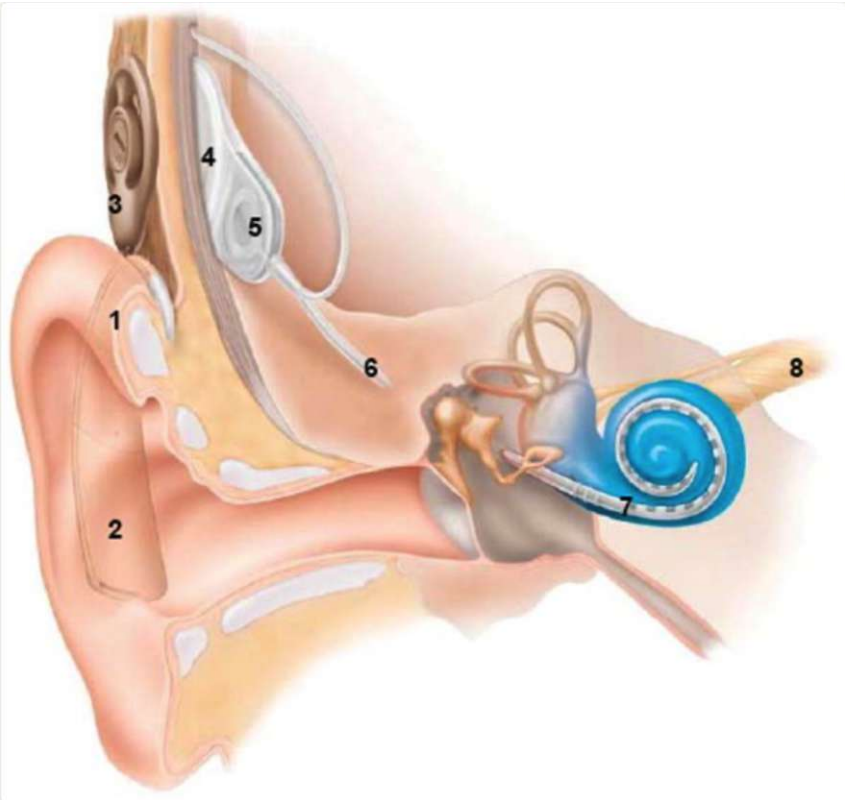

Figure 10: Basic components of a CI: (1) Microphone, (2) Behind-the-ear processor with battery, (3) External headpiece with antenna, (4) Internal receiver, (5) Hermetically sealed stimulator with active electronics, (6) Electrode lead wires, (7) Electrode array, (8) Auditory nerve (Zeng et al., 2008)

2.3 Electrical Stimulation of the Auditory Nerve

2.3.1 Extracellular Stimulation of the Auditory Nerve

In their pioneering voltage-clamp experiments, Hodgkin and Huxley investigated the relationship between membrane voltage and ionic currents in the giant squid axon. By inserting electrodes directly into the axon, they were able to inject current and measure voltage responses, laying the groundwork for the development of the HHM (Hodgkin and Huxley, 1952a). Since these experiments involved intracellular stimulation, where the electrode is placed inside the axon, the HHM primarily describes such conditions. For extracellular stimulation, where the electrode is located outside the neuron in the extracellular medium, the model must be extended to account for the complex interactions between the extracellular space and the neuron's geometry (Rattay, 1990).

While the initiation and location of an AP in intracellular stimulation is relatively straightforward, typically occurring near the site of current injection, extracellular stimulation introduces additional complexity. When an electrode delivers current into the extracellular space, it generates an electric field that causes spatial changes in the extracellular potential along the neuron (Rattay, 1999).

The transmembrane voltage is defined as follows:

$$V_m = V_i - V_e \tag{20}$$

A local increase in V_e elicited by the electrode leads to a decrease in V_m (depolarization) while a local decrease in V_e causes an increase in V_m (hyperpolarization). If the depolarization at an active side of the membrane (e.g. NoR) reaches the threshold, an AP is elicited and propagates along the axon (Rattay, 1999).

The extracellular potential V_e of a spherical electrode can be approximated (Equation 21)[1] (Rattay, 1990).

$$V_e = \frac{\rho_e \cdot I_{el}}{4\pi r} \tag{21}$$

where
V_e is the extracellular potential $[V]$
ρ_e is the resistivity of the extracellular medium $[\Omega \cdot cm]$
I_{el} is the electrode current $[A]$
r is the distance to the axon $[cm]$, calculated using the Pythagorean theorem

2.3.2 Multi-Compartment Modeling

In order to apply this to a multi-compartment model, some assumptions have to be made. The fiber is segmented into compartments. It is crucial that the compartments are so small, that the behavior of each compartment can be approximated by a mean voltage and current value. Essentially, this means that each compartment is treated as an isopotential segment and all calculations assume a single membrane voltage per compartment. This allows the multi-compartment model to simulate the fiber using one

[1] Valid exactly in an infinite, homogeneous medium

differential equation (voltage equation coupled with the gating variable equations) per compartment (Rattay, 1990).

For a single compartment, the membrane voltage can be calculated using the Hodgkin-Huxley equation (Equation 15). Expanding this model to a multi-compartment model, connections between compartments are added which allow current to flow from one compartment to another through axial resistances (Rattay, 1990).

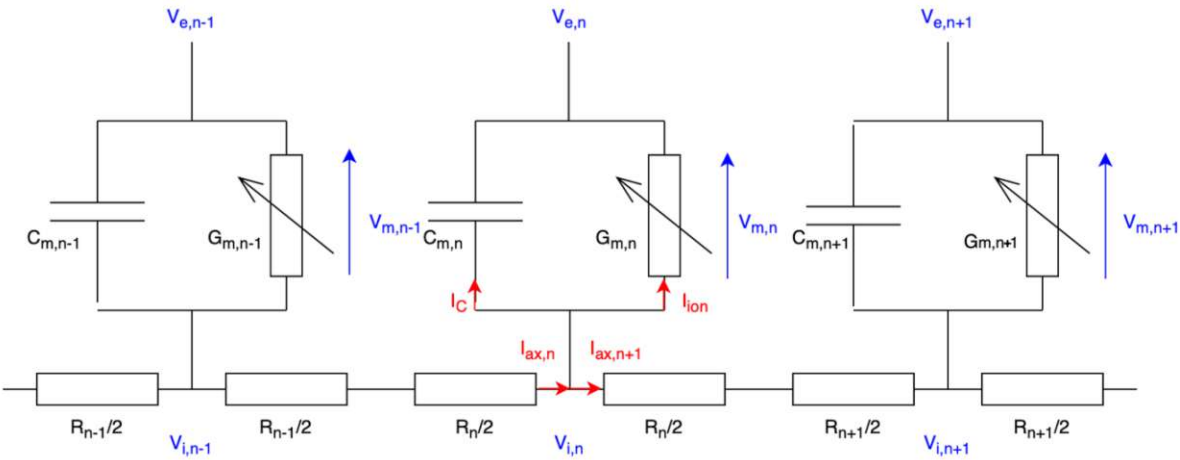

Figure 11: Equivalent circuit for a multi-compartment neuronal model. Each segment of the neuron is modeled as an RC circuit with C_m as the membrane capacitance and G_m as the membrane conductance. Compartments are connected through axial resistances R_n allowing longitudinal current flow I_{ax} between compartments. Ionic I_{ion} and capacitive currents I_C are also shown. The membrane voltage V_m is defined as the potential difference between the intracellular voltage V_i and the extracellular voltage V_e (Adapted from (Rattay, 1990) drawn with *diagrams.net* (JGraph Ltd., 2023)).

Unless otherwise indicated, the following equations and descriptions are based on Rattay (Rattay, 1990). Using Kirchhoff's law for the n-th compartment yields the following equation:

$$0 = i_{c,n} + i_{ion,n} - i_{ax,n} + i_{ax,n+1} \tag{22}$$

The axial currents can be rewritten using Ohm's law.

$$i_{ax,n} = \frac{V_{i,n-1} - V_{i,n}}{R_{n-1}/2 + R_n/2} \tag{23}$$

$$i_{ax,n+1} = \frac{V_{i,n} - V_{i,n+1}}{R_n/2 + R_{n+1}/2} \tag{24}$$

Substituting Equation 23 and 24 into Equation 22 yields the following equation:

$$0 = \frac{dV_{m,n}}{dt} \cdot C_{m,n} + I_{ion,n} + \frac{V_{i,n} - V_{i,n-1}}{R_{n-1}/2 + R_n/2} + \frac{V_{i,n} - V_{i,n+1}}{R_n/2 + R_{n+1}/2} \tag{25}$$

For analytical convenience, the reduced membrane voltage (Equation 26) is used. By subtracting the resting membrane potential from the total membrane potential, the reduced voltage becomes zero under steady-state conditions, simplifying calculations.

$$V_m = V_i - V_e - V_{rest} \tag{26}$$

Considering the reduced membrane voltage, the following equations can now be used to calculate the time course for the voltage in the n-th compartment (V_n).

$$\begin{aligned}\frac{dV_n}{dt} = \frac{1}{C_{m,n}}\Big[- I_{\text{ion}} + \frac{V_{n-1} - V_n}{R_{n-1}/2 + R_n/2} + \frac{V_{n+1} - V_n}{R_n/2 + R_{n+1}/2} \\ + \frac{V_{e,n-1} - V_{e,n}}{R_{n-1}/2 + R_n/2} + \frac{V_{e,n+1} - V_{e,n}}{R_{n+1}/2 + R_n/2}\Big]\end{aligned} \tag{27}$$

The parameter R symbolizes the axial resistance of the compartment and depends on the resistivity ρ_i of the neuronal cytoplasm and on the geometry of the compartment. If the compartment is modeled as a cylinder with length l and radius r, R can be calculated as follows:

$$R = \rho_i \cdot \frac{l}{r^2 \cdot \pi} \tag{28}$$

The parameter C symbolizes the membrane capacitance. In order to calculate it, the membrane surface area A of every compartment has to be determined. C_m is the product of surface area A and specific membrane capacitance c which is inversely proportional to the number of myelin sheaths. For the n-th compartment, it can be calculated as follows (Rattay et al., 2001):

$$C_{m,n} = A_n \cdot c_{m,n} \tag{29}$$

In multi-compartment modeling of neurons, the soma is often treated differently from dendrites and axons due to its distinctive geometry. Dendrites and axons are typically modeled as cylindrical cables. The soma can be represented as a spherical or ellipsoidal structure. This is an important fact, as this leads to a significantly larger membrane surface area compared to the dendritic or axonal segments, directly impacting membrane capacitance. The larger surface area leads to a much higher capacitance for the soma compared to other compartments. This increased capacitance means that the soma can store more charge and responds more slowly to changes in membrane potential, effectively acting as an electrical sink within the neuron (Dayan and Abbott, 2001).

2.3.3 Activating Function

The activating function is useful for predicting the influence of extracellular electrodes on the fiber. It was introduced for a homogeneous fiber (Rattay, 1986) and in a generalized form for neurons of arbitrary shape (Rattay, 1999). The activating function gives a first approximation of where the membrane will be most depolarized or hyperpolarized due to an extracellular stimulus. Positive values of the activating function indicate regions of depolarization where APs are more likely elicited. Negative values indicate hyperpolarized regions which likey inhibit AP generation. In multi-compartment models, the activating function is particularly valuable, as it helps to identify potential sites of AP initiation without requiring the full solution of the nonlinear Hodgkin-Huxley equations. This is important in the context of extracellular stimulation, where APs are not necessarily initiated in the first compartment of the model. If the cell is in the resting state, the activating function represents the slope $\frac{dVm}{dt}$ of the membrane at the first moment after stimulus application (Rattay, 1990).

The last terms of Equation 27 represent the activating function:

$$f_n = \frac{1}{C_n} \cdot \frac{V_{e,n-1} - V_{e,n}}{R_{n-1}/2 + R_n/2} + \frac{V_{e,n+1} - V_{e,n}}{R_{n+1}/2 + R_n/2} \tag{30}$$

Here, R_n represents the intracellular resistance between adjacent compartments. It is important to note that the resistance between presomatic compartment and soma and soma and postsomatic compartment have to be calculated separately. Rattay et al. (2002) state a formula to calculate the somatic resistance to the border of the j-th process with $z_j = \sqrt{r_{soma}^2 - r_{process,j}^2}$:

$$\frac{R_{\text{soma,j}}}{2} = \frac{\rho_i}{2\pi r_{process}} \cdot \ln(\frac{r_{soma} + z_j}{r_{soma} - z_j}) \tag{31}$$

2.3.4 Stochastic Behavior and Electrode Effects

In ANF models, the generations of APs is often treated deterministically. This means that a binary approach is applied, an AP either occurs or not depending on whether a stimulus threshold is reached or not. However, in biological systems, AP generation is a stochastic process that is influenced by random fluctuations in ion channel behavior, synaptic noise and other sources of variability (Faisal et al., 2008). Plotting stimulus intensity vs. spiking probability, Rattay et al. (2022) visualized the S-shaped behavior of this stochastic process.

Building upon the theoretical framework established by FitzHugh (1961), Hochmair and Hochmair-Desoyer (1984) have introduced stochastic firing behavior into auditory models by incorporating random fluctuations in the excitation process. The importance of stochastic modeling has been reinforced by more recent studies. Rattay (2022) has demonstrated that electrode position significantly affects the dynamic range of ANF responses and that only stochastic models can realistically reproduce the broad distribution of firing thresholds that has been observed experimentally. Ignoring stochasticity can lead to overly simplistic or misleading predictions of neural behavior.

Stochasticity can be introduced in various ways. Rattay and Tanzer (2022) incorporate a Gaussian noise term into the membrane potential dynamics to simulate random channel activity.

2.3.5 Modern Multi-Compartment Models

The development of multi-compartment cable models of ANFs plays a crucial role in advancing CI design and functionality. Improving computational technology and increasing insights from in vivo and in vitro experiments have allowed this models to incorporate a high level of morphological and physiological details. However, the existence of multiple models utilizing different strategies makes it challenging to determine the most appropriate one for a given study (Bachmaier et al., 2019).

In their work, Bachmaier et al. (2019) have provided a comparative analysis of the three most popular multi-compartment models. These include the Rattay et al. model (RM) (2001), the Briaire and Frijns model (BFM) (2005) and the Smit et al. model (SMM) (2010).

The RM (Rattay et al., 2001) represents the ANF as a chain of connected compartments with simplified morphology for computational efficiency. It makes use of the HHM (Section 2.2.2) to model the membrane potential and ion channels and includes stochastic channel behavior via Gaussian noise. This stochastic component allows the RM to capture the inherent variability in neural firing. The model is sensitive to parameter variation especially in the somatic region. The models of this thesis are based on this model and use the same approximations and considerations.

In contrast, the BFM (Briaire and Frijns, 2005) and SMM (Smit et al., 2010) models do not originally incorporate stochasticity in their simulations. Both models treat ion channel dynamics deterministically, which limits their ability to reproduce the variability and randomness observed in biological neural responses (Bachmaier et al., 2019).

The BFM (Briaire and Frijns, 2005) uses a higher number of compartments to model peripheral process, soma and the central axon. Instead of using the HHM to model ion channel behavior, it employs a phenomenological representation that simplifies these dynamics based on observed behavior.

The SMM (Smit et al., 2010) refines the BFM by increasing the number of compartments and improving the representation of ion channels. It also incorporates features like fiber tapering (gradual change in diameter of a nerve fiber along its length) and detailed modeling of refractory periods and conduction block. However, its AP duration is significantly longer than physiological values, leading to abnormally large absolute refractory periods.

The RM offers a balance between computational efficiency and physiological accuracy making it suitable for large-scale simulations with limited computational resources. With its detailed morphological and physiological parameters, the BFM provides a more precise simulation of electrical stimulation. However, the higher accuracy comes at a greater computational cost. The SM works best for detailed biophysical investigations, allowing an accurate representation of AP propagation and refractory behavior. Among the three of the models it has the highest computational cost (Bachmaier et al., 2019).

A big challenge for multi-compartment modeling is to predict pulse-train responses (response to electrical pulses delivered at regular intervals) in a range comparable to experimental results. Key temporal effects like pulse-train integration and adaption need to be included for realistic simulation of ANF responses (Bachmaier et al., 2019). Pulse-train integration refers to how an ANF accumulates the effect of closely spaced pulse-train impulses over time rather than responding to each one in isolation (Zhou et al., 2015). Neural adaptation refers to the gradual decrease in neural responsiveness to a constant stimulus over time (He et al., 2022). Since these long-term effects significantly influence the perception of CI users, it would be valuable for future models to incorporate these mechanisms.

3 Materials and Methods

3.1 Model Description

3.1.1 Intracellular Stimulation

This model aims to simulate the natural process of signal conduction in human myelinated ANF of Type-I with intact hair cells. To simulate the synaptic input from the sensory hair cells, which is usually in the range of pA (Grant et al., 2010; Rattay and Danner, 2014), a stimulating current is applied to the first compartment (P0) of the model (Figure 12). If this current is strong enough to exceed the excitation threshold, an AP is elicited that propagates along the nerve fiber toward the auditory brainstem. This multi-compartment model approximates the ANF by assigning distinct biophysical parameters to each compartment. The dendritic region begins with the P0 compartment. The model then alternates between passive, myelinated internodal compartments and active compartments symbolizing the NoRs which are enriched with voltage-gated ion channels critical for AP propagation. The presomatic compartment is modeled using three compartments for computational efficiency. The soma itself is modeled as a sphere. Directly after the soma, there is one compartment for the postsomatic region, the model then proceeds with alternating internodes and NoR. The P0 region, NoR, presomatic region, soma and postsomatic region are unmyelinated. According to compartment, different HHM-dynamics are applied. P0 region, NoR, presomatic and postsomatic region are modeled with a modified HHM with higher ion channel density. The dendrite is modeled with approximately half as many myelin sheaths as the axon, while the soma is approximated by a small number of layers of myelin sheaths to represent the insulating effect of satellite glial cell wrapping. Although the soma is not truly myelinated, this approximation captures its electrical insulation in the model. Additionally, the diameter of the dendrite is roughly half that of the axon (Rattay et al., 2013). All compartments except the soma are represented as cylindrical segments to approximate their geometry.

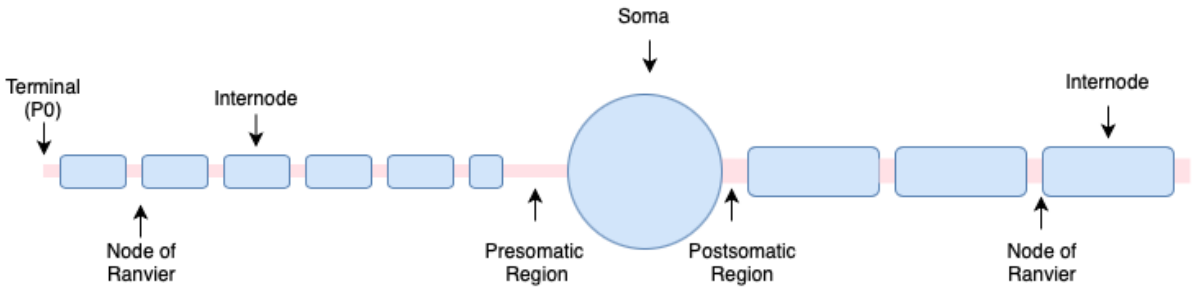

Figure 12: Schematic representation of the multi-compartment model of a myelinated Type-I ANF. At the terminal compartment (P0), a stimulating current simulates the synaptic input from sensory hair cells. The ANF alternates between passive, myelinated internodal compartments and active NoR which are enriched in voltage-gated ion channels essential for AP propagation. The presomatic region is represented by three compartments to improve computational efficiency, followed by a spherical soma. The model continues with one compartment for the postsomatic region and resumes again with alternating compartments for internodes and NoR. Redrawn after Rattay et al. (2001).

3.1.2 Extracellular Stimulation

The extracellular model builds upon the framework of the intracellular model described in the previous section. The main difference lies in the AP initiation mechanism. In this model, the fiber is assumed to lie along the x-axis at y=0, with the origin defined at the beginning of the terminal region P0. A point electrode that is positioned outside the neuron at coordinates $elecX$ and $elecY$ is used to stimulate the fiber extracellularly. The coordinates are used to calculate the extracellular potential V_e at each compartment based on the distance between electrode and compartment center. The reference point is the distant extracellular medium, assumed to be at zero potential far away from the electrode. For each compartment, one single value V_e is calculated relative to this reference. The effect of extracellular stimulation on neuronal activity depends on the polarity of the applied current. A cathodic (negative) current lowers the extracellular potential V_e near the electrode, leading to membrane depolarization (V_m=V_i-V_e), therefore increasing the likelihood of AP generation in nearby compartments. In contrast, an anodic (positive) current raises V_e hyperpolarizing adjacent compartments. Due to the spatial gradient of V_e, distal regions might see a smaller or opposite change in V_m, a behavior that can be studied by the activating function (Section 2.3.3).

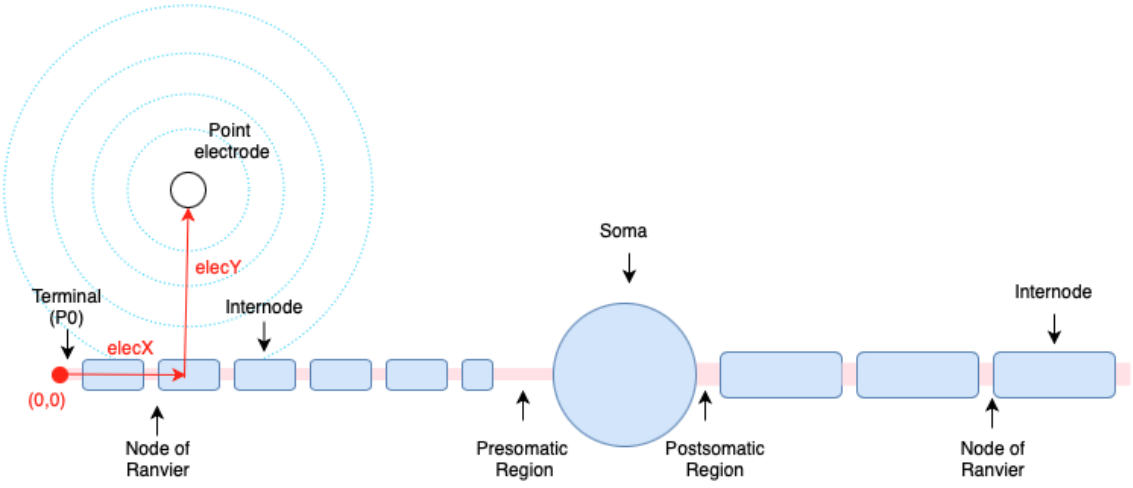

Figure 13: Schematic representation of the multi-compartment model of a myelinated Type-I ANF. Modeling of the ANF as in Figure 12, with a point electrode placed at *elecX* and *elecY* in the homogeneous extracellular medium. Blue dotted circles represent equipotentials according to Equation 21.

3.2 Model Parameters

The model parameters were selected based on previous multi-compartment models of the standard ANF (Rattay et al., 2001, 2013; Rattay and Tanzer, 2022; Bucek, 2023) and literature (Section 2.1.2).

3.2.1 Intracellular Stimulation

	Value
Lengths	
Terminal (P0)	10 μm
Node of Ranvier	1.5 μm
Dendritic Internode	200 μm
Last Dendritic Internode	100 μm
Presomatic Region	100 μm
Postsomatic Region	5 μm
Axonal Internode	400 μm
Diameters	
Dendrite	1.35 μm
Soma	20 μm
Axon	2.67 μm
Myelin Layers	
Dendrite	40 layers
Axon	80 layers
Soma	3 layers
Capacities	
Node of Ranvier	1 $\mu F/cm^2$
Dendritic Internode	0.025 $\mu F/cm^2$
Axonal Internode	0.0125 $\mu F/cm^2$
Soma	0.3333 $\mu F/cm^2$
Presomatic Region	1 $\mu F/cm^2$
Postsomatic Region	1 $\mu F/cm^2$
Conductances	
Sodium (HHM10)	1200 mS/cm^2
Potassium (HHM10)	360 mS/cm^2
Leak (HHM10)	3 mS/cm^2
Sodium (HHM)	120 mS/cm^2
Potassium (HHM)	36 mS/cm^2
Leak (HHM)	0.3 mS/cm^2
Dendritic Internode	0.025 mS/cm^2
Axonal Internode	0.0125 mS/cm^2

Table 1: Summary of morphological and biophysical parameters used in the multi-compartment model of the Type-I ANF. The table lists compartment lengths and diameters, number of myelin layers, membrane capacitances and ion channel conductances for active and passive regions. These parameters were selected based on experimental data and published literature values (Section 2.1.2).

3.2.2 Extracellular Stimulation

The extracellular model uses the default parameters from the intracellular model. It only varies in current injection, thus a variable for the extracellular resistivity ρ_e is introduced that is used for the calculation of V_e and by default set to 300Ω (Rattay et al., 2013). The electrode position is set by the coordinates *elecX* and *elecY* with the fiber along the x axis at y=0 with origin at the start of the P0 region.

3.3 Computational Workflow

The multi-compartment model has been implemented by using MATLAB R2023b. The ANF model developed in this thesis adopts a function-based implementation in MATLAB. The code builds upon the framework introduced by Rattay et al. (2001). Some portions of the code have been adapted from Bucek's master thesis (2023), with modifications to fit the current model. The model is organized into several MATLAB functions, each responsible for specific aspects of the simulation. The functions are executed and coordinated within the scripts *intracellular_calling* and *extracellular_calling*. The corresponding code is provided in the Appendix (Intracellular Model: Appendix 1, Extracellular Model: Appendix 2).

- *compartment_vec*

  This function generates the labels for an ANF with one compartment for the unmyelinated P0 region, compartments for the alternating nodes and internodes in the dendrite, three compartments for the presomatic region, one compartment for the soma, one compartment for the postsomatic region and again compartments for alternating nodes and internodes in the axon. The model ends with an axonal NoR. The number of dendritic and axonal internodes can be selected. Standard values are 6 dendritic and 11 axonal internodes.

- *store_parameters*

  This function generates a matrix that contains the morphological and biophysical parameters for each compartment. The default parameters used are specified in Section 3.2.1.

- *HHM_natural*

  This function simulates the propagation of an AP along the myelinated nerve fiber using the HHM. The membrane potential is calculated over time across multiple compartments representing the segments of a neuron with varying properties and parameters for each compartment. In this model, the stimulating current is applied to the terminal region of the model (P0).

- *threshold_AP*

  This function calculates the minimum threshold current that initiates an AP for either cathodic or anodic stimulating currents using a binary search method. The compartment for which the threshold is calculated can be specified. This is mainly used to determine the threshold that initiates an AP in the dendrite and the threshold that initiates an AP that propagates over the soma to the axon.

- *plotting*

  This function visualizes the results of the intracellular simulation. Based on plot number, different results are shown: AP in each compartment (1), Propagation of AP along the fiber (2), AP in first compartment (3), Conduction velocities and presomatic delay (4), Latency of AP (5), Strength duration curve (6).

- *HHM_extracellular*

  This function builds upon the framework of *HHM_natural*. Instead of a stimulating current directly injected into the cell, an external point electrode is used for stimulation of the ANF.

- *minimum_threshold*

  This function is used to find the electrode current needed to elicit an AP in the somatic compartment using a binary search algorithm.

- *plotting_ex*

  This function visualizes the results of extracellular stimulation. Based on plot number, different results are shown: AP in each compartment (1), AP in selected compartments (2), AP propagation along the fiber (3), Activating function (4), Extracellular potential (5).

4 Results

4.1 Intracellular Stimulation

The aim of the following results is to provide an understanding of the natural process of signal conduction in an ANF of Type-I. This section visualizes the influence of various geometric and physiological parameters on AP propagation. The results have been generated using the code provided in Appendix 1. Unless stated otherwise, simulations were carried out with the default parameters stated in Section 3.2.1 with 6 dendritic and 11 axonal internodes.

4.1.1 Cathodic and Anodic Stimulating Currents

The HHM has one peculiarity. A positive and negative current can trigger an AP if strong enough. Figure 14a and 14b show the time course of the membrane potential in the first compartment (P0) during an AP. While an anodic current (red) directly elevates the membrane potential (blue), a cathodic current first leads to hyperpolarization before the AP is triggered by a rebound depolarization. To visualize this phenomenon without interference that might occur directly at threshold level (e.g. backpropagation, Section 4.1.3), a current of slightly higher magnitude than the threshold current was chosen. The threshold current for anodic stimulation is with 34.76pA of smaller magnitude than the cathodic threshold current of -124.21pA.

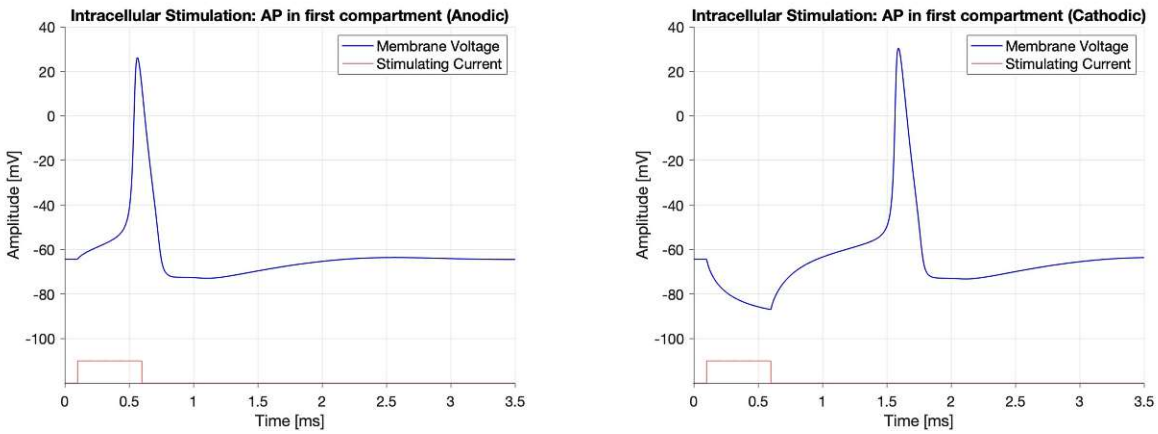

(a) AP triggered by anodic current (40pA, 0.5ms)

(b) AP triggered by cathodic current (-130pA, 0.5ms)

Figure 14: APs in the first compartment of the model (P0) under anodic and cathodic stimulation. While anodic stimulation directly elevates the membrane potential, cathodic stimulation first leads to hyperpolarization before eliciting an AP.

The polarity of the current has also an impact on latency. Latency is defined as the time between stimulus onset and first triggered AP. Figure 15a and 15b visualize this effect, with the blue dot indicating stimulus onset and the red dot showing when the threshold, at which an AP is considered (here -20mV), is reached. The latency is the time between these dots and is with 0.429ms for the anodic stimulation (40pA, 0.5ms) significantly

lower than for cathodic stimulation, where the threshold is reached after 1.456ms (-130pA, 0.5ms), as the cathodic current first hyperpolarizes the membrane before triggering the AP through a rebound reaction.

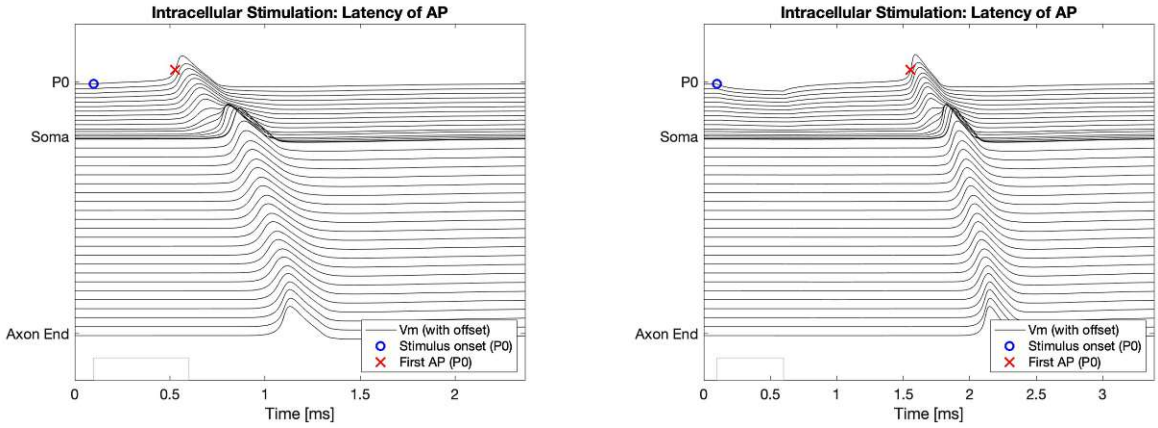

(a) Latency: anodic current (40pA, 0.5ms)

(b) Latency: cathodic current (-130pA, 0.5ms)

Figure 15: Stimulus onset (blue dot) and first triggered AP (red cross) for cathodic and anodic stimulation. As recovery from hyperpolarization takes time, the latency is of larger magnitude for the cathodic stimulation.

4.1.2 Influence of Soma Size and Presomatic Length on AP Propagation

Influencing factors on AP propagation are soma size and length of the presomatic region. This effect is visualized by Figure 16. Increasing the soma diameter increases presomatic delay for all presomatic compartment lengths. This effect remains relatively constant for lengths of 100, 80 and 60μm, showing similar values for presomatic delay for varying presomatic lengths. Smaller presomatic compartment lengths in the range of 40 to 10μm lead to a notable increase in presomatic delay for larger soma diameters. For a soma diameter of of 35μm, this even results in the failure of AP propagation for a presomatic compartment length of 20 and 10μm, while all other cases allow propagation over the soma into the axon. For smaller soma diameters, shortening the presomatic compartment can be beneficial, leading to a shorter presomatic delay. For this simulation, an anodic current of 40pA with 0.5ms pulse duration was used. An AP was considered to occur if a threshold of -40mV was reached.

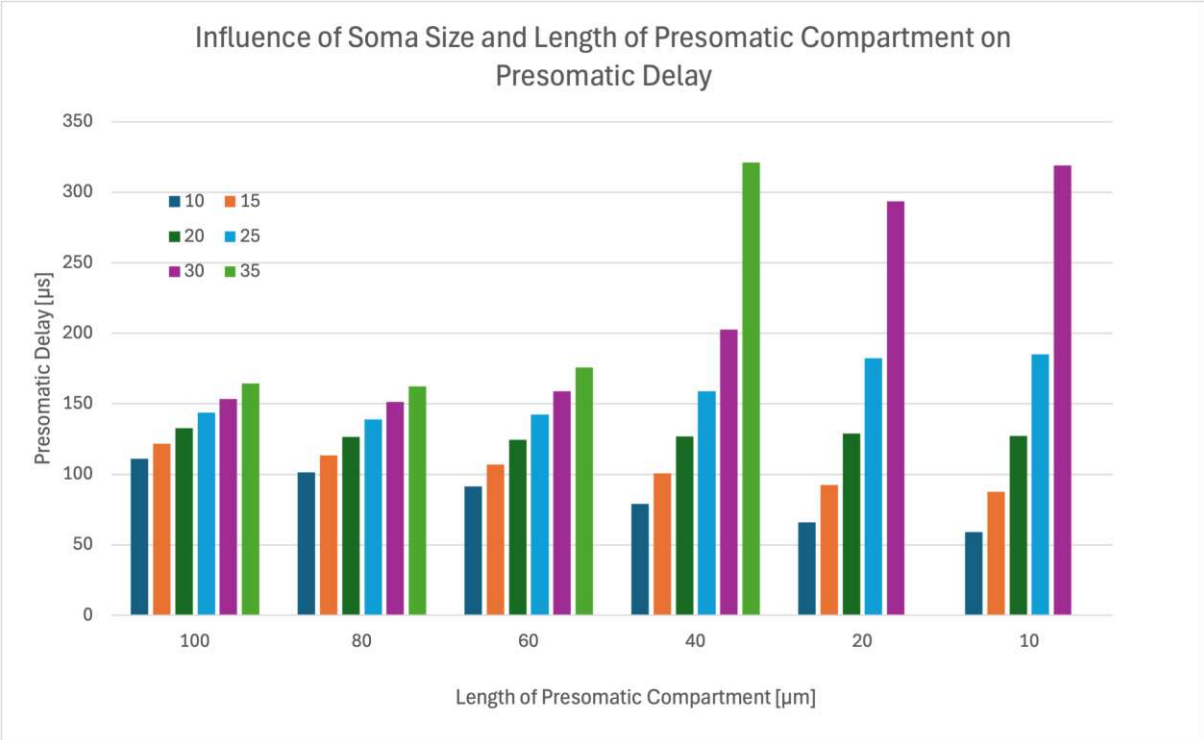

Figure 16: Impact of soma diameter and presomatic compartment length on presomatic delay. For longer presomatic compartments (100, 80, 60 μm), the delay remains relatively constant across all soma diameters. For shorter compartments (40 to 10μm), the presomatic delay increases rapidly for larger soma diameters (30 and 35 μm). For a soma diameter of 35μm, AP propagation fails for presomatic compartment lengths of 20 and 10μm. For all other cases, the AP successfully propagates over the soma into the axon. Stimulating current: 40pA, 0.5ms. This figure was created with Microsoft Excel.

4.1.3 Backpropagation

An interesting phenomenon called backpropagation occurs at larger soma diameters and smaller presomatic lengths. Figure 17 visualizes voltage dynamics in the ANF with a soma diameter of 30μm and a presomatic length of 20μm. Subfigures 17a and 17b show that a current of 34.81pA (0.5ms) is strong enough to elicit an AP in the dendrite, but the AP fails to propagate over the soma. A slightly higher current of 34.85pA is able to overcome the soma-barrier and also leads to APs traveling back in the dendrite, also known as backpropagation (Subfigure 17c and 17d). At larger currents (38pA), backpropagation does no longer occur (Subfigures 17e and 17f).

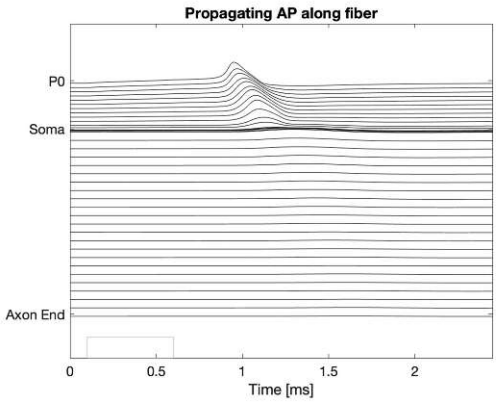

(a) 34.81pA: AP propagation

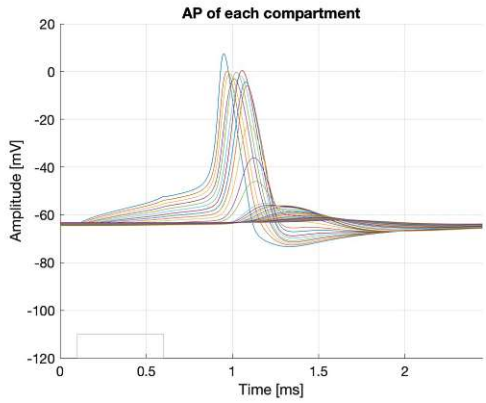

(b) 34.81pA: AP of each compartment

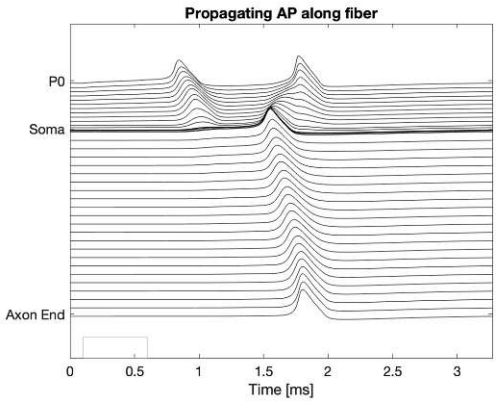

(c) 34.85pA: AP propagation

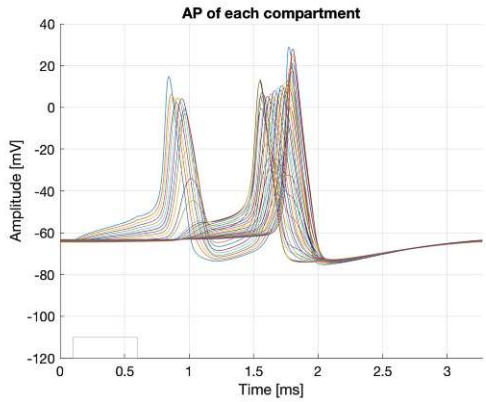

(d) 34.85pA: AP of each compartment

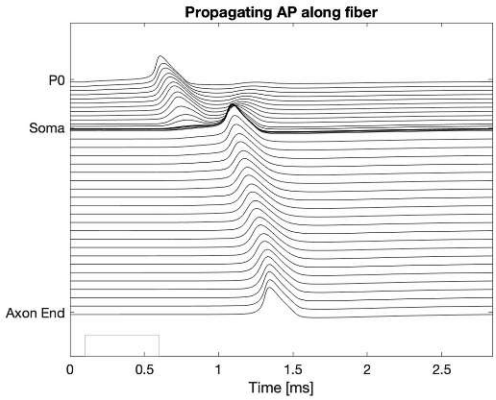

(e) 38pA: AP propagation

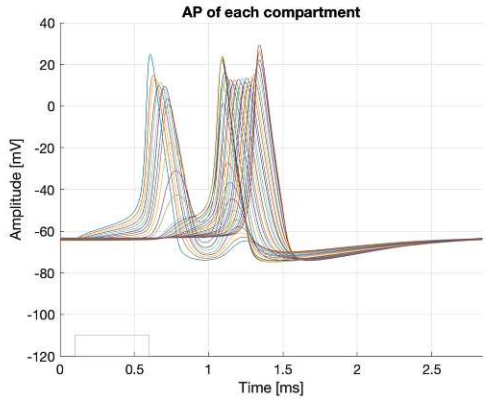

(f) 38pA: AP of each compartment

Figure 17: Membrane voltage dynamics in the ANF with soma diameter of 30μm and presomatic compartment length of 20μm. Subfigures (a) and (b) show voltage response to a 34.81pA current with a duration of 0.5ms: an AP is generated and propagates in the dendrite but fails to propagate over the soma. Subfigures (c) and (d) show the response for a current of 34.85pA with duration of 0.5ms: the AP crosses the soma and additionally elicits backpropagation of APs into the dendrite. Subfigures (e) and (f) illustrate the response to a current of 38pA, 0.5ms duration: backpropagation does no longer occur, the AP propagates unidirectionally.

4.1.4 Impact of Fiber Diameter on Threshold and Conduction Velocity

Another influencing factor on AP propagation, especially on conduction velocity, is the diameter of the axon and dendrite. Table 2 shows that larger diameters lead to faster conduction velocities for the dendrite and axon. Larger diameters of dendrite and axon also elevate the threshold current necessary to trigger an AP. This simulation was carried out for a pulse duration of $0.5ms$ and soma diameter of $20\mu m$.

Diameter		**Threshold**	**Conduction Velocity**	
Dendrite $[\mu m]$	Axon $[\mu m]$	Anodic $[pA]$	Dendrite $[mm/ms]$	Axon $[mm/ms]$
0.5	1	8.7	4.04	9.50
1	2	22.51	4.88	13.69
1.5	3	40.65	5.36	17.14
2	4	63.08	5.52	20.28

Table 2: Anodic threshold currents $[pA]$ and conduction velocities $[mm/ms]$ for varying dendritic and axonal diameters. Stimulating current for the conduction velocities was set to displayed threshold with a current duration of $0.5ms$. Larger diameters elevate the threshold current and lead to faster conduction velocities.

4.1.5 Influence of Channel Density and Node Length on Conduction and Threshold

Ion channel density and length of the NoRs can also have an impact on conduction velocity and threshold. Table 3 shows that for both node lengths the conduction velocity increases with enhanced ion channel density, while the threshold current needed to trigger an AP decreases. Here it is important to note that 'channel density' refers in this context to the scaling factor for the HHM used in the P0 region, the NoRs, the presomatic region and the postsomatic region.

The table also displays, that dendritic conduction velocity is higher for longer NoRs while axonal conduction velocity is larger for shorter NoRs. This simulation was carried out for a current duration of $0.1ms$. The impact of this shortened current duration on threshold magnitude (Table 3) is visible when comparing the threshold currents to the diameter experiments (Table 2), that were carried out with a current duration of $0.5ms$. For a shorter current duration, significantly larger magnitudes are necessary to trigger an AP. This phenomenon will be discussed in the next section.

NoR length [μm]	Channel Density -	Anodic Threshold [pA]	Velocity Dendrite [mm/ms]	Velocity Axon [mm/ms]
1.5	8	92.59	4.19	15.26
	10	88.53	5.27	16.07
	12	85.76	6.07	16.75
2.5	8	96.58	5.30	15.18
	10	92.34	5.96	15.89
	12	89.44	6.57	16.49

Table 3: Conduction velocities [mm/ms] in dendrite and axon and anodic threshold currents [pA] at varying ion channel densities for shorter ($1.5\mu m$) and longer ($2.5\mu m$) NoRs. For measurement of the conduction velocity, the stimulating current was set to the threshold current. Increasing channel density leads to increasing conduction velocity and lower threshold currents for both short and long NoRs. Simulation was carried out for a current duration of $0.1ms$.

4.1.6 Strength-Duration Curve

The higher threshold current values in Table 3 with a pulse duration of $0.1ms$ compared to Table 2 with a pulse duration of $0.5ms$ suggest that pulse duration also has a major influence on AP initiation. Figure 18 visualizes an important concept of stimulation: the relationship between pulse duration and strength. The figure visualizes that shorter pulses need larger amplitudes for AP initiation. Two key parameters characterize this curve: Chronaxie and Rheobase. Rheobase refers to the minimum current amplitude that can elicit APs with a theoretically infinite pulse duration representing the baseline excitability of the fiber. Chronaxie is the pulse duration at which the threshold current required to elicit an AP is exactly twice the rheobase current (Rattay, 1990).

Chronaxie and rheobase were determined for four different cases:

- Case 1: Standard parameters (Section 3.2.1)
- Case 2: Altered fiber diameter (Dendrite: $2\mu m$, Axon: $4\mu m$)
- Case 3: Altered NoR length ($2.5\mu m$)
- Case 4: Altered soma diameter ($30\mu m$)

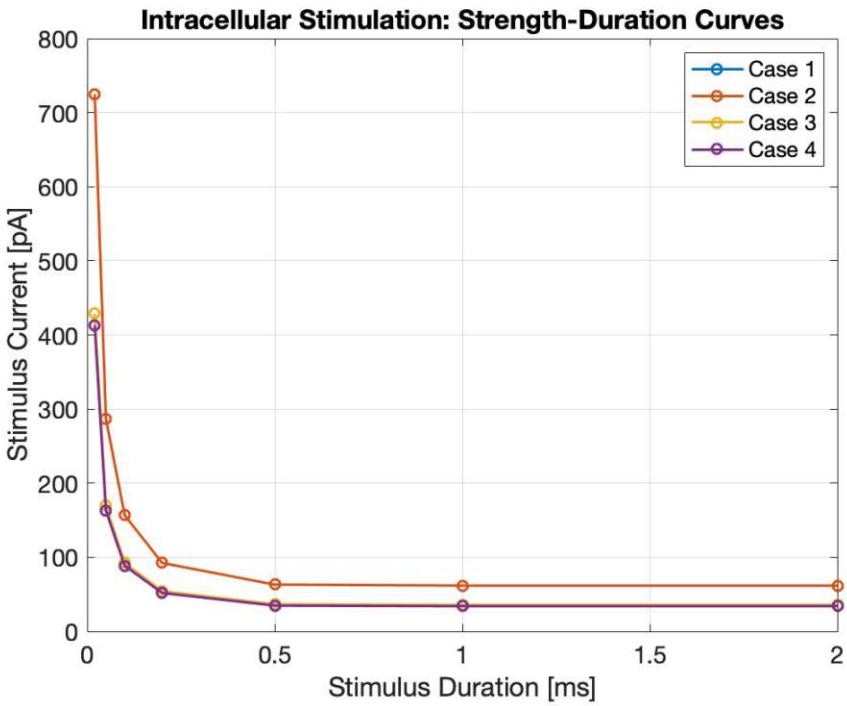

Figure 18: Relationship between pulse duration and current strength for four different cases. Case 1: Standard parameters, Case 2: Altered fiber diameter for dendrite and axon, Case 3: Longer NoR length, Case 4: Larger soma diameter. Shorter pulses have to be of larger magnitude in order to elicit an AP. Only case 2 deviates from the others with larger currents needed to elicit an AP.

Table 4 visualizes the rheobase and chronaxie values for all four cases. While NoR length and soma diameter have only a marginal impact, changing the fiber diameter leads to almost double current magnitudes needed to elicit APs. Chronaxie values are uniform for all four cases.

Case	**Chronaxie** $[ms]$	**Rheobase** $[pA]$
1	0.156	33.97
2	0.151	61.80
3	0.155	35.74
4	0.156	33.99

Table 4: Chronaxie and Rheobase for four different cases. Rheobase refers to minimum current amplitude needed to trigger an AP. Chronaxie is the pulse duration at which the threshold current required to elicit an AP is exactly twice the rheobase current. Case 1: Standard parameters, Case 2: Altered fiber diameter for dendrite and axon, Case 3: longer NoR length, Case 4: Larger soma diameter. Only case 2 has a noticable impact on rheobase value.

4.1.7 Impact of Myelination on Threshold and AP Propagation

Myelination is also an influencing factor on AP propagation that should not be overlooked. Table 5 shows that with decreasing myelination the threshold required to trigger an AP increases and the conduction velocities for the dendrite and axon decrease. It is important to note that 'Myelin layers' in this context represents the number of myelin layers wrapping the dendritic and axonal internodes. The soma itself is not myelinated, but wrapped with glial cells, which is simplified in this code by using a small number of myelin layers. This number of layers for the soma has a clear impact on presomatic delay. The simulation was carried out for current durations of $0.5ms$.

Myelin Layers				**Velocity**		
Axon	Dendrite	Soma	**Threshold** $[pA]$	Dendrite $[mm/ms]$	Axon $[mm/ms]$	**Presomatic Delay** $[\mu s]$
100	60	3	32.19	6.67	18.17	130.21
80	40	3	34.76	5.05	16.07	129.87
60	20	3	41.53	3.22	13.46	130.03
60	20	1.5	41.52	3.08	13.39	220.60

Table 5: Effect of varying number of myelin layers in axon, dendrite, and soma on threshold current, dendritic and axonal conduction velocity and presomatic delay. For conduction velocity and presomatic delay, the displayed threshold currents were used with a duration of $0.5ms$. Fewer myelin layers lead to higher threshold currents and slower conduction velocities. The number of layers for the soma representing the glial cell wrapping has a big impact on presomatic delay.

4.2 Extracellular Stimulation

4.2.1 Cathodic and Anodic Electrode Currents

The extracellular stimulation also allows triggering APs with currents of both polarity. Figure 19 visualizes, how APs at minimum threshold current necessary for the AP to cross the soma propagate for a cathodic electrode current (-17.31μA, 0.1ms duration, Subfigure 19a) and for an anodic electrode current (45.14μA, 0.1ms duration, Subfigure 19b) applied to a point electrode in distance x=100μm and y=80μm. The electrode coordinates and position (red dot) in the plot indicate that the electrode is not directly at the beginning of the fiber but rather above the first internode. The AP is in both cases still elicited in the first compartment (P0), as indicated by the red line. At the compartment closest to electrode position (first dendritic internode, compartment 2), the voltage behaves differently depending on current polarization. Cathodic currents directly elevate the membrane potential at the compartment below, while anodic currents lead in the same compartment to hyperpolarization.

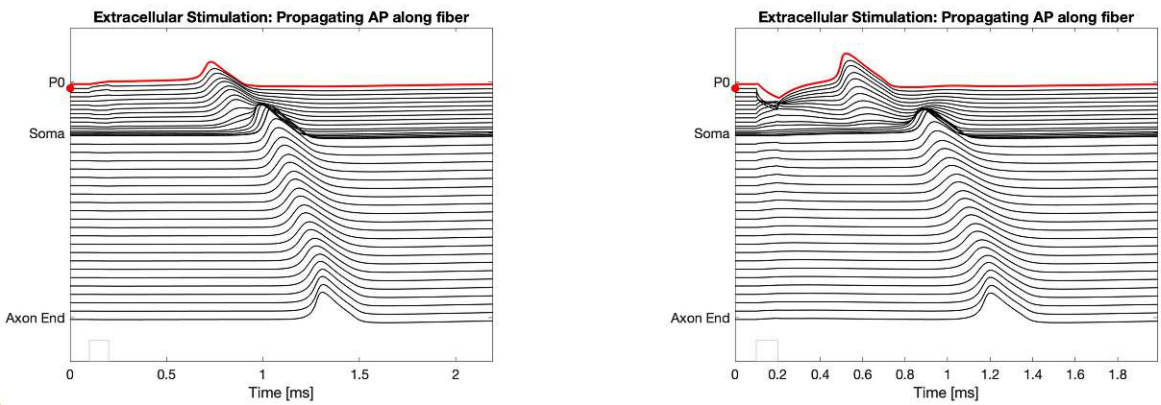

(a) AP propagation for cathodic current (-17.31μA, 0.1ms)

(b) AP propagation for anodic current (45.14μA, 0.1ms)

Figure 19: AP propagation for cathodic and anodic electrode current, applied to a point electrode at position x=100μm, y=80μm (position indicated by red dot). The red line symbolizes the compartment where the first AP is triggered, which is the first compartment for both cases. Directly below the electrode, cathodic currents lead to depolarization, while anodic currents hyperpolarize.

To better visualize this effect, Figure 20 shows the AP in selected compartments. As the electrode is with x=100μm and y=80μm closest to compartment 2, the plots show the APs in the first five compartments (1: P0, 2: Internode, 3: NoR, 4: Internode, 5: NoR) for the same electrode currents used in Figure 19.

Subfigure 20a shows the APs for stimulation with the cathodic electrode current. The compartment directly below the point electrode (compartment 2: internode, orange) is depolarized. Flanking compartments (compartment 1: P0, blue; compartment 3: NoR, yellow) also experience depolarization but of lower magnitude. Compartments further from the electrode (compartment 4: internode, violet; compartment 5: NoR, green) are hyperpolarized.

Subfigure 20b visualizes the APs in the selected compartments for stimulation with the anodic electrode current. The compartment directly below the electrode (compartment 2: internode, orange) is hyperpolarized. Flanking regions (compartment 1: P0, blue; compartment 3: NoR, yellow) are also hyperpolarized but with lower magnitude. Compartments further from the electrode (compartment 4: internode, violet; compartment 5: NoR, green) are depolarized.

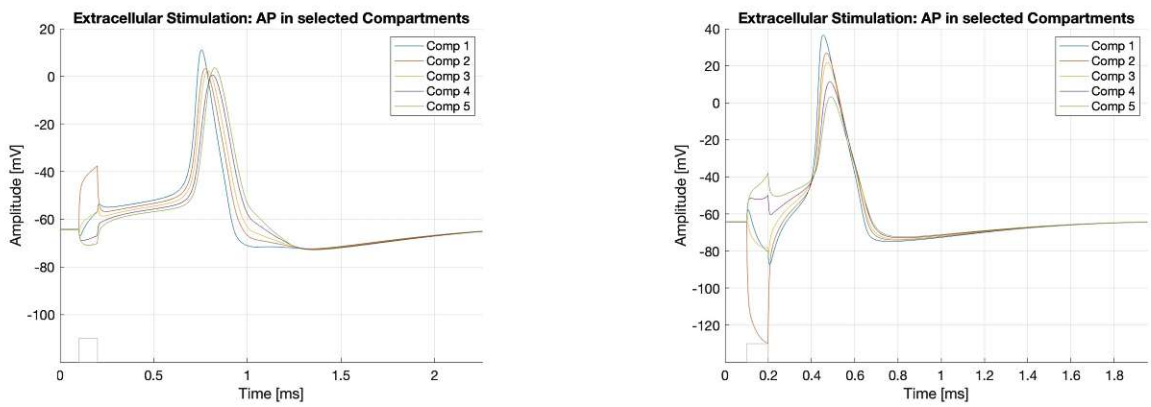

(a) APs in selected compartments, cathodic current (-17.31μA, 0.1ms)

(b) APs in selected compartments, anodic current (45.14μA, 0.1ms)

Figure 20: APs in selected compartments (1: P0, 2: Internode, 3: NoR, 4: Internode, 5: NoR) for cathodic and anodic electrode current, applied to a point electrode at position x=100μm, y=80μm. Directly below the electrode and in flanking regions cathodic currents depolarize, while anodic currents hyperpolarize.

For the same conditions as in Figure 19 and 20, Figure 21 visualizes the influence of the point electrode on the extracellular potential V_e. Subigure 21a shows that under the influence of a cathodic electrode current the extracellular potential decreases with a minimum peak directly below the point electrode (position indicated by dashed red line). Subfigure 21b visualizes that this effect is reversed for an anodic electrode current. The anodic electrode current increases the extracellular potential with a maximum peak directly below the point electrode.

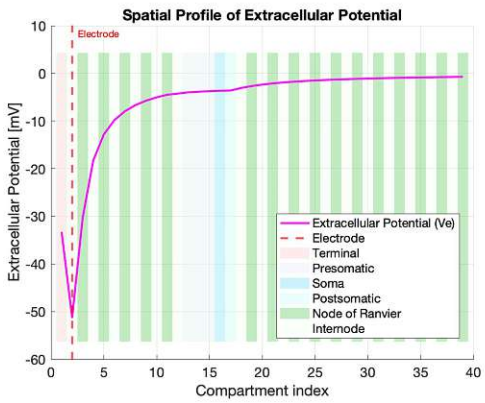

(a) Extracellular potential: cathodic electrode current (-17.31μA, 0.1ms)

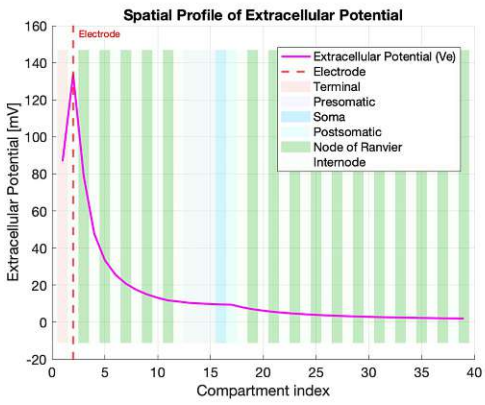

(b) Extracellular potential: anodic electrode current (45.14μA, 0.1ms)

Figure 21: Change in extracellular potential under cathodic and anodic extracellular stimulation with a point electrode at position x=100μm, y=80μm. The patches represent the compartment type, the red dashed line indicates the electrode position. Cathodic electrode currents decrease the extracellular potential directly below the electrode, while anodic electrode currents lead to an increase.

Figure 22 shows the activating function for both polarities. The activating function indicates where depolarization and hyperpolarization along the fiber might occur. In this master thesis, positive values indicate regions where depolarization is most likely, while negative values indicate hyperpolarizing regions. Subigure 22a represents stimulation with the cathodic electrode current and shows a positive peak directly below the electrode indicating a region where depolarization might occur. At compartment 4 it shows a negative peak indicating hyperpolarization. Subfigure 22b visualizes the activating function for stimulation with an anodic current. Directly at the electrode position, it shows a negative peak indicating hyperpolarization. Compartment 4 exhibits a positive peak, showing a region where likely depolarizaiton occurs.

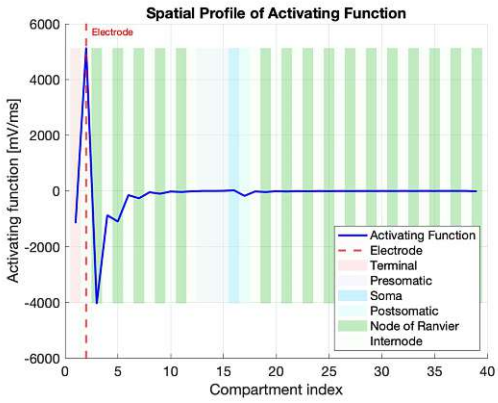

(a) Activating function for cathodic electrode current (-17.31μA, 0.1ms)

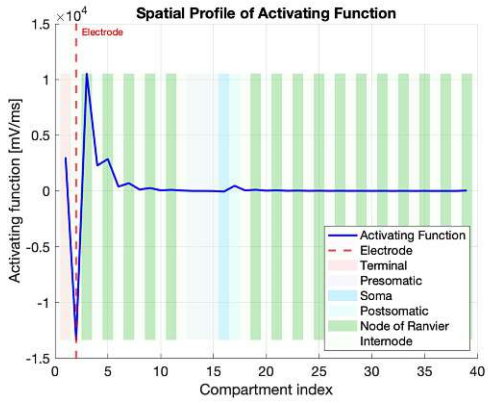

(b) Activating function for anodic electrode current (45.14μA, 0.1ms)

Figure 22: Activating function for stimulation with cathodic and anodic electrode current (x=100μm, y=80μm). Positive values indicate regions of depolarization, negative values regions of hyperpolarization. Cathodic stimulation leads to a positive peak at electrode position, indicating a depolarizing region, while anodic stimulation exhibits a negative peak indicating a hyperpolarizing region.

Results obtained with an electrode distance of y=80μm are not practically feasible but remain theoretically interesting, as certain phenomena observed at this small scale do not appear at larger electrode distances. To ensure practical relevance, the previous and following experiments will be calculated for a small distance (y=80μm) and a more realistic electrode distance of y=300μm.

Figure 23 visualizes the same situation as in Figure 19 with an altered electrode position of x=100μm and y=300μm. For both the cathodic (-62.56μA, 0.1ms; Subfigure 23a) and anodic (387.39μA, 0.1ms; Subfigure 23b) electrode current, the first AP is elicited in the first compartment P0. Comparing the threshold currents needed to elicit an AP that propagates over the soma from Figure 19 and Figure 23, it shows that larger electrode distances require larger current magnitudes.

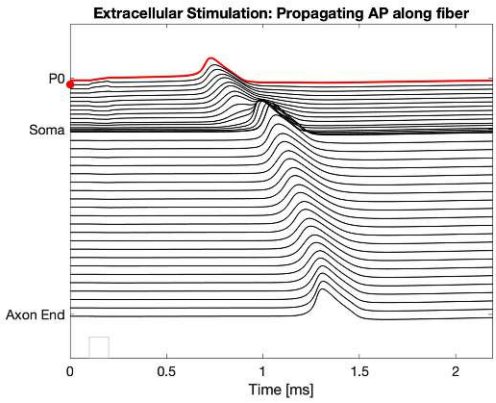

(a) AP propagation for cathodic current (-62.56μA, 0.1ms)

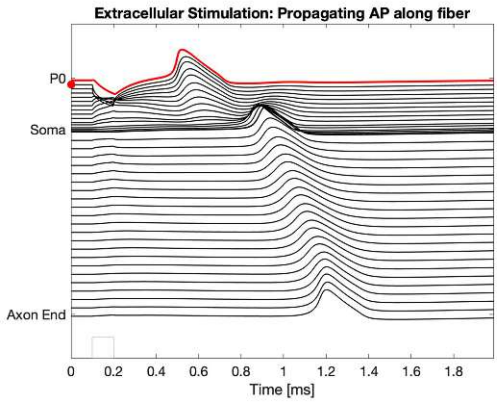

(b) AP propagation for anodic current (387.39μA, 0.1ms)

Figure 23: AP propagation for cathodic and anodic electrode current, applied to a point electrode at position x=100μm, y=300μm (position indicated by red dot). The red line symbolizes the compartment where the first AP is triggered, which is the first compartment for both cases.

Again, the influence of the electrode on nearby compartments is examined, analogous to Figure 20 with electrode position x=100μm, y=300μm. Figure 24 indicates that for larger electrode distances directly below the electrode and in flanking compartments cathodic currents depolarize (Subfigure 24a) and anodic currents hyperpolarize (Subfigure 24b). The effect of reverse polarization in flanking regions shown in Figure 20 can be observed for an electrode distance of y=300μm as well, it is shifted to more distal compartments which is why it does not appear in Figure 24.

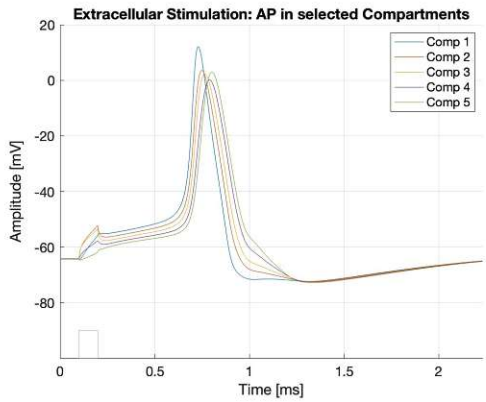

(a) APs in selected compartments, cathodic current (-62.56μA, 0.1ms)

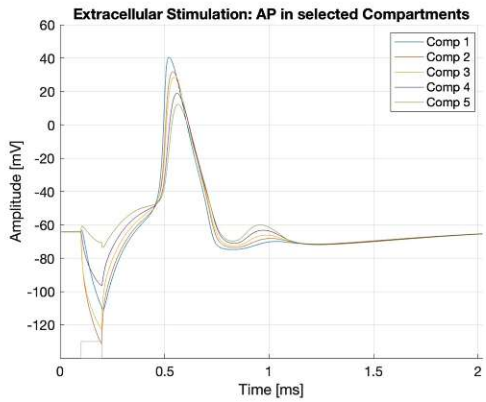

(b) APs in selected compartments, anodic current (387.39μA, 0.1ms)

Figure 24: APs in selected compartments (1: P0, 2: Internode, 3: NoR, 4: Internode, 5: NoR) for cathodic and anodic electrode current, applied to a point electrode at position x=100μm, y=300μm. Directly below the electrode and in flanking regions cathodic currents depolarize, while anodic currents hyperpolarize.

Figure 25 visualizes the influence of the point electrode placed at x=100μm and y=300μm on the extracellular potential V_e (analogous to Figure 21). Subfigure 25a shows that V_e is increasing with a minimum peak directly below the electrode. For an anodic electrode current, V_e decreases with a maximum peak directly below the electrode (Subfigure 25b). Compared to the relatively steep increase or decrease at shorter electrode distances (Figure 21, y=80μm), the slope is noticeably more gradual for larger electrode distances of y=300μm.

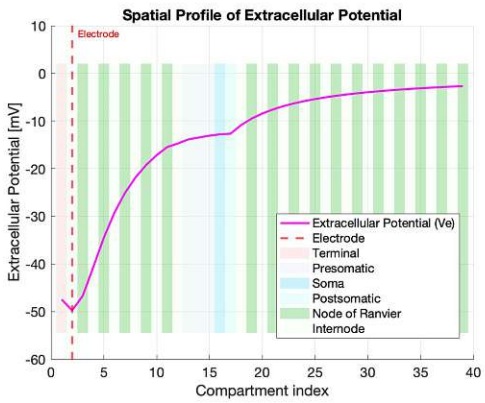

(a) Extracellular potential: cathodic electrode current (-62.56μA, 0.1ms)

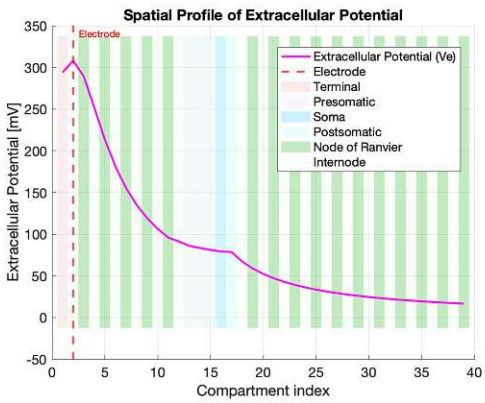

(b) Extracellular potential: anodic electrode current (387.39μA, 0.1ms)

Figure 25: Change in extracellular potential under cathodic and anodic extracellular stimulation with a point electrode at position x=100μm, y=300μm. The patches represent the compartment type, the red dashed line indicates the electrode position. Cathodic electrode currents decrease the extracellular potential directly below the electrode, while anodic electrode currents lead to an increase.

Analogous to Figure 22, Figure 26 visualizes the activating function for both polarities at an electrode distance of x=100μm, y=300μm. Subfigure 26a indicates that up to compartment 5, the fiber exhibits only depolarization, which aligns with the results of Subfigure 24a. For an anodic electrode current, the first 5 compartments exhibit solely hyperpolarization (Subfigure 26b), which also aligns with the results of Subfigure 24b. Figure 22 shows that smaller electrode distances lead to more pronounced peaks in electrode proximity and only a few, less prominent local extrema along the fiber. For larger electrode distances, Figure 26 visualizes again prominent peaks directly below the electrode, but also more pronounced local extrema along the fiber, especially in the postsomatic region.

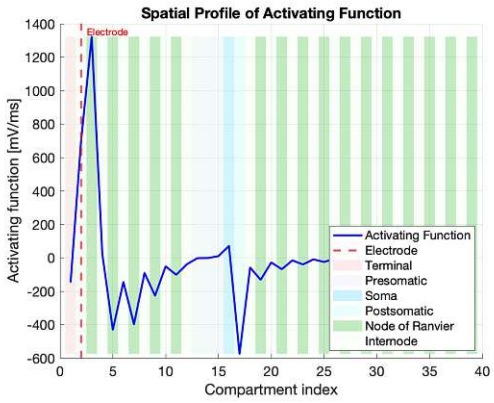

(a) Activating function for cathodic electrode current (-62.56μA, 0.1ms)

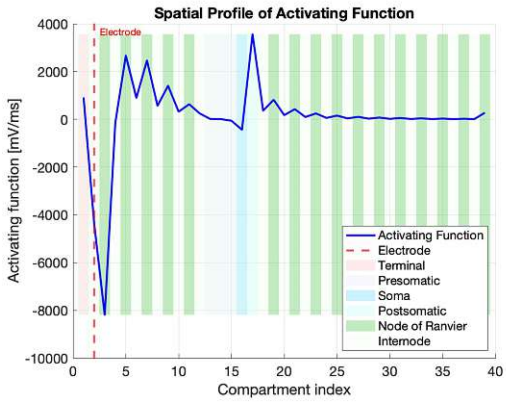

(b) Activating function for anodic electrode current (387.39μA, 0.1ms)

Figure 26: Activating function for stimulation with cathodic and anodic electrode current (x=100μm, y=300μm). Positive values indicate regions of depolarization, negative values regions of hyperpolarization. Cathodic stimulation leads to a positive peak at electrode position, indicating a depolarizing region, while anodic stimulation exhibits a negative peak, indicating a hyperpolarizing region.

4.2.2 Influence of Current Strength and Electrode Position on AP Propagation

To determine the influence of electrode position on location of AP initiation, five different electrode positions have been chosen.

- Position 1 (x=400, y=80): Above dendritic NoR (Compartment 5)
- Position 2 (x=1100, y=80): Above internode, close to presomatic compartment
- Position 3 (x=1220, y=80): Above soma
- Position 4 (x=1400, y=80): Approximately above postsomatic compartment
- Position 5 (x=2800, y=80): Above axonal NoR

For this analysis, only the cathodic electrode currents were considered, as cathodic electrode currents are preferred in extracellular stimulation because they directly depolarize the ANF below the electrode. For this simulation, a duration of $0.1ms$ has been chosen. The threshold currents and respective AP initiation site were determined, then simulation was run again with a current 1.5 times the threshold current to visualize the effect of current strength on initation site.

Table 6 visualizes how electrode position affects threshold and AP initiation site (compartment where first AP is initiated). For the simulation at threshold current, the results display that close to the soma thresholds of larger magnitude are needed and that the preferred AP initation sites are the presomatic compartments. In the dendrite, the AP is elicited at the NoR directly below the electrode. In the axon, the first AP occurs at the last NoR of the axon. Larger currents show AP initation in compartments closer to the point electrode compared to AP initation at threshold level.

Electrode Position			**Threshold**	**First AP**	**First AP: 1.5·Thresh.**
x [μm]	y [μm]	Closest Comp.	[μA]	Comp.	Comp.
400	80	5 (NoR Dendrite)	-9.62	5 (NoR Dendrite)	5 (NoR Dendrite)
1100	80	12 (Internode)	-12.33	14 (Presomatic)	13 (Presomatic)
1220	80	16 (Soma)	-18.75	13 (Presomatic)	15 (Presomatic)
1300	80	17 (Postsoma)	-22.10	13 (Presomatic)	16 (Soma)
2800	80	25 (NoR Axon)	-10.22	39 (NoR Axon)	25 (NoR Axon)

Table 6: AP initiation sites and threshold currents for five different electrode positions. Position 1: Dendrite, directly above dendritic NoR. Position 2: Dendrite, directly above internode but close to presomatic compartments. Position 3: Directly above the soma. Position 4: Directly above postsomatic compartment. Position 5: Axon, directly above NoR. Simulation was carried out for displayed threshold current with a duration of $0.1ms$, then again for a current 1.5 times the threshold current. Close to the soma, threshold currents have a higher magnitude and APs are initiated in the presomatic compartments. Larger currents lead to more localized AP initiation.

The same simulation was carried out again with y=150μm to visualize the effect of electrode distance. Table 7 displayed that if the electrode is further away from the fiber, larger threshold currents are necessary to elicit an AP and the AP is more likely elicited at regions of high ionic channel density, as shown by the results of the first position. Higher currents again lead to more localized AP initiation at NoRs.

Electrode Position			**Threshold**	**First AP**	**First AP: 1.5·Thresh.**
x [μm]	y [μm]	Closest Comp.	[μA]	Comp.	Comp.
400	150	5 (NoR Dendrite)	-22.4	1 (P0)	5 (NoR Dendrite)
1100	150	12 (Internode)	-32.99	14 (Presomatic)	13 (Presomatic)
1220	150	16 (Soma)	-45.8	13 (Presomatic)	15 (Presomatic)
1300	150	17 (Postsoma)	-46.7	13 (Presomatic)	16 (Soma)
2800	150	25 (NoR Axon)	-19.31	39 (NoR Axon)	25 (NoR Axon)

Table 7: AP initiation sites and threshold currents for five different electrode positions. Position 1: Dendrite, directly above dendritic NoR. Position 2: Dendrite, directly above internode but close to presomatic compartments. Position 3: Directly above the soma. Position 4: Directly above postsomatic compartment. Position 5: Axon, directly above NoR. Simulation was carried out for displayed threshold current with a duration of 0.1ms, then again for a current 1.5 times the threshold current. Close to the soma, threshold currents have a higher magnitude and APs are initiated in the presomatic compartments. Larger currents lead to more localized AP initiation.

While an electrode distance of y=80μm is theoretically interesting, it is not practically feasible. y=150μm still represents a relatively small distance. Therefore, the simulations were repeated using a more practical and realistic value of y=300μm. Table 7 and 8 yield similar results, especially for larger current magnitudes where APs are elicited more locally. For AP initiation at threshold level, larger electrode distances (y=300μm) are mainly elicited at the first compartment P0. The current magnitudes are largest for y=300μm.

Electrode Position			**Threshold**	**First AP**	**First AP: 1.5·Thresh.**
x [μm]	y [μm]	Closest Comp.	[μA]	Comp.	Comp.
400	300	5 (NoR Dendrite)	-64.48	1 (P0)	5 (NoR Dendrite)
1100	300	12 (Internode)	-107.20	13 (Presomatic)	13 (Presomatic)
1220	300	16 (Soma)	-122.75	1 (P0)	15 (Presomatic)
1300	300	17 (Postsoma)	-128.03	1 (P0)	15 (Presomatic)
2800	300	25 (NoR Axon)	-46.05	39 (NoR Axon)	25 (NoR Axon)

Table 8: AP initiation sites and threshold currents for five different electrode positions. Position 1: Dendrite, directly above dendritic NoR. Position 2: Dendrite, directly above internode but close to presomatic compartments. Position 3: Directly above the soma. Position 4: Directly above postsomatic compartment. Position 5: Axon, directly above NoR. Simulation was carried out for displayed threshold current with a duration of 0.1ms, then again for a current 1.5 times the threshold current. Close to the soma, threshold currents have a higher magnitude and APs are initiated in the presomatic compartments. Larger currents lead to more localized AP initiation.

4.2.3 Influence of Soma Geometry and Presomatic Length on AP Propagation

The results of the intracellular stimulation (Section 4.1.2) indicate that the length of the presomatic compartment and soma diameter have a major influence on signal propagation, which is why this influence has also been studied for the extracellular stimulation. For this simulation, only electrode positions 2-4 have been examined, as they are closest to the soma. Two soma diameters have been tested, 15 and 30μm. For the presomatic length the default value of 100μm and 10μm have been chosen.

Table 9 displays the anodic threshold current and AP initiation site at threshold level and for a current 1.5 times the threshold current. Shorter presomatic lengths (10μm) lead to larger threshold currents for both soma diameters (15, 30 μm). Except for the combination of large soma diameter (30 μm) and short presomatic length (10μm), AP initiation at threshold level occurs at the presomatic or postsomatic compartment. Only for the short presomatic length (10μm) and large soma diameter(30 μm) does AP initiation occur at the first compartment P0. For larger currents, this effects vanishes and the AP initiation site becomes more localized. What strikes the eye is that Position 4, which is approximately above the postsomatic compartment, seems to be a difficult position for AP initiation, as large current magnitudes are needed to trigger the AP and the initiation site is either the soma or the postsomatic compartment.

Electrode Position			**Threshold**	**First AP**	**First AP: 1.5·Thresh.**
x [μm]	y [μm]	$d\_soma/l\_presoma$ [μm]	[μA]	Comp.	Comp.
1100	80	15/100	-12.4	13 (Presomatic)	13 (Presomatic)
1220	80	15/100	-15.17	13 (Presomatic)	15 (Presomatic)
1300	80	15/100	-19.44	13 (Presomatic)	16 (Soma)
1100	80	15/10	-12.82	13 (Presomatic)	13 (Presomatic)
1220	80	15/10	-18.57	13 (Presomatic)	14 (Presomatic)
1300	80	15/10	-39.86	17 (Postsomatic)	17 (Postsomatic)
1100	80	30/100	-12.08	13 (Presomatic)	13 (Presomatic)
1220	80	30/100	-28.79	13 (Presomatic)	15 (Presomatic)
1300	80	30/100	-28.7	13 (Presomatic)	16 (Soma)
1100	80	30/10	-29.10	1 (P0)	13 (Presomatic)
1220	80	30/10	- 35.78	1 (P0)	13 (Presomatic)
1300	80	30/10	-75.62	1 (P0)	17 (Postsomatic)

Table 9: Threshold currents and AP initiation site for threshold current and a current 1.5 times the threshold current for a pulse duration of 0.1ms and varying soma diameter and presomatic length. Higher current magnitudes are needed for shorter presomatic compartments and larger soma diameters. AP initiation site mainly focuses on sites with high ion channel density.

Figure 27 visualizes the activating function for position 4, which shows a large peak at the postsomatic region and large flanking hyperpolarizing regions. Simulations have been carried out with a current duration of $0.1ms$.

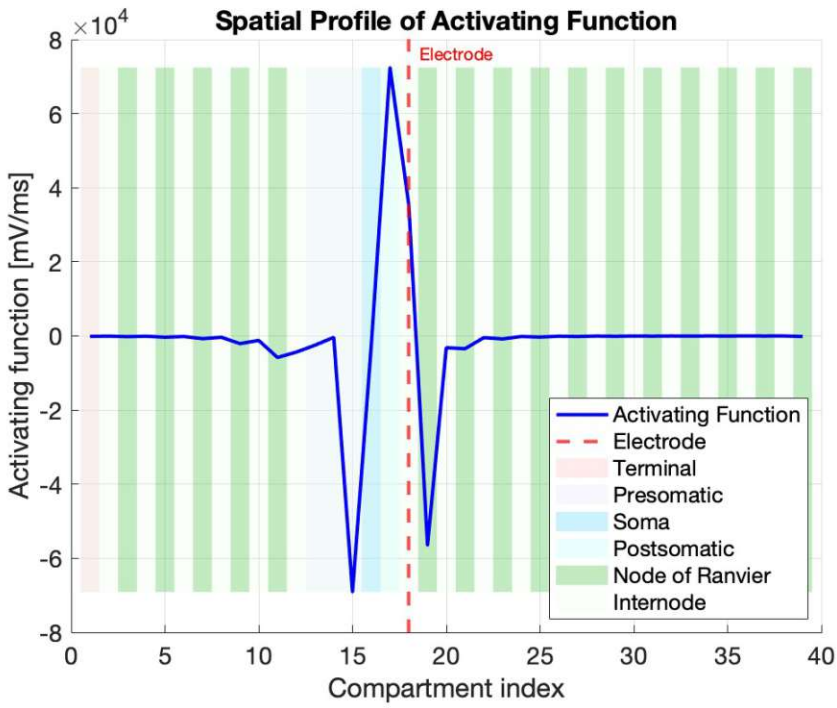

Figure 27: Activating function for electrode position x=1300, y=80. The red dashed line indicates the electrode position, the shaded regions visualize the compartments. The large depolarizing peak at the postsomatic compartment is flanked by large hyperpolarizing regions at the adjacent NoR and presomatic compartment.

In order to gain practically applicable results, the electrode distance has been set to y=300μm and the simulation has been repeated (Table 10). The results of Table 10 show that at threshold current the first compartment is favored for AP initiation, especially for smaller presomatic compartments (10μm). This effect is also visible in Table 9 for an electrode distance of 80μm, but is more pronounced for larger electrode distances. Larger currents initiate APs mainly at the presomatic region. For larger electrode distances to the fiber higher current magnitudes are needed.

Electrode Position			**Threshold**	**First AP**	**First AP: 1.5·Thresh.**
x [μm]	y [μm]	$d\_soma/l\_presoma$ [μm]	[μA]	Comp.	Comp.
1100	300	15/100	-96.09	14 (Presomatic)	13 (Presomatic)
1220	300	15/100	-100.11	13 (Presomatic)	15 (Presomatic)
1300	300	15/100	-105.13	1 (P0)	15 (Presomatic)
1100	300	15/10	-67.30	13 (Presomatic)	13 (Presomatic)
1220	300	15/10	-73.33	1 (P0)	14 (Presomatic)
1300	300	15/10	-87.93	1 (P0)	13 (Presomatic)
1100	300	30/100	-123.57	13 (Presomatic)	13 (Presomatic)
1220	300	30/100	-187.34	13 (Presomatic)	14 (Presomatic)
1300	300	30/100	-192.34	1 (P0)	15 (Presomatic)
1100	300	30/10	-158.78	1 (P0)	13 (Presomatic)
1220	300	30/10	-169.31	1 (P0)	13 (Presomatic)
1300	300	30/10	-198.68	1 (P0)	17 (Postsomatic)

Table 10: Threshold currents and AP initiation site for threshold current and a current 1.5 times the threshold current for a current duration of 0.1ms and varying soma diameter and presomatic length. Higher current magnitudes are needed for shorter presomatic compartments and larger soma diameters. AP initiation site mainly focuses on sites with high ion channel density.

4.2.4 Backpropagation

Backpropagation describes the conduction of an AP back to the dendrite. This phenomenon has been shown for intracellular stimulation 4.1.3, but it can also be observed under certain conditions in extracellular stimulation, which resemble the conditions where backpropagation occurs in intracellular stimulation. The soma diameter has been set to $30\mu m$ and the length of the presomatic compartment to $20\mu m$. The electrode has been placed at x=0μm and y=80μm. The minimum electrode current needed to trigger an AP has been determined as -3.73μA for a pulse duration of 0.5ms. In order to display the phenomenon of backpropagation which is limited to a small current range, this level of precision is not sufficient enough. Figure 28 shows that for a current of -3.7263μA, the AP is not strong enough to propagate over the soma (Subfigure 28a). Elevating the current to -3.72631 up to -3.72632μA leads to the AP propagating over the soma, but also back into the dendrite like displayed in the intracellular case (Subfigure 28b). Backpropagation does no longer occur at a current magnitude of -3.72633μA and above (Subfigure 28c).

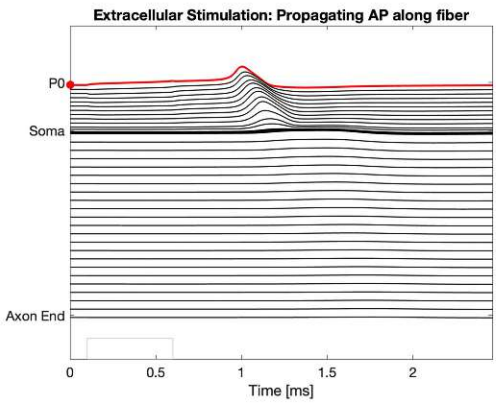

(a) -3.7263μA: AP propagation

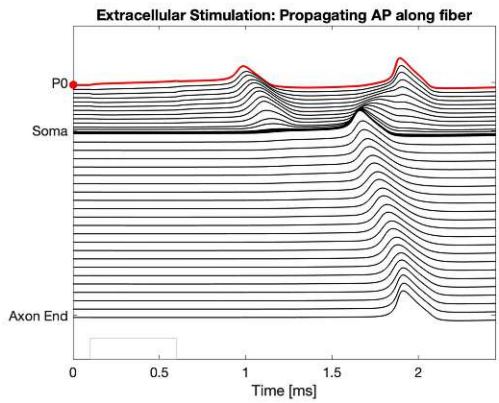

(b) -3.72631μA: AP propagation

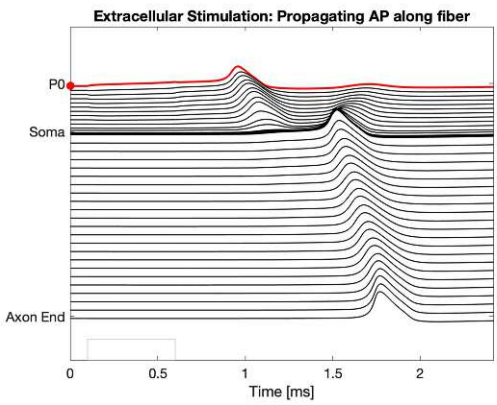

(c) -3.76233μA: AP propagation

Figure 28: Membrane voltage dynamics in the ANF with soma diameter of $30\mu m$ and presomatic compartment length of $20\mu m$: Subfigure (a) -3.7263μA with 0.5ms pulse duration: an AP is generated in the dendrite, but fails to propagate over the soma. Subfigure (b) -3.72631μA and 0.5ms pulse duration: the AP propagates over the soma and additionally back into the dendrite. Subfigure (c) shows that the pheonomenon of backpropagation does no longer occur at a current magnitude of -3.76233μA and above.

In the extracellular stimulation, a different type of backpropagation can be observed as well (Figure 29). The electrode is placed far from the soma above the axon at position x=4000μm, y=80μm. An electrode current of -15μA with a pulse duration of 0.1ms elicits an AP in the NoR below (compartment 31). The AP travels to the axonal end, but also back to the soma and the dendrite.

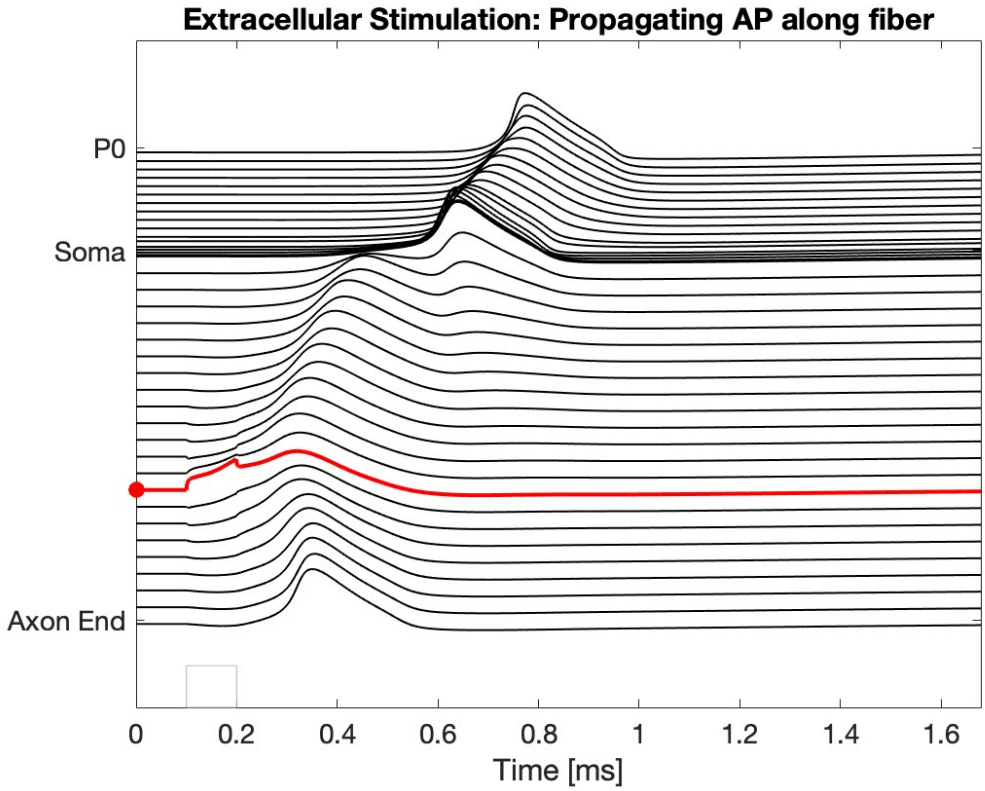

Figure 29: The electrode is placed far from the soma above an axonal NoR (x=4000μm, y=80μm). This leads to the AP being elicited in the NoR below the electrode. The AP propagates to the end of the axon, but also back to the soma and dendrite. This phenomenon is also known as backpropagation. Current magnitude of -15μA, pulse duration of 0.1ms.

This phenomenon can be observed for electrodes placed behind the soma above the axon. In contrast to the results for the other type of backpropagation, this form of backpropagation is not limited to a narrow current range, as it also occurs at larger current magnitudes (e.g. doubling the current magnitude in this example also allows backpropagation), highlighting the fact that the backpropagation shown in 4.1.3 displays a different type of backpropagation than shown here.

5 Discussion

5.1 Intracellular Stimulation

5.1.1 Cathodic and Anodic Stimulating Currents

The results of Section 4.1.1 and Section 4.2.1 showcase the big difference between extra- and intracellular stimulation concerning current polarity. While for intracellular stimulation it is advantageous to stimulate with a positive (anodic) current, the effects are reversed for extracellular stimulation, where a negative (cathodic) current is the one that leads to direct depolarization. The mechanisms on how membrane potential V_m is elevated are different for both stimulation types.

In the resting state, the inside potential V_i is more negative compared to the outside potential V_e. In intracellular stimulation, the membrane potential V_m=V_i - V_e is elevated through the inside potential V_i. A current is injected into the cell. If that current is an anodic, positive current (Figure 14a), this brings V_i and thus also V_m to more positive values. If the membrane potential V_m then reaches the threshold necessary for AP initiation, ionic channels open and the AP progresses as discussed in the introductory chapter 2.1.3. This mechanism is pretty straightforward.

Surprisingly, as shown in Figure 14b, also the injection of a negative current is able to trigger an AP. Rattay (1990) explains this phenomenon as follows: During injection of the current, hyperpolarization occurs. When the current pulse ends, the membrane potential V_m returns towards the resting potential. As a consequence of the relative slow gating variables, the voltage crosses the resting potential. The sodium current becomes the dominant part of the total ionic currents, leading to the initiation of a normal AP, if the rebound reaction is strong enough. The results also indicate that stimulation through the rebound reaction needs larger current magnitudes to trigger an AP. Whether current magnitudes of the model are in a reasonable range will be discussed in Section 5.1.6.

As shown in Figure 14, the anodic current directly initiates an AP, while the cathodic current first hyperpolarizes the membrane before triggering a membrane potential through the rebound reaction. This means that for the cathodic stimulation it takes longer to reach the threshold necessary for AP initiation. Figure 15 visualizes that for current values close to threshold, the AP is initiated approximately $1ms$ later for cathodic stimulation compared to anodic stimulation.

Stimulation with anodic currents in the extracellular case also allows the initiation of an AP, but the mechanism behind the inverse extracellular stimulation is quite different and will be discussed in Section 5.2.1. While inverse extracellular stimulation is extensively discussed in literature, the intracellular cathodic stimulation only finds little recognition.

5.1.2 Influence of Soma Size and Presomatic Length on AP Propagation

Whether an AP propagates over the soma or not is highly dependent on soma geometry and length of presomatic compartment. Figure 16 visualizes the impact of soma diameter on presomatic delay. For all presomatic lengths, the presomatic delay increases with increasing soma diameter. This is attributed to the capacitive load of the soma. The capacitance of the soma is the product of surface area and specific membrane capacitance (Equation 29). Simplifying the soma geometry to a sphere (in the code axon and dendrite junction are considered as well), the surface area is $A = d^2\pi$. This means that the capacitance increases quadratically with soma diameter. Doubling the soma diameter therefore leads to a fourfold increase in total membrane capacitance which has a significant impact on signal conduction as shown by the results and can lead in extreme cases (soma diameter of $35\mu m$, presomatic length of 10, 20 μm) to failure of signal conduction. Capacitance defines how much electrical charge can accumulate across the membrane. Higher values mean that more charge can be stored. A soma of high capacitance therefore acts like a 'charge sink'. This means that it absorbs a lot of current before the voltage changes significantly. Simply speaking, more current is needed to bring the soma to threshold. This also slows down propagation, leading to increasing presomatic delay with increasing soma diameter.

The impact of the presomatic compartment length is also clearly visible in the results of Figure 16. This can be attributed to the lower axial resistance, which is dependent on the length of the compartment (Equation 28). A shorter presomatic compartment has lower axial resistance. This means that the depolarizing current from the dendrite reaches the soma more quickly instead of building up voltage in the presomatic region. Due to the high capacitance of the soma, this current can get 'absorbed' in the soma without significantly changing membrane voltage. This may lead to the AP failing to propagate over the soma. For longer presomatic compartments, the presomatic segment is more depolarized before reaching the soma, making it easier to reach threshold value in the soma.

5.1.3 Backpropagation

Under certain conditions, APs can travel back into the dendrite like depicted by Figure 17. The results indicate that backpropagation occurs only at threshold level, but the effect vanishes for higher current magnitudes.

Tsay et al. (2002) explain this phenomenon with the properties of the voltage-gated sodium channels, especially their inactivation kinetics. If an AP is triggered at threshold, the sodium channels in the dendrite are not yet significantly inactivated. This allows the AP to propagate back into the dendrite, as enough sodium channels support depolarization and can elevate the membrane potential to threshold level. At higher currents, sodium channels are more and faster inactivated in the dendrite, reducing the number of available channels to support backpropagation. This leads to the prevention of propagation back into the dendrite, as not enough sodium channels are available to elevate the membrane potential in the dendrite to threshold level. This results in a narrow current range within which backpropagation can occur, making it highly dependent on timing.

5.1.4 Impact of Fiber Diameter

Table 2 shows that increasing fiber diameter leads to faster conduction velocities in axon and dendrite. This can be explained with the reduced axial resistance in fibers of larger diameter. As stated in 3.1.1, the axial resistance of a cylindrical conductor is calculated as follows:

$$R = \frac{\rho_i \cdot l}{A} \tag{32}$$

where R is the axial resistance, ρ_i is the intracellular resistivity, l the compartment length and A the cross-sectional area which the current passes. For a circular cross-section, A is calculated with $r^2\pi$. Doubling the diameter quadruples A, so the axial resistance R is reduced to one quarter of its original value, assuming that all other parameters remain constant. Taking a look at the parameters 3.2.1, the diameter of the axon is twice the one of the dendrite, leading to a larger cross-sectional area and consequently lower axial resistance which allows faster conduction of axial currents. This also explains why increasing the diameter of axon and dendrite leads to increased conduction velocity. It is important to keep in mind that the length of the respective compartment also factors in, as the compartment length in the axonal internodes is with $400\mu m$ significantly larger than the dendritic internodal length of $200\mu m$. These simple cable-theory assumptions apply to both myelinated and unmyelinated fibers but do not account for active membrane properties like voltage-gated ion channels that shape AP initiation and propagation.

Rattay (1990) reports a linear dependence of diameter and conduction velocity for myelinated fibers and a square root dependence on the diameter for unmyelinated fibers (Equation 1,2). The data from Table 2 supports these relationships.

Table 2 also suggests that fibers of larger diameter need higher stimulating currents to trigger an AP. This can be explained by two mechanisms. For the first, Ohm's law for a given voltage change is considered:

$$\Delta V = I \cdot R \tag{33}$$

As stated above, doubling the diameter leads to a decrease of the axial resistance R by a factor of 4. Applying this to Equation 33, this means that doubling the diameter requires four times the current to achieve the same voltage change ΔV.

The second mechanism influencing required current strength focuses on the membrane capacitance. The capacitive current can be approximated as follows:

$$I_c = C_m \cdot \frac{dV}{dt} \approx C_m \cdot \frac{\Delta V}{\Delta t} \tag{34}$$

The capacitance C_m has a linear dependence on the area of the compartment, so fibers of larger diameter require more capacitive current to change the membrane potential sufficiently. This increase in capacitive current is linear for cylindrical segments and quadratic for the spherical soma.

Taking a look at the results of Table 2, doubling the diameter $0.5\mu m$ for the dendrite and $1\mu m$ for the axon leads to a threshold current increase from $8.7pA$ to $22.51pA$. This is an increase by a factor of 2.6. If the diameter is again doubled, the current increases from $22.51pA$ to $63.08pA$, an increase by a factor of 2.8. As both effects discussed above factor in, these values are well within bounds.

5.1.5 Channel Density and Node Length

As expected, increasing ion channel density significantly reduces the threshold current needed to trigger an AP (Table 3). This principle is pretty straightforward, as higher ion channel density provides a larger inward sodium conductance, which allows more rapid depolarization and easier AP initiation. Conduction velocity is also increased, as the next NoR is activated more rapidly due to the stronger and faster depolarizing current. Interestingly, the length of the NoR has different effects on conduction velocity in the dendrite and axon. Longer nodes lead to higher dendritic conduction velocity. The dendrite in the human ANF is largely unmyelinated or less myelinated than the axon. This allows larger ionic currents to flow through these longer exposed membrane regions, leading to faster signal regeneration. The axon is more heavily myelinated and excessively long nodes may increase capacitive load and reduce conduction efficiency (Rattay, 1990).

The higher threshold currents compared to previous experiments can be attributed to the shorter stimulus duration. As discussed in Section 5.1.6, shorter pulses require larger amplitudes to reach threshold.

5.1.6 Strength-Duration Curve

The results of Table 2 for a duration of $0.5ms$ and Table 3 for a duration of $0.1ms$ show quite a difference in the magnitude of anodic threshold current. This can be explained with the differing pulse duration. The relationship between pulse duration and current strength has been researched since the 19th century with the earliest publication by Hoorweg in 1892 and is best described with chronaxie and rheobase. Rheobase refers to the minimum current needed to trigger an AP regardless of the pulse duration. Below rheobase, no current will ever be able to trigger an AP. Chronaxie reflects the responsiveness of a neuron with smaller values representing more responsive neurons and is defined as the stimulus duration required to elicit an AP using twice the rheobase current.

Chronaxie values of myelinated fibers cluster around $100\mu s$, unmyelinated fibers have much larger values in the range of 500-600μs as a consequence of the high capacity caused by the much larger amount of exposed membrane (Rattay, 1990). The chronaxie values for this simulation are with $151\mu s$-$156ms$ in a reasonable range. Validating the rheobase values with literature posed quite a challenge, as human data is due to ethical reasons scarce. Dagostin et al. (Dagostin et al., 2015) report for neurons in the auditory system of birds values around 82-317pA. Of course this cannot be directly translated to humans, but it indicates that the values for rheobase from Table 4 are with $33.97pA$-$61.8pA$ in appropriate units and approximately in the correct order of magnitude, possibly on the lower end.

Table 4 shows, that standard parameters, larger soma diameter and longer NoR have almost the same values for rheobase and chronaxie. As shown in Table 3, changing the NoR length does not have a major impact on the threshold current. A larger soma diameter alone does also not significantly impact AP initiation and propagation, unless it is in combination with a short presomatic compartment (Figure 16). What has a big impact on current magnitude, is the change of fiber diameter (Table 2), which is why the rheobase value is almost doubled for Case 2 with the larger fiber diameter. It is also important to explain why the chronaxie value is still the same as in the other cases. As

chronaxie is defined as a fixed ratio (2 times rheobase), its absolute current value does not influence it - only the timing dynamics matter.

Weiss (1901) has published an equation based on experimental data, that can be used to calculate the minimum threshold current at a given pulse duration:

$$I = I_{rheobase} \cdot (1 + \frac{t_{chronaxie}}{t}) \tag{35}$$

with $I_{rheobase}$ being the minimum current able to elicit an AP for an infinitely long duration, $t_{chronaxie}$ being the duration at which the required current is twice the rheobase current, t as the pulse duration and I being the stimulation current needed to trigger an AP. Applying the obtained values for rheobase and chronaxie for a pulse duration of $0.1ms$ yields a threshold value of $86.96pA$ with the Weiss equation (Case 1, Standard parameters). The simulated value is with $88.53pA$ in accordance with that.

5.1.7 Myelination

As stated in the introduction (Section 2.1.2), in the human ANF, the Type-I fibers are bipolar myelinated cells. The dendrite is mostly unmyelinated or only thinly myelinated, while the axon exhibits more consistent and thicker myelination. Table 5 visualizes how this affects signal propagation. Myelin electrically isolates the membrane at the internodes. This insulation prevents ionic currents (sodium, potassium) from flowing through the myelinated regions and restricts activity to the NoRs. This means that instead of depolarizing the entire membrane along the fiber, the AP only regenerates at the nodes, which is much faster compared to unmyelinated signal conduction. The depolarizing current travels passively and rapidly through insulated segments, creating the illusion that the AP jumps from node to node - a phenomenon known as saltatory conduction. Capacitive currents are minimal for myelinated compartments, because the capacitance decreases with increasing number of myelin layers. This means essentially that less capacitive current is needed to change the membrane potential, allowing faster signal conduction for more myelin layers (Rattay, 1990).

The results from Table 5 align well with these considerations. A larger number of myelin layers leads to enhanced conduction velocities in dendrite and axon. Changing only the number of layers for the axon and dendrite, the impact on presomatic delay is negligible.

For more myelin layers, the threshold currents needed to trigger an AP in Table 5 are lower. The membrane is modeled as a parallel connection of membrane resistance and membrane capacitance. Myelin increases the membrane resistance, as the insulation blocks ion flow across the membrane. In the simulation, this effect is accounted for by setting the ionic currents in the internodes to zero. As discussed above, myelin also decreases membrane capacitance. Both effects reduce the leakage of current across the membrane, reducing the load that stimulation must overcome. This means that most of the injected current travels as the axial current along the fiber instead of leaking out. That makes it easier for the depolarization to reach threshold level, as less current is lost (Rattay, 1990).

What strikes the eye is the increase in presomatic delay when the number of myelin layers for the soma is changed from 3 to 1.5. Presomatic delay increases from $130.03\mu s$ to $220.60\mu s$, which is quite a strong increase for such a small change. This highlights how

important it is in neuron modeling to account for the satellite glial cells that wrap the soma, as neglecting them can lead to an underestimation of the presomatic delay, which is a crucial factor in signal propagation.

5.2 Extracellular Stimulation

5.2.1 Cathodic and Anodic Stimulation

The results of Section 4.1.1 and Section 4.2.1 show that for extracellular stimulation with a point electrode, a cathodic electrode current is advantageous, as it directly leads to depolarization below the electrode. This is in contrast to intracellular stimulation, where anodic currents had that effect. To understand the basics behind this phenomenon, it is crucial to look at how and where current is injected. While - as discussed in 4.1.1 - in intracellular stimulation the current is directly injected into the cell, the mechanism for triggering APs with a point electrode is different. Intracellular stimulation depolarizes, by elevating the inside potential V_i. In extracellular stimulation, the electrode is placed outside the cell, so a current alters the extracellular potential V_e. Taking a look at the formula for the membrane potential $V_m = V_i$ - V_e, this leads to the following considerations. If a cathodic, negative current is applied to the extracellular space, this makes V_e more negative (Figure 21a) which depolarizes the membrane potential V_m. For an anodic, positive current, the effect is reversed, as V_e gets more positive (Figure 21b) effectively hyperpolarizing V_m.

Figure 19 and 20 indicate that these considerations hold true for compartments below or close to the point electrode, but for further compartments the results show flanking regions with the opposing effect. This can be explained by the spread of the electric field through the extracellular medium. If current is injected through a point electrode, the electric field spreads radially through the surrounding tissue (Figure 13). This creates a non-uniform, spatial distribution of extracellular potential V_e. Directly under the point electrode, the field is the strongest. With distance, the extracellular potential changes rapidly. Lateral compartments can even experience the reverse effect (depending on polarity of injected current), because the extracellular voltage gradient reverses direction on the flanks causing an opposing electric field relative to the central region. The effect of the point electrode on the ANF can be best visualized with the activating function displayed in Figure 22 (second spatial derivative of V_e), which indicates regions of depolarization and hyperpolarization along the ANF. With the help of the activating function, it is possible to analyze different geometrical situations without the need of calculating the whole multi-compartment model each time, which makes it a useful tool in neural engineering.

Additionally, it is important to keep in mind that in extracellular stimulation AP initiation does not necessarily happen directly below the electrode. The electrode in 19 was with x=100μm placed above the first dendritic internode, but the AP was still initiated at the P0 region. APs cannot be elicited at an internode due to the high level of myelination, which prevents the flow of ionic currents and - compared to the adjacent NoR - the P0 region has a higher ion channel density facilitating AP initiation.

The results for the more realistic electrode position of y=300μA underline these considerations, but also show that changing the y position of the electrode only 220μm can already have a substantial impact. The most obvious difference is the significantly higher current magnitude. This can be explained with the spatial decay of the electric field generated by the point-electrode. If the electrode is further away from the fiber, the electric field at the fiber is weaker, leading to less depolarization and the need for larger current magnitudes.

Comparing the impact on compartments in close proximity to the electrode also visualizes another important aspect. While Figure 20 shows reverse polarization effects in adjacent compartments, this cannot be seen in Figure 24. Reverse polarization still occurs in this case, but it is shifted to compartments further away from the electrode, as the electric field covers a wider area with less steep gradients. This effect is also visualized by the activating function (Figure 26). The comparison of Figure 22 and Figure 26 indicates that if the electrode is placed in close proximity to the fiber, the effects are more localized. This means that the activating function has one clear peak and almost none local maxima and minima for y=80μm. For larger electrode distances, the electric field broadens and the activating function shows lots of local maxima and minima. This is reflected in the behavior of V_e. Small electrode-fiber distance leads to steep slopes, while large distances have a less steep change of extracellular potential. This directly affects the likelihood of AP initiation. For close electrode proximity, the AP is likely initiated below or close to the electrode. Larger electrode distances make it easier for the AP to be initiated further away from the electrode.

An important aspect that should not be overlooked is the striking difference in current magnitude for intracellular and extracellular stimulation. Intracellular stimulation can elicit APs with pA currents, while for extracellular stimulation currents in the μA range are required. Intracellular current is directly injected into the cell, altering the intracellular membrane potential V_i. In contrast, extracellular stimulation influences the membrane potential by changing the extracellular potential V_e. Current has to pass through the resistive and capacitive extracellular medium, making this indirect mechanism less efficient. Higher current magnitudes are needed to sufficiently change the membrane potential V_m and trigger APs.

5.2.2 Influence of Current Strength and Electrode Position on AP Propagation

The position of the point electrode along the fiber does have an influence on AP initiation site, as indicated by the results of Table 6 and 7. The results of Table 6 visualize that for a point electrode in close proximity to the fiber (y=80μm), the APs are at threshold current for electrode positions close to the soma primarily initiated at the presomatic compartment. This is expected, as the presomatic compartment is with a default length of 100μm and enhanced HHM-dynamics a place of high ion channel density. At threshold current, AP initiation site in the dendrite is - as expected - in the closest NoR. What strikes the eye is the first AP initiation of the last electrode position (x=2800, y=80), which is with the last compartment far off from electrode position. This unexpected result can be attributed to the model structure. The ANF model terminates with a NoR, which is due to enhanced HHM-dynamics capable of initiating APs. The fiber ends at this compartment, there is no downstream segment for axial current to flow into. The reduced current leakage leads to stronger local depolarization, meaning that this boundary condition can artificially favor AP initiation at the fiber end, especially at threshold current level. To avoid this effect, one possiblilty would be to extend the model by adding more internodes beyond the terminal node.

While at threshold current, multiple compartments may be near the threshold needed for AP initiation, which promotes variablity in AP initiation site, larger electrode currents

lead to more localized AP initiation. This is due to the more pronounced extracellular potential gradient. A single compartment - typically the one closest to the peak of activating function - recieves the strongest depolarizing input. If the current is strong enough, APs are initatied at the nearest NoR and not necessarily at a region of enhanced ion channel density like the P0 region, presomatic region or postsomatic region.

The higher threshold currents necessary for AP initiation for electrode positions near the soma can be explained by several factors. The soma has due to its large diameter a large surface area, resulting in higher capacitance and lower input resistance. More current is required to generate a comparable change in membrane potential V_m. Currents at the soma also tend to disperse rather than building up locally. In contrast to that, NoR are small and have higher input resistances, making them more sensitive to the extracellular field gradients. They are easier to excite and lower threshold currents are needed.

Table 7 and 8 visualize how the electrode-fiber distance (y-value) impacts threshold current and AP initiation site. y=150μm and y=300μm lead to higher threshold currents compared to y=80μm. The electric field generated by a point electrode in a homogeneous medium decays with distance. An increasing distance between electrode and fiber leads to a decreased extracellular potential V_e. Therefore, more current is needed to elevate the membrane potential to threshold level. At larger distances from the fiber, AP initiation mainly takes place at regions of high ion channel density, as these regions are more sensitive to weak stimulation and reach threshold first. This effect is more prominent for y=150μm than y=80μm and most prominent for y=300μm. For y=300μm, the first compartment P0 is favored for AP initiation, which is expected. This compartment corresponds to the AIS, as in the healthy case synaptic input from the IHCs leads to AP initiation at this compartment. For larger currents, this effect is lost and AP initiation becomes again more localized.

5.2.3 Influence of Soma Geometry and Presomatic Length on AP Propagation

The results for the intracellular stimulation indicated that soma geometry and presomatic length have a major impact on signal conduction. While other effects like myelination, node length, channel density and fiber diameter also factor in, failure of AP propagation mainly depends on the interplay between these two geometric parameters. The results of Table 9 demonstrate that both soma diameter and length of presomatic compartment influence threshold currents and AP initiation site in the extracellular stimulation.

Shorter presomatic lengths (10μm) consistently lead to higher threshold currents compared to the default length (100μm). This can be explained by the reduction in axial resistance for shorter compartments. Shorter presomatic compartments lead to tighter coupling of soma and presomatic compartment. This makes the presomatic membrane more sensitive to the capacitive load of the soma. As a consequence, threshold currents are higher. The shorter length also reduces the available membrane area with high ion channel density, which limits AP initiation. This effect is especially prominent for a combination of a large soma (30μm) and a short presomatic compartment (10μm). Large somas have an increased membrane capacitance and lower input resistance, which makes them act like current sinks. Combined with the short presomatic compartment, this shifts AP

initiation away from the presomatic region to the first compartment, which has a length of 10μm and also enhanced HHM-dynamics, making it favorable for AP initiation. This indicates that for positions close to the soma a combination between large soma diameter and short presomatic compartment makes the soma electrically dominant and local spike initiation less likely.

Electrode Position 4 (x=1300, y=80) consistently required the highest threshold current, especially for the combination of large soma and short presomatic length. This can be explained by taking a look at the activating function at this position (Figure 27). The activating function has a strong depolarizing peak at the postsomatic compartment, but also strong adjacent hyperpolarizing flanks at the soma, presomatic compartments and adjacent NoR. These flanking regions suggest that AP initiation at these sites is less likely. The postsomatic compartment itself is not favored as AP initiation site, likely due to its short length (5μm) and its proximity to the large soma, which acts as a current sink. Especially for the combination of large soma and short presomatic compartment, this effect is visible, as a current of high magnitude (-75.62μA) is needed to elicit an AP.

At current magnitudes above threshold current, AP initiation becomes more localized. This behavior is consistent with previous observations and reflects the increasing dominance of the peak of the activating function at higher stimulation amplitudes.

These considerations also hold true for y=300μA. The main difference between Table 9 and 10 is that at threshold level, the first compartment corresponding to the AIS becomes the favored AP initiation site for larger electrode distances. This occurs, because the electric field is more spatially diffuse for larger distances to the fiber. As a result, strong depolarization of compartments with lower ion channel density is less likely and AP initiation reverts to the most excitable regions of the fiber - the AIS, which is also the physiological AP initiation site in the healthy case and the presomatic compartments.

5.2.4 Backpropagation

In extracellular stimulation, two different types of backpropagation can be observed, depending on electrode position and current magnitude. The first type (Figure 28) closely resembles the backpropagation of the intracellular case (Figure 17) and has been discussed in Chapter 5.1.3. This form of backpropagation highly depends on voltage-gated sodium channel kinetics and is therefore limited to a narrow current range at threshold level. In extracellular stimulation, this behavior can only be found if the conditions of intracellular stimulation are closely mirrored, as this form of backpropagation is highly dependent on timing.

In contrast, the second observed form of backpropagation does not depend on current magnitude, but rather electrode position. The electrode is positioned behind the soma above the axon, as shown in Figure 29. The AP is initiated at an axonal NoR and travels bidirectionally - toward the axon terminal and also back to the soma and dendrite. Timing is in this type of backpropagation not important, as the channels are in the initial state ready to support AP propagation regardelss of its direction.

6 Conclusion and Outlook

The intracellular stimulation visualizes that myelination, NoR geometry, channel density and fiber diameter mainly influence the conduction velocity, but under the tested conditions do not lead to failure of AP propagation. The major influencing factor for successful AP propagation proves to be the geometry of soma and presomatic segment. Larger somas and shorter presomatic segments increase presomatic delay and in extreme cases even inhibit AP propagation over the soma.

Extracellular stimulation introduces an additional factor: the location of AP initiation. The results indicate that the position of the electrode has an influence on needed threshold current and initiation site. Larger currents or the electrode in close proximity to the fiber lead to more localized initiation sites. The interplay between soma and presomatic compartments has an impact on threshold currents with larger currents needed for the combination of short presomatic segment and large soma. AP initation site also depends on position of the electrode, indicating an unfavorable electrode position (Position 4) above the postsomatic segment. Currents of large magnitude are needed, as the soma acts like a current sink and the adjacent NoR is in an hyperpolarized state.

To sum up, while parameters like number of myelination layers, NoR geometry, ion channel density and fiber diameter show an influence on conduction velocity and presomatic delay, under the tested conditions they show a minor impact on AP propagation over the soma. The main influence proves to be the combination of soma diameter and presomatic delay and the position of the electrode.

It is important to emphasise that the model has limitations. Due to the scarce anatomical data on human ANFs, not all parameters can be verified. As most available data is based on cats, validation of the results also poses a challenge. It is also crucial to note that this model simplifies the process of AP initiation and propagation, as it only focuses on potassium, sodium and leakage conductance. The stochasticity of AP generation in nature and neural adaption is also not considered in this model and should be incorporated in future evaluations. Moreover, the model has only been tested under simple conditions, as e.g. pulse-train responses have not been considered.

Appendix 1: MATLAB Code for Intracellular Stimulation

```
%% MODEL 1: INTRACELLULAR STIMULATION OF THE ANF

%% ENVIRONMENT SETUP
% Clear command window and workspace variables, close all figures
clc;
clear;
close all;

%% CREATE COMPARTMENT VECTOR
% Define number of myelinated internodes for dendrite and axon
n_inter_dendrite=6; % default 6
n_inter_axon=11; % default 11

% Call function compartment_vec to create cell array containing the
% labels for each compartment
labels=compartment_vec(n_inter_dendrite, n_inter_axon);

%% CREATE PARAMETER MATRIX
% Call function store_parameters with labels as input to create parameter
% matrix
% Columns: length [ m ], capacity [ F /cm^2], gNa [mS/cm^2], gK [mS/cm^2], gL [mS/cm^2], diameter [ m ]
parameter_matrix=store_parameters(labels);

%% HHM - CALCULATE MEMBRANE POTENTIAL
% Define strength, duration and polarity of stimulating current
iStim=41.52; % negative sign: cathodic current, positive sign: anodic current [pA]
dur=0.5; % [ms]

% Calculate membrane potential and corresponding time vector
[Vm, time]=HHM_natural(labels, parameter_matrix, iStim, dur);

%% FIND MINIMUM THRESHOLD CURRENTS
% Choose one compartment in the dendrite (e.g. first compartment)
% and the somatic compartment to show whether the soma barrier prevents or
% % allows AP propagation
threshold_AP(labels, parameter_matrix, 'anodic', dur, [1,16])
threshold_AP(labels, parameter_matrix, 'cathodic', dur, [1,16])

%% PLOT RESULTS
% Plot the results: 6 different plots can be shown
```

```
% Last input: number(s) of plot to display (single integer or list of integers)
% 1: AP in each compartment
% 2: Propagation of AP along fiber
% 3: AP in first compartment
% 4: Conduction velocities and presomatic delay
% 5: Latency of the AP
% 6: Strength-Duration Curve
plotting(labels, parameter_matrix, Vm, time, iStim, dur, [1,2,3,4,5,6])
```

```
function compartment_labels=compartment_vec(n_internodes_dendrite, n_internodes_axon)
%% DESCRIPTION OF FUNCTION:
%---------------------------
% FUNCTION:
% This function creates a cell array containing the labels for each
% compartment of the multi-compartment model of the ANF. It starts with an
% unmyelinated terminal region (P0), alternating myelinated internodes and
% Nodes of Ranvier (NoR) for the dendrite, 3 compartments for the presomatic
% region, 1 compartment for the soma, 1 compartment for the postsomatic
% region and alternating internodes and NoR for the axon. The
% model ends with an axonal NoR.
%
% INPUT:
% number of internodes for the dendrite and axon (myelinated)
%
% OUTPUT:
% cell array of character vectors containing the compartment lables
%---------------------------

%% NUMBER OF COMPARTMENTS IN MODEL
P0=1; % P0
n_nodes_dendrite=n_internodes_dendrite-1; % NoR dendrite
n_soma=1; % Soma
n_nodes_axon=n_internodes_axon; % NoR axon
n_presomatic=3; % Presomatic compartments
n_postsomatic=1; % Postsomatic compartments

% Total number of compartments
total_compartments=P0+n_nodes_dendrite+n_internodes_dendrite+n_presomatic+n_soma+n_postsomatic+n_nodes_axon+n_internodes_axon;
```

```
%% COMPARTMENT VECTOR
% Preallocate cell array for speed
compartment_labels=cell(1, total_compartments);
index=1; % Tracking index

% P0
compartment_labels{index}='P0';
index=index+1;

% Dendritic compartments
for i=1:n_internodes_dendrite
    % Internode
    compartment_labels{index}='Internode_Dendrite';
    index=index+1;
    % Node
    if i<n_internodes_dendrite
        compartment_labels{index}='Node_Dendrite';
        index=index+1;
    end
end

% Presomatic region
for i=1:n_presomatic
    compartment_labels{index}='Presomatic_Region';
    index=index+1;
end

% Soma
compartment_labels{index}='Soma';
index=index+1;

% Postsomatic region
compartment_labels{index}='Postsomatic_Region';
index=index+1;

% Axonal compartments
for i=1:n_internodes_axon
    % Internode
    compartment_labels{index}='Internode_Axon';
    index=index+1;
    % Node
    compartment_labels{index}='Node_Axon';
    index=index+1;
end

end
```

```
function compartment_matrix=store_parameters(compartment_labels)
```

```
%% DESCRIPTION OF FUNCTION:
%---------------------------
% FUNCTION:
% This function creates a parameter matrix containing the following
% parameters for each compartment:
% Column 1: Length
% Column 2: Capacity
% Column 3: Sodium conductance
% Column 4: Potassium conductance
% Column 5: Leak conductance
% Column 6: Diameter
%
% INPUT:
% compartment_labels cell array created by compartment_vec function
% containing the labels of each compartment
%
% OUTPUT:
% matrix with parameters for each compartment:
% Columns: length [ m ], capacity [ F /cm^2], conductance sodium [mS/cm^2],
% conductance potassium [mS/cm^2], leak conductance [mS/cm^2], diameter [ m ]
%
% REFERENCE VALUES:
% Based on literature and experiments, see Section 3.2
%---------------------------

%% DEFINE PARAMETERS
% Length of compartments
len_terminal=10; % P0 [ m ]; default 10
len_node=1.5; % NoR [ m ]; default 1.5
len_internode_dendrite=200; % Dendritic internode [ m ]; default 200
len_last_internode_dendrite=100; % Last dendritic internode [ m ]; default 100
len_presomatic=100; % Presomatic region [ m ]; default 100
len_postsomatic=5; % Postsomatic region [ m ]; default 5
len_internode_axon=400; % Axonal internode [ m ]; default 400

% Diameters of compartments
diam_dendrite=1.35; % Dendrite [ m ]; default 1.35
diam_soma=20; % Soma [ m ]; default 20
diam_axon=2.67; % Axon [ m ]; default 2.67

% Number of myelin layers
myelin_dendrite=20; % Dendrite; default 40
myelin_axon=60; % Axon; default 80
```

```
myelin_soma=1.5; % Soma (not myelinated, wrapped by glial cells - use 3 to account for that)

% Capacities of compartments
c_node=1; % NoR [ F /cm^2]; default 1
c_presomatic=1; % Presomatic region [ F /cm^2]; default 1
c_postsomatic=1; % Postsomatic region [ F /cm^2]; default 1
c_internode_dendrite=c_node/myelin_dendrite; % Dendritic internode [ F /cm^2]
c_internode_axon=c_node/myelin_axon; % Axonal internode [ F /cm^2]
c_soma=c_node/myelin_soma; % Soma [ F /cm^2]

% Conductances, scaled for special regions (P0, pre- and postsomatic region, NoR)
gNa_HHM=120; % Sodium; default 120 [mS/cm^2]
gK_HHM=36; % Potassium; default 36 [mS/cm^2]
gL_HHM=0.3; % Leak; default 0.3 [mS/cm^2]
dens_fac=10; % Scale factor for active compartments; default 10
gNa_HHM10=gNa_HHM*dens_fac; % Sodium [mS/cm^2]
gK_HHM10=gK_HHM*dens_fac; % Potassium [mS/cm^2]
gL_HHM10=gL_HHM*dens_fac; % Leak [mS/cm^2]

% Conductances for passive compartments
g_internode_dendrite=1/myelin_dendrite; % Dendritic internodes [mS/cm^2]
g_internode_axon=1/myelin_axon; % Axonal internodes [mS/cm^2]

%% INITIALIZE VECTORS
% Preallocate for speed
num_compartments=length(compartment_labels);
lcomp=zeros(num_compartments, 1);
ccomp=zeros(num_compartments, 1);
gNacomp=zeros(num_compartments, 1);
gKcomp=zeros(num_compartments, 1);
gLcomp=zeros(num_compartments, 1);
dcomp=zeros(num_compartments, 1);

%% ASSIGN VALUES BASED ON LABEL

for i=1:num_compartments
    label=compartment_labels{i};
    if contains(label, 'P0')
        lcomp(i)=len_terminal;
        dcomp(i)=diam_dendrite;
        ccomp(i)=c_node;
        gNacomp(i)=gNa_HHM10;
        gKcomp(i)=gK_HHM10;
        gLcomp(i)=gL_HHM10;
```

```
    elseif contains(label, 'Internode_Dendrite')
        lcomp(i)=len_internode_dendrite;
        dcomp(i)=diam_dendrite;
        ccomp(i)=c_internode_dendrite;
        gNacomp(i)=0;
        gKcomp(i)=0;
        gLcomp(i)=g_internode_dendrite;
    elseif contains(label, 'Node_Dendrite')
        lcomp(i)=len_node;
        dcomp(i)=diam_dendrite;
        ccomp(i)=c_node;
        gNacomp(i)=gNa_HHM10;
        gKcomp(i)=gK_HHM10;
        gLcomp(i)=gL_HHM10;
    elseif contains(label, 'Presomatic_Region')
        lcomp(i)=len_presomatic/3;
        dcomp(i)=diam_dendrite;
        ccomp(i)=c_presomatic;
        gNacomp(i)=gNa_HHM10;
        gKcomp(i)=gK_HHM10;
        gLcomp(i)=gL_HHM10;
    elseif contains(label, 'Soma')
        lcomp(i)=diam_soma;
        dcomp(i)=diam_soma;
        ccomp(i)=c_soma;
        gNacomp(i)=gNa_HHM;
        gKcomp(i)=gK_HHM;
        gLcomp(i)=gL_HHM;
    elseif contains(label, 'Postsomatic_Region')
        lcomp(i)=len_postsomatic;
        dcomp(i)=diam_axon;
        ccomp(i)=c_postsomatic;
        gNacomp(i)=gNa_HHM10;
        gKcomp(i)=gK_HHM10;
        gLcomp(i)=gL_HHM10;
    elseif contains(label, 'Internode_Axon')
        lcomp(i)=len_internode_axon;
        dcomp(i)=diam_axon;
        ccomp(i)=c_internode_axon;
        gNacomp(i)=0;
        gKcomp(i)=0;
        gLcomp(i)=g_internode_axon;
    elseif contains(label, 'Node_Axon')
        lcomp(i)=len_node;
        dcomp(i)=diam_axon;
        ccomp(i)=c_node;
        gNacomp(i)=gNa_HHM10;
        gKcomp(i)=gK_HHM10;
        gLcomp(i)=gL_HHM10;
```

```
    end

    % Change lenght of the last dendritic internode
    if i<num_compartments-1 && contains(compartment_labels{i + 1}, 'Presomatic_Region') && contains(label, 'Internode_Dendrite')
        lcomp(i)=len_last_internode_dendrite;
    end
end

%% CREATE MATRIX
% Columns: length [ m ], capacity [ F /cm^2], gNa [mS/cm^2], gK [mS/cm^2], gL [mS/cm^2], diameter [ m ]

compartment_matrix=[num2cell(lcomp), num2cell(ccomp), num2cell(gNacomp), ...
                    num2cell(gKcomp), num2cell(gLcomp), num2cell(dcomp)];

% Convert to numeric matrix
compartment_matrix=cell2mat(compartment_matrix);

end
```

```
function[Vm, time]=HHM_natural(compartments, compartment_matrix, iStim, dur)
%% DESCRIPTION OF FUNCTION:
%---------------------------
% FUNCTION:
% This function simulates the membrane potential (Vm) over time in a
% multi-compartment ANF using the HHM. The stimulating current is injected
% into the first compartment and can - if strong enough - elicit an AP that
% propagates along the fiber.
%
% INPUT:
% compartments: Label for each compartment
% compartment_matrix: Parameters for each compartment:
% length [ m ], capacity [ F /cm^2], conductance sodium [mS/cm^2],
% conductance potassium [mS/cm^2], leak conductance [mS/cm^2], diameter [ m ]
% iStim: Strength of stimulus current [pA]
% dur: Duration of stimulus [ms]
%
% OUTPUT:
% Vm: Membrane potential matrix [mV]
```

```
% time: Time vector corresponding to simulation steps [ms]
%
% Code adapted from:
% F. Bucek, "Simulation of auditory nerve fiber excitation with
% prostheses implanted in the scala vestibuli"
% Diploma thesis, Technische Universit t Wien. reposiTUm, 2023.
%---------------------------

%% TEMPORAL PARAMETERS
start=0; % Start of simulation [ms]
del=5; % Delay of stimulus [ms]
stop=15; % Duration of simulation [ms]
dt=0.001; % Step size [ms]
pretime=0.1; % Time before stimulus [ms]
t=start:dt:stop; % Time vector [ms]
time=start:dt:(stop-del+pretime); % Time vector excluding
    stimulus delay, with pre-stimulus buffer [ms]

%% HHM PARAMETERS
% Set parameters for the HHM

% Voltage
Vrest=-65; % Rest [mV]
V_Na=115; % Sodium [mV]
V_K=-12; % Potassium [mV]
V_L=10.6; % Leakage [mV]

% Reversal potentials
E_Na=V_Na+Vrest; % Sodium [mV]
E_K=V_K+Vrest; % Potassium [mV]
E_L=V_L+Vrest; % Leak [mV]

% Temperature
T=29; % [ C ]
k=3^(0.1*T-0.63); % Temperature coefficient: 6.3  C  k=1; 29  C
    k = 12.11 % []

%% MODEL PARAMETERS
rhoi=50; % axial resistivity [Ohm*cm]

%% DEFINE MODEL PARAMETERS
% Extract parameters of parameter matrix
lcomp=double(compartment_matrix(:, 1)); % Lengths
ccomp=double(compartment_matrix(:, 2));% Capacitances
gNacomp=double(compartment_matrix(:, 3)); % Sodium conductance
gKcomp=double(compartment_matrix(:, 4)); % Potassium conductance
gLcomp=double(compartment_matrix(:, 5)); % Leak conductance
dcomp=double(compartment_matrix(:, 6)); % Diameters

```

```
% Number of compartments
ncomp=length(lcomp);

%% CALCULATE AXIAL RESISTANCES
R=(rhoi*lcomp*1e-4)./(pi*((dcomp/2)*1e-4).^2); % [Ohm]
R_kOhm=R*1e-3; % [kOhm]

% Special case: Soma
% Find indices of soma, presomatic compartments and postsomatic compartment
soma_index=find(strcmp(compartments, 'Soma'), 1); % Soma
presomatic_second=soma_index-2; % Middle presomatic region
presomatic_third=soma_index-1; % Presomatic region directly before soma
postsomatic=soma_index+1; % Postsomatic region

% Extract diameters for soma, dendrite and axon
d_soma=dcomp(soma_index); % Soma
d_dendrite=dcomp(soma_index-4); % Diameter dendrite
d_axon=dcomp(soma_index+2); % Diameter axon

% Calculate the resistance for the two exceptions:
% Presomatic compartment to soma
R_presoma_soma=1e-03*rhoi/(pi*d_dendrite*1e-04)*log(...
    (d_soma/2+sqrt((d_soma/2)^2-(d_dendrite/2)^2))/((d_soma/2-sqrt((d_soma/2)^2-(d_dendrite/2)^2)))); % [kOhm]
% Soma to postsomatic compartment
R_soma_postsoma=1e-03*rhoi/(pi*d_axon*1e-04)*log(...
    (d_soma/2+sqrt((d_soma/2)^2-(d_axon/2)^2))/((d_soma/2-sqrt((d_soma/2)^2-(d_axon/2)^2)))); % [kOhm]

% Calculate the half resistance
R_half=R_kOhm./2; % [kOhm]
R_presoma_soma=R_presoma_soma/2; % [kOhm]
R_soma_postsoma=R_soma_postsoma/2; % [kOhm]
R_half(soma_index,1) = NaN; % Set soma resistance to NaN - will be bridged later so it does not affect calculations

%% CALCULATE SURFACE AREA
% Cylindric compartments
A=2*(dcomp/2).*pi.*lcomp*1e-08; % [cm^2]

% Calculate the surface area for the soma:
% Height of the spherical cap removed by the dendrite attachment
capHeight_dendrite=(d_soma/2-sqrt((d_soma/2)^2-(d_dendrite/2)^2)); % [ m ]
% Height of the spherical cap removed by the axonal attachment
capHeight_axon=(d_soma/2-sqrt((d_soma/2)^2-(d_axon/2)^2)); % [ m ]
```

```
% Calculate the surface area of the soma and subtract the parts cut out by
% attachments from dendrite and axon
A_soma=(4*(d_soma/2)^2.*pi-((d_soma*pi*capHeight_dendrite)+(d_soma*pi*capHeight_axon)))*1e-08; % [cm^2]
A(soma_index,1)=A_soma;

%% CALCULATE MEMBRANE CAPACITANCE
C=ccomp.*A; % [ F ]

%% CAPACITANCE-CONDUCTANCE MATRIX
% Shift R_half to get resistance of previous and next compartment
R_half_previous=circshift(R_half, 1); % Shift right by 1, resistance of previous compartment (i-1)
R_half_next=circshift(R_half, -1); % Shift left by 1, resistance of next compartment (i+1)

% Construct matrix:
% Own compartment's contribution
AC_diagonal=[1+(dt/C(1))*(1/(R_half(1)+R_half(2)));
    ones(ncomp-2, 1)+(dt./C(2:end-1)).*( ...
        1./(R_half_previous(2:end-1)+R_half(2:end-1)) + ...
        1./(R_half_next(2:end-1)+R_half(2:end-1)) );
    1+(dt/C(end))*(1/(R_half(end-1)+R_half(end)))]; % []
% Contribution from previous compartment
AC_lower=-(dt./C(2:end)).*(1./(circshift(R_half(2:end), 1)+R_half(2:end))); % []
% Contribution from next compartment
AC_upper=-(dt./C(1:end-1)).*(1./(circshift(R_half(1:end-1), -1)+R_half(1:end-1))); % []

% Special treatment for soma and start and end region - bridge soma
% resistance value (set to NaN, replace with previous/next compartment)
AC_diagonal(presomatic_third)=1+(dt./C(presomatic_third)).*(1./(R_half(presomatic_second)+R_half(presomatic_third))+1./(R_presoma_soma+R_half(presomatic_third)));
AC_diagonal(soma_index)=1+(dt./C(soma_index)).*(1./(R_half(presomatic_third)+R_presoma_soma)+1./(R_soma_postsoma+R_half(postsomatic)));
AC_diagonal(postsomatic)=1+(dt./C(postsomatic)).*(1./(R_half(postsomatic)+R_soma_postsoma)+1./(R_half(postsomatic+1)+R_half(postsomatic)));
AC_lower(presomatic_third)=-(dt./C(soma_index)).*(1./(R_presoma_soma+R_half(presomatic_third)));
AC_lower(soma_index)=-(dt./C(postsomatic)).*(1./(R_soma_postsoma+R_half(postsomatic)));
```

```
AC_upper(presomatic_third)=-(dt./C(presomatic_third)).*(1./(R_presoma_soma+R_half(presomatic_third)));
AC_upper(soma_index)=-(dt./C(soma_index)).*(1./(R_soma_postsoma+R_half(postsomatic)));
AC_lower(1)=-(dt./C(2)).*(1./(R_half(2)+R_half(1)));
AC_upper(ncomp-1)=-(dt./C(ncomp-1)).*(1./(R_half(ncomp-1)+R_half(ncomp)));

% Build capacitance-conductance matrix from main, upper and lower diagonal
AC_matrix = diag(AC_diagonal,0) + diag(AC_lower,-1) + diag(AC_upper,1); % []

%% SOLVE HHM-MODEL
% Initialize the membrane potential and set it to the resting potential
V=zeros(ncomp, length(t));
V(:,1)=Vrest; % [mV]

% Membrane Potential without initializing phase
Vm=zeros(ncomp, length(time)); % [mV]

% Initialize gating variables for all compartments over time
m=zeros(ncomp, length(time));
n=zeros(ncomp, length(time));
h=zeros(ncomp, length(time));

% Calculate rate constants at initial potential (resting potential)
% m
alpha_M=solve_alpham(V(1), Vrest); % [1/ms]
beta_M=solve_betam(V(1), Vrest); % [1/ms]
% n
alpha_N=solve_alphan(V(1), Vrest); % [1/ms]
beta_N=solve_betan(V(1), Vrest); % [1/ms]
% h
alpha_H=solve_alphah(V(1), Vrest); % [1/ms]
beta_H=solve_betah(V(1), Vrest); % [1/ms]

% Calculate initial value for gating variables
m(:,1)=alpha_M/(alpha_M+beta_M);
n(:,1)=alpha_N/(alpha_N+beta_N);
h(:,1)=alpha_H/(alpha_H+beta_H);

% Additional BE Voltage: improve stability
inclVadd=1; % 1: Yes, 0: No
Vadd=0.001; % Auxiliary voltage [mV]
s=1; % index for post-stimulus recording

```

```
% Loop through time vector
for i=1:length(t)

    % Apply stimulating current in specified time window
    if i>del/dt && i<=(del+dur)/dt
        istim=zeros(ncomp, 1);
        iStim_uA=iStim*1e-6; % [ A ], convert from pA
        istim(1)=iStim_uA/A(1); % Inject into first compartment [ A /cm^2]
    else
        istim=zeros(ncomp, 1); % No stimulation outside of window
    end

    % Calculate ionic conductances
    gNa(:,i)=gNacomp.*m(:,i).^3.*h(:,i); % [mS/cm^2]
    gK(:,i)=gKcomp.*n(:,i).^4; % [mS/cm^2]
    gL(:,i)=gLcomp; % [mS/cm^2]

    % Use conductances to calculate ionic currents
    I_Na(:,i)=gNa(:,i).*(V(:,i)-E_Na); % [ A /cm^2]
    I_K(:,i)=gK(:,i).*(V(:,i)-E_K); % [ A /cm^2]
    I_L(:,i)=gL(:,i).*(V(:,i)-E_L); % [ A /cm^2]
    % Total ionic current is the sum of sodium, potassium and leak
    % current
    Iion(:,i)=I_Na(:,i)+I_K(:,i)+I_L(:,i); % [ A /cm^2]

    % To improve stability of BE add auxiliary currents (if Vadd is set to
    % 1)
    if inclVadd==1
        I_Naadd(:,i)=gNacomp.*m(:,i).^3.*h(:,i).*(V(:,i)+Vadd-E_Na); % [ A /cm^2]
        I_Kadd(:,i)=gKcomp.*n(:,i).^4.*(V(:,i)+Vadd-E_K); % [ A /cm^2]
        I_Ladd(:,i)=gLcomp.*(V(:,i)+Vadd-E_L); % [ A /cm^2]
        Iionadd(:,i)=(I_Naadd(:,i)-I_Na(:,i)+I_Kadd(:,i)-I_K(:,i)+I_Ladd(:,i)-I_L(:,i))/Vadd; % [( A  /cm^2)/mV]
    else
        Iionadd(:,i)=0;
    end

    % Calculate right side of equation
    b=V(:,i)+(dt./ccomp).*(-Iion(:,i)+Iionadd(:,i).*V(:,i)+istim); %[mV]

    % Add auxiliary currents to other side of equation (main diagonal)
    AC_matrix(1:1+length(AC_matrix):end)=AC_diagonal+Iionadd(:,i)
```

```
        .*(dt ./ ccomp);

    % Solve for V+1 using b and the AC_matrix
    V(:,i+1)=sparse(AC_matrix)\b; % [mV]

    % Get values for time window of interest
    if i>((del/dt)-(pretime/dt))
        Vm(:,s)=V(:,i);
        s=s+1;
    end

    % Get next m, n, h values
    m(:,i+1)=(m(:,i)+k*dt*solve_alpham(V(:,i+1), Vrest))./(1+k*dt
       *(solve_alpham(V(:,i+1), Vrest)+solve_betam(V(:,i+1), Vrest
       )));
    n(:,i+1)=(n(:,i)+k*dt*solve_alphan(V(:,i+1), Vrest))./(1+k*dt
       *(solve_alphan(V(:,i+1), Vrest)+solve_betan(V(:,i+1), Vrest
       )));
    h(:,i+1)=(h(:,i)+k*dt*solve_alphah(V(:,i+1), Vrest))./(1+k*dt
       *(solve_alphah(V(:,i+1), Vrest)+solve_betah(V(:,i+1), Vrest
       )));
end

V(:,end)=[]; % necessary so t and V have same length, not further
    used just for completeness

%% GATING FUNCTIONS
% Sodium channel activation gate: opening rate
function alpha_m=solve_alpham(V, Vrest)
    alpha_m=(2.5-0.1*(V-Vrest))./(exp(2.5-0.1*(V-Vrest))-1);
end

% Sodium channel activation gate: closing rate
function beta_m=solve_betam(V, Vrest)
    beta_m=4*exp((Vrest-V)/18);
end

% Potassium channel activation gate: opening rate
function alpha_n=solve_alphan(V, Vrest)
    alpha_n=(1-0.1*(V-Vrest))./(10*(exp(1-0.1*(V-Vrest))-1));
end

% Potassium channel activation gate: closing rate
function beta_n=solve_betan(V, Vrest)
    beta_n=0.125*exp((Vrest-V)/80);
end

% Sodium channel inactivation gate: opening rate
function alpha_h=solve_alphah(V, Vrest)
```

```
    alpha_h=0.07*exp((Vrest-V)/20);
end

% Sodium channel inactivation gate: closing rate
function beta_h=solve_betah(V, Vrest)
    beta_h=1./(exp(3-0.1*(V-Vrest))+1);
end

end
```

```
function [] = threshold_AP(compartments, compartment_matrix, current_type, dur, test_compartments)
%% DESCRIPTION OF FUNCTION:
%---------------------------
% FUNCTION:
% Calculates the minimum threshold current to initiate an AP using a binary search algorithm,
% for either cathodic or anodic stimulation. The threshold is computed separately for each specified
% compartment, allowing analysis of whether the stimulation elicits an AP
% only in the dendrite or one that propagates across the soma.
%
% INPUT:
% compartments: Labels of compartments
% compartment_matrix: length [ m ], capacity [ F /cm^2], conductance sodium [mS/cm^2],
% conductance potassium [mS/cm^2], leak conductance [mS/cm^2], diameter [ m ]
% current_type: 'anodic' (positive current) or 'cathodic' (negative current)
% dur: Duration of stimulus [ms]
% test_compartments: Array of compartment indices to test
%
% OUTPUT:
% Threshold current for each tested compartment [pA]
%---------------------------

%% SET PARAMETERS
threshold_level=-20;  % Voltage at which AP is considered [mV]
tol=0.01; % Desired level of precision [pA]
max_current=500; % Set current search range, adjust if code does not work properly

%% DETERMINE CURRENT SIGN
switch lower(current_type)
    case 'anodic'
        sign_factor=1;
    case 'cathodic'
```

```
        sign_factor=-1;
    otherwise
        error('Invalid current type. Use "anodic" or "cathodic".');
end

% print header based on current type
fprintf('--- %s Threshold Currents Per Compartment ---\n', upper(current_type));

%% BINARY SEARCH FOR THRESHOLD CURRENT

% Loop through test_compartments
for i=1:length(test_compartments)
    comp_idx=test_compartments(i);
    low=0; % lower bound: lowest current to test
    high=max_current; % upper bound: highest current to test

    % Binary search until bounds converge to tolerance level
    while (high-low)>tol
        mid=(low+high)/2;
        % Calculate midpoint current and apply sign factor
        stim_current=sign_factor*mid;
        % Get membrane voltage using HHM function with the midpoint current
        [Vm, ~]=HHM_natural(compartments, compartment_matrix, stim_current, dur);
        % Find maximum membrane voltage
        max_voltage=max(Vm(comp_idx, :));

         % Update bounds based on whether AP threshold is reached or not
        if max_voltage>threshold_level
            high=mid; % AP triggered, lower upper bound
        else
            low=mid; % No AP, raise lower bound
        end
    end

    % Threshold is approximately the upper bound after convergence
    threshold=high*sign_factor;
    fprintf('Compartment %-3d | Threshold Current: %7.2f pA\n', comp_idx, threshold);

end

end
```

```
function [] = plotting(compartments, compartment_matrix, Vm, time, iStim, dur, plot_number)
%% DESCRIPTION OF FUNCTION:
%---------------------------
% FUNCTION:
% This function visualizes the results of the simulation based on specified plot
% number
%
% INPUT:
% compartments: Labels of compartments
% compartment_matrix: length [ m ], capacity [ F /cm^2], conductance sodium [mS/cm^2],
% conductance potassium [mS/cm^2], leak conductance [mS/cm^2], diameter [ m ]
% Vm: Membrane potential over time [mV]
% time: Corresponding time vector to membrane potential [ms]
% iStim: Stimulating current [pA]
% dur: Duration of stimulation [ms]
% plot number: Integer or list of integers specifying which plot is desired
% (1 = AP in each compartment, 2 = Propagation of AP along fiber, 3 = AP in first compartment,
% 4 = Conduction velocities and presomatic delay, 5 = Latency of AP, 6 = Strength-Duration-Curve)
%
% OUTPUT:
% Specified figure
%---------------------------

%% SET PARAMETERS
pretime=0.1; % Time before stimulus [ms]
ncomp=size(compartment_matrix, 1); % Number of compartments

%% DEFINE SCALE AND OFFSET FOR PLOTTING
% Scale
scale=7; % amplify voltage values for visualization
lcomp=double(compartment_matrix(:, 1));
lfiber=sum(lcomp)-Vm(end, end)*scale; % adjusted fiber length for plotting

% Compute offset for each compartment
% Preallocate for speed
offset=zeros(ncomp, 1);
for i=1:ncomp
    if i==1
        offset(i)=lfiber-lcomp(i)/2; % special case for first compartment
    else
```

```
        offset(i)=offset(i-1)-((lcomp(i-1)+lcomp(i))/2); % stack voltage traces vertically
    end
end

%% ENSURE PLOT NUMBER IS VALID
if isempty(plot_number)
    plot_number=1:4;
elseif ~isvector(plot_number)
    error('plot_number must be a scalar or a vector.');
end

%% DEFINE BUFFER FOR LIMITS BASED ON PEAK OCCURANCE
% Find maximum voltage across all compartments and times
[~, idx_max]=max(Vm(:));
[~, max_col]=ind2sub(size(Vm), idx_max);
% get time where this maximum voltage occurs
t_peak=time(max_col);
% Define a buffer window
buffer=1.5;

%% PLOT 1: AP IN EACH COMPARTMENT
if any(plot_number==1)
    figure;
    hold on; box off;
    plot(time, Vm); % plot all compartments
    % Plot rectangle to indicate stimulating current
    rectangle('Position', [pretime, -120, dur, 10], 'EdgeColor', [0.7 0.7 0.7]);
    grid on;
    % Set limit based on maximum voltage occurance
    xlim([0, min(t_peak + buffer, time(end))]);
    xlabel('Time [ms]');
    ylabel('Amplitude [mV]');
    title('Intracellular Stimulation: AP of each compartment');
    set(gca, 'FontSize', 14);
end

%% PLOT 2: PROPAGATING AP ALONG FIBER
if any(plot_number==2)
    figure;
    plot(time, scale*Vm+offset, 'k'); % plot Vm with an offset to visualize AP propagation
    label_shift=0.07*(max(offset)-min(offset));
    soma_index=strcmp(compartments, 'Soma');
    % Create ticklabels to indicate location on fiber
    yticks([offset(end)-label_shift, offset(soma_index)-label_shift, offset(1)-label_shift]);
    yticklabels({'Axon End', 'Soma', 'P0'});
```

```
    set(gca, 'TickLabelInterpreter', 'tex');
    xlim([0, min(t_peak+buffer, time(end))]); % Set limit based on maximum peak occurance
    rectangle('Position', [pretime, -1000, dur, 500], 'EdgeColor', [0.7 0.7 0.7]); % Indicate stimulating current
    xlabel('Time [ms]');
    title('Intracellular Stimulation: Propagating AP along fiber');
    set(gca, 'FontSize', 14);
end

%% PLOT 3: AP PROPAGATION IN FIRST COMPARTMENT
    if any(plot_number==3)
        figure;
        hold on; box off; grid on;
        set(gca, 'TickDir', 'out');
        % Plot AP only in first compartment
        p1=plot(time, Vm(1, :), 'b', 'LineWidth', 1, 'DisplayName', 'Membrane Voltage');
        ylabel('Amplitude [mV]', 'FontSize', 16);
        ylim([-120, 40]);
        % Construct a function for iStim
        stim_start=pretime;
        stim_end=pretime+0.5;
        stim_strength=10;
        Istim=zeros(size(time));
        Istim(time>=stim_start & time<stim_end)=stim_strength;
        p2 = plot(time, Istim-120, 'r', 'LineWidth', 0.5, 'DisplayName', 'Stimulating Current');
        xlim([0, 3.5]);
        xlabel('Time [ms]', 'FontSize', 16);
        % Make title specific to current input
        if iStim>0
            stim_type='Anodic';
        else
            stim_type='Cathodic';
        end
        title(['Intracellular Stimulation: AP in first compartment (' stim_type ')'], 'FontSize', 18);
        set(gca, 'FontSize', 14);
        legend([p1, p2], 'Location', 'northeast', 'FontSize', 14);
    end

%% PLOT 4: CONDUCTION VELOCITY AND PRESOMATIC DELAY
    if any(plot_number == 4)
        presomatic_delay(compartments, Vm, scale, offset, time); % Call seperate function for plotting

```

```
    end

%% PLOT 5: LATENCY
if any(plot_number == 5)
    % Calculate index after pretime (=stimulus onset)
    after_pretime = find(time >= pretime, 1);
    threshold = -20;
    % Search for first time where threshold is reached (will be compartment
    % P0)
    first_AP = find(Vm(1, after_pretime:end) > threshold, 1);

    % Check if AP is reached - if yes plot red dot on first threshold reach
    if ~isempty(first_AP)
        figure;
        plot(time, scale*Vm + offset, 'k'); % Vm for all compartments
        hold on;
        stim_start = scale * Vm(1, after_pretime) + offset;
        h1=plot(pretime(1), stim_start(1), 'bo', 'MarkerSize', 8, 'LineWidth', 2);  % Blue circle for stimulus onset
        AP_time = time(after_pretime + first_AP);
        AP_voltage = scale * Vm(1, after_pretime + first_AP) + offset;
        % Calculate latency
        latency = AP_time - pretime;
        fprintf('AP latency = %.3f ms\n', latency); % Display latency
        h2=plot(AP_time(1), AP_voltage(1), 'rx', 'MarkerSize', 10, 'LineWidth', 2); % Red circle for first threshold reach
        label_shift=0.07*(max(offset)-min(offset));
        soma_index=strcmp(compartments, 'Soma');
        % Create ticklabels to indicate location on fiber
        yticks([offset(end)-label_shift, offset(soma_index)-label_shift, offset(1)-label_shift]);
        yticklabels({'Axon End', 'Soma', 'P0'});
        set(gca, 'TickLabelInterpreter', 'tex');
        xlim([0, min(t_peak+buffer, time(end))]); % Set limit based on maximum peak occurance
        rectangle('Position', [pretime, -1000, dur, 500], 'EdgeColor', [0.7 0.7 0.7]); % Indicate stimulating current
        xlabel('Time [ms]');
        title('Intracellular Stimulation: Latency of AP');
        set(gca, 'FontSize', 14);
        h3 = plot(nan, nan, 'k'); % Dummy handle for Vm trace
        legend([h3 h1 h2], {'Vm (with offset)', 'Stimulus onset (
```

```
            P0)', 'First AP (P0)'}, 'Location', 'southeast');
    else
        fprintf('No AP detected.\n');
    end
end

%% PLOT 6: STRENGTH-DURATION CURVE
if any(plot_number == 6)
    % pulse duration
    t = [0.02, 0.05, 0.1, 0.2, 0.5, 1.0, 2.0];

    % threshold currents [pA]
    I_1 = [412.67, 162.81, 88.53, 51.76, 34.76, 33.97, 33.97];
    I_2=[724.79, 286.8, 156.62, 92.32, 63.07, 61.8, 61.8];
    I_3=[428.65, 169.4, 92.34, 54.18, 36.55, 35.74, 35.74];
    I_4=[412.9, 162.9, 88.58, 51.79, 34.79, 33.99, 33.99];

    % plot
    figure;
    plot(t, I_1, '-o', 'MarkerSize', 6, 'LineWidth', 1.5, '
       DisplayName', 'Case 1')
    hold on;
    plot(t, I_2, '-o', 'MarkerSize', 6, 'LineWidth', 1.5, '
       DisplayName', 'Case 2')
    hold on;
    plot(t, I_3, '-o', 'MarkerSize', 6, 'LineWidth', 1.5, '
       DisplayName', 'Case 3')
    hold on;
    plot(t, I_4, '-o', 'MarkerSize', 6, 'LineWidth', 1.5, '
       DisplayName', 'Case 4')
    hold on


    % axis, title, legend
    grid on;
    xlabel('Stimulus Duration [ms]', 'FontSize', 14);
    ylabel('Stimulus Current [pA]', 'FontSize', 14);
    title('Intracellular Stimulation: Strength-Duration Curves',
       'FontSize', 14);
    legend('Location', 'northeast');
    set(gca, 'FontSize', 14)
    hold off;

end

end
```

```
function []=presomatic_delay(compartments, Vm, scale, offset, time)

%% GET INDICES OF COMPARTMENTS
node_first=find(strcmp(compartments, 'Terminal')); % P0 region
node_den_indices=find(strcmp(compartments, 'Node_Dendrite')); % NoR dendrite
node_soma=find(strcmp(compartments, 'Soma')); % Soma
node_axon_indices=find(strcmp(compartments, 'Node_Axon')); % NoR axon
dendrite_indices=[node_first, node_den_indices]; % Combine for dendrite
axon_indices=[node_soma, node_axon_indices]; % Combine for axon
indices=[dendrite_indices, node_soma, node_axon_indices]; % Get all indices of active compartments

%% FIND THRESHOLD CROSSING INDICES
threshold=-40; % Threshold level at which AP is considered [mV], default -40
threshold_times=NaN(length(indices), 1); % Preallocate crossing times
for i=1:length(indices)
    Vm_node=Vm(indices(i), :);
    crossing_indices=find(Vm_node>threshold, 1);
    if ~isempty(crossing_indices)
        threshold_times(i)=time(crossing_indices);
    end
end

%% PLOTTING

figure;
hold on;
grid on;

% loop through crossing indices and set a marker based on location (blue:
% dendrite, red: axon)
for i=1:length(indices)
    y_marker=scale*threshold+offset(indices(i));
    if ismember(indices(i), node_den_indices)
        plot(threshold_times(i), y_marker, 'bx', 'MarkerSize', 5);
    elseif ismember(indices(i), node_axon_indices)
        plot(threshold_times(i), y_marker, 'rx', 'MarkerSize', 5);
    end
end

```

```
%% FIT LINE THROUGH CROSSINGS TO DETERMINE VELOCITY

% Dendrite
dendrite_offsets=offset(dendrite_indices);
dendrite_times=threshold_times(1:length(dendrite_indices));
dendrite_fit_coeffs=polyfit(dendrite_offsets, dendrite_times, 1);
fine_offsets=linspace(min(dendrite_offsets), max(dendrite_offsets
    ), 100);
fitted_times=polyval(dendrite_fit_coeffs, fine_offsets);
fitted_y=scale*threshold+fine_offsets;
plot(fitted_times, fitted_y, 'b-', 'LineWidth', 1);

% Interpolation for estimated soma value, calculation real soma
    value
soma_offset=offset(node_soma);
soma_time_interp=polyval(dendrite_fit_coeffs, soma_offset);
real_soma_time=threshold_times(length(dendrite_indices) + 1);
plot(soma_time_interp, scale*threshold+soma_offset, 'bo', '
    MarkerSize', 5);
plot(real_soma_time, scale*threshold+soma_offset, 'ro', '
    MarkerSize', 5);

% Axon
[~, loc]=ismember(axon_indices, indices);
axon_times=threshold_times(loc);
axon_offsets=offset(axon_indices);
[axon_offsets_sorted, sort_idx]=sort(axon_offsets);
axon_times_sorted=axon_times(sort_idx);
axon_fit_coeffs=polyfit(axon_offsets_sorted, axon_times_sorted,
    1);
fine_axon_offsets=linspace(min(axon_offsets_sorted), max(
    axon_offsets_sorted), 100);
axon_fitted_times=polyval(axon_fit_coeffs, fine_axon_offsets);
axon_fitted_y=scale*threshold+fine_axon_offsets;
plot(axon_fitted_times, axon_fitted_y, 'r-', 'LineWidth', 1);

%% PLOT Vm
plot(time, scale*Vm+offset, 'k', 'LineWidth', 0.5);
label_shift=0.07*(max(offset)-min(offset));
yticks([offset(end)-label_shift, offset(node_soma)-label_shift,
    offset(1)-label_shift]);
yticklabels({'Axon End', 'Soma', 'P0'});
xlabel('Time [ms]');
ylabel('Fiber Location');
title('Presomatic delay and propagation velocities');
set(gca, 'FontSize', 14);

% Legend
h1=plot(NaN, NaN, 'bx', 'MarkerSize', 5);
```

```
h2=plot(NaN, NaN, 'bo', 'MarkerSize', 5);
h3=plot(NaN, NaN, 'ro', 'MarkerSize', 5);
h4=plot(NaN, NaN, 'rx', 'MarkerSize', 5);
h5=plot(NaN, NaN, 'b-', 'LineWidth', 1);
h6=plot(NaN, NaN, 'r-', 'LineWidth', 1);
h7=plot(NaN, NaN, 'k', 'LineWidth', 0.5);
legend([h1 h2 h3 h4 h5 h6 h7], ...
       {'Dendrite Threshold','Soma (Interpolated)', 'Soma (Actual)', ...
        'Axon Threshold', 'Dendrite Linear Fit', 'Axon Linear Fit', 'Vm Propagation'}, ...
       'Location', 'southeast');

% Calculate buffer value to find perfect time window for visualization
[~, idx_max]=max(Vm(:));
[~, max_col]=ind2sub(size(Vm), idx_max);
t_peak=time(max_col); % find time of maximum peak
buffer=2;
xlim([0, min(t_peak+buffer, time(end))]);

%% PRESOMATIC DELAY AND CONDUCTION VELOCITIES
% Presomatic delay
presomatic_delay=(real_soma_time-soma_time_interp) * 1e3; % [ s ]
fprintf('Presomatic Delay: %.2f  s \n', presomatic_delay);

% Dendritic and axonal velocity
slope_dendrite=dendrite_fit_coeffs(1);
slope_axon=axon_fit_coeffs(1);
velocity_dendrite_mm=-1/slope_dendrite/1000;
velocity_axon_mm=-1/slope_axon/1000;
fprintf('Velocity along dendrite: %.2f mm/ms\n', velocity_dendrite_mm);
fprintf('Velocity along axon: %.2f mm/ms\n', velocity_axon_mm);

%% ANNOTATE PLOT
% Use box to display velocities and presomatic delays
velocity_text=sprintf(['\\bfVelocity and Soma Delay Info\\rm\n' ...
                       'Dendritic Velocity: %.2f mm/ms\n' ...
                       'Axonal Velocity: %.2f mm/ms\n' ...
                       'Pre-somatic Delay: %.2f  s '], ...
                       velocity_dendrite_mm, velocity_axon_mm, presomatic_delay);

annotation('textbox', [0.18, 0.2, 0.3, 0.07], 'String', velocity_text, ...
           'FitBoxToText', 'on', 'BackgroundColor', 'white', ...
           'EdgeColor', 'black', 'FontSize', 10);
```

```
330
331 end
```

Appendix 2: MATLAB Code for Extracellular Stimulation

```
%% MODEL 2: EXTRACELLULAR STIMULATION OF THE ANF
%% ENVIRONMENT SETUP
% clear command window and workspace variables, close all figures
clc;
clear;
close all;

%% CREATE COMPARTMENT VECTOR
% Define number of internodes for dendrite and axon
n_inter_dendrite=6; % default 6
n_inter_axon=11; % default 11

% Call function compartment_vec to create a cell array containing the
% labels for each compartment
labels=compartment_vec(n_inter_dendrite, n_inter_axon);

%% CREATE PARAMETER MATRIX
% Call function store_parameters with labels as input to create parameter
% matrix
% Columns: length [ m ], capacity [ F /cm^2], gNa [mS/cm^2], gK [mS/cm^2], gL [mS/cm^2], diameter [ m ]
parameter_matrix=store_parameters(labels);

%% HHM - CALCULATE MEMBRANE POTENTIAL
% Define strength, duration and polarity of stimulating current
I_el=-10.84; % Negative sign: cathodic current, positive sign: anodic current [ A ]
dur=0.1; % [ms]
elecX=800; % Electrode position along fiber
elecY=80; % Electrode position away from fiber

% Calculate membrane potential and corresponding time vector
[Vm, time, actfct, Ve, t, closest_idx]=HHM_extracellular(labels, parameter_matrix, I_el, dur, elecX, elecY);

%% GET THRESHOLD CURRENT TO TRIGGER AP AT SOMA
minimum_threshold(labels, parameter_matrix, 'cathodic', dur, elecX, elecY)
minimum_threshold(labels, parameter_matrix, 'anodic', dur, elecX, elecY)
%% PLOT RESULTS
% a function is used to plot the results, 4 different plots can be shown
```

```
% specified by the last input element either a list of numbers or single
% number can be passed
% 1: AP in each compartment
% 2: AP in selected compartments
% 3: Propagating AP along the fiber with electrode position
% 4: Activating function
% 5: Extracellular Potential
plotting_ex(labels, parameter_matrix, Vm, time, dur, closest_idx, actfct, Ve, [1,2,3,4,5])
```

```
function[Vm, time, actfct, Ve, t, closest_idx]=HHM_extracellular(compartments, compartment_matrix, Iel, dur, elecX, elecY)
%% DESCRIPTION OF FUNCTION:
%---------------------------
% FUNCTION:
% This function simulates the membrane potential (Vm) over time in a
% multi-compartment ANF using the HHM. The stimulating current is applied
% to a point electrode and can - if strong enough - elicit an AP in one of
% the compartments that propagates along the fiber
%
% INPUT:
% compartments: contains label for each compartment
% compartment_matrix: contains parameters length [ m ], capacity [ F /cm^2], conductance sodium [mS/cm^2],
% conductance potassium [mS/cm^2], leak conductance [mS/cm^2], diameter [ m ]
% Iel: Strength of electrode current [ A ]
% dur: Duration of stimulus [ms]
% elecX: Position of the electrode along fiber
% elecY: Position of the electrode away from fiber
%
% OUTPUT:
% Vm: Membrane potential matrix [mV]
% time: Time vector corresponding to simulation steps [ms]
% actfct: Activating function [mV/ms]
% Ve: Extracellular potential [mV]
% t: Time vector for whole simulation [ms]
% closest_index: Index of closest compartment to electrode []
%
% Code adapted from:
% F. Bucek, "Simulation of auditory nerve fiber excitation with
% prostheses implanted in the scala vestibuli"
% Diploma thesis, Technische Universit t Wien. reposiTUm, 2023.
%---------------------------

```

```
%% TEMPORAL PARAMETERS
start=0; % start of simulation [ms]
del=5; % delay of stimulus [ms]
stop=15; % duration of simulation [ms]
dt=0.001; % time steps [ms]
pretime=0.1; % time before stimulus [ms]
t=start:dt:stop; % time vector [ms]
time=start:dt:(stop-del+pretime); % time without initializing
    phase

%% HHM PARAMETERS
% Set parameters for the HHM

% Voltage
Vrest=-65; % Rest [mV]
V_Na=115; % Sodium [mV]
V_K=-12; % Potassium [mV]
V_L=10.6; % Leakage [mV]

% Reversal potentials
E_Na=V_Na+Vrest; % Sodium [mV]
E_K=V_K+Vrest; % Potassium [mV]
E_L=V_L+Vrest; % Leak [mV]

% Temperature
T=29; % [ C ]
k=3^(0.1*T-0.63); % Temperature coefficient: 6.3  C  k=1; 29  C
    k = 12.11 % []

%% MODEL PARAMETERS
rhoi=50; % axial resistivity [Ohm*cm]
rhoe=300; % extracellular resistivity [Ohm*cm]

%% DEFINE MODEL PARAMETERS
% Extract parameters of parameter matrix
lcomp=double(compartment_matrix(:, 1)); % Lengths
ccomp=double(compartment_matrix(:, 2));% Capacitances
gNacomp=double(compartment_matrix(:, 3)); % Sodium conductance
gKcomp=double(compartment_matrix(:, 4)); % Potassium conductance
gLcomp=double(compartment_matrix(:, 5)); % Leak conductance
dcomp=double(compartment_matrix(:, 6)); % Diameters

% Number of compartments
ncomp=length(lcomp);

%% CALCULATE AXIAL RESISTANCES
R=(rhoi*lcomp*1e-4)./(pi*((dcomp/2)*1e-4).^2); % [Ohm]
R_kOhm=R*1e-3; % [kOhm]

```

```
% Special case: Soma
% Find indices of soma, presomatic compartments and postsomatic compartment
soma_index=find(strcmp(compartments, 'Soma'), 1); % Soma
presomatic_second=soma_index-2; % Middle presomatic region
presomatic_third=soma_index-1; % Presomatic region directly before soma
postsomatic=soma_index+1; % Postsomatic region

% Extract diameters for soma, dendrite and axon
d_soma=dcomp(soma_index); % Soma
d_dendrite=dcomp(soma_index-4); % Diameter dendrite
d_axon=dcomp(soma_index+2); % Diameter axon

% Calculate the resistance for the two exceptions:
% Presomatic compartment to soma
R_presoma_soma=1e-03*rhoi/(pi*d_dendrite*1e-04)*log(...
    (d_soma/2+sqrt((d_soma/2)^2-(d_dendrite/2)^2))/((d_soma/2-sqrt((d_soma/2)^2-(d_dendrite/2)^2)))); % [kOhm]
% Soma to postsomatic compartment
R_soma_postsoma=1e-03*rhoi/(pi*d_axon*1e-04)*log(...
    (d_soma/2+sqrt((d_soma/2)^2-(d_axon/2)^2))/((d_soma/2-sqrt((d_soma/2)^2-(d_axon/2)^2)))); % [kOhm]

% Calculate the half resistance
R_half=R_kOhm./2; % [kOhm]
R_presoma_soma=R_presoma_soma/2; % [kOhm]
R_soma_postsoma=R_soma_postsoma/2; % [kOhm]
R_half(soma_index,1) = NaN; % Set soma resistance to NaN - will be bridged later so it does not affect calculations


%% CALCULATE SURFACE AREA
% Cylindric compartments
A=2*(dcomp/2).*pi.*lcomp*1e-08; % [cm^2]

% Calculate the surface area for the soma:
% Height of the spherical cap removed by the dendrite attachment
capHeight_dendrite=(d_soma/2-sqrt((d_soma/2)^2-(d_dendrite/2)^2)); % [ m ]
% Height of the spherical cap removed by the axonal attachment
capHeight_axon=(d_soma/2-sqrt((d_soma/2)^2-(d_axon/2)^2)); % [ m ]

% Calculate the surface area of the soma and subtract the parts cut out by
% attachments from dendrite and axon
A_soma=(4*(d_soma/2)^2.*pi-((d_soma*pi*capHeight_dendrite)+(d_soma*pi*capHeight_axon)))*1e-08; % [cm^2]
```

```
A(soma_index,1)=A_soma;

%% CALCULATE MEMBRANE CAPACITANCE
C=ccomp.*A; % [ F ]

%% CONDUCTANCE MATRIX
% Shift R_half to get resistance of previous and next compartment
R_half_previous=circshift(R_half, 1); % Shift right by 1, resistance of previous compartment (i-1)
R_half_next=circshift(R_half, -1); % Shift left by 1, resistance of next compartment (i+1)

% Construct matrix:
% Own compartment's contribution
G_diagonal=[-1/(R_half(1)+R_half(2));
             -1./(R_half_previous(2:end-1)+R_half(2:end-1))-1./(R_half_next(2:end-1)+R_half(2:end-1));
             -1/(R_half(end-1)+R_half(end))]; % [mS]
% Contribution from previous compartment
G_lower=1./(circshift(R_half(2:end),1)+R_half(2:end)); % [mS]
% Contribution from next compartment
G_upper=1./(circshift(R_half(1:end-1),-1)+R_half(1:end-1)); % [mS]

% Special treatment for soma and start and end region - bridge soma
% resistance value (set to NaN, replace with previous/next compartment)
G_diagonal(presomatic_third)=-1./(R_half(presomatic_third)+R_half(presomatic_second))-1./(R_half(presomatic_third)+R_presoma_soma);
G_diagonal(soma_index)=-1./(R_half(presomatic_third)+R_presoma_soma)-1./(R_half(postsomatic)+R_soma_postsoma);
G_diagonal(postsomatic)=-1./(R_half(postsomatic)+R_soma_postsoma)-1./(R_half(postsomatic+1)+R_half(postsomatic));
G_lower(presomatic_third)=1./(R_presoma_soma+R_half(presomatic_third));
G_lower(soma_index)=1./(R_soma_postsoma+R_half(postsomatic));
G_upper(presomatic_third)=1./(R_half(presomatic_third)+R_presoma_soma);
G_upper(soma_index)=1./(R_half(postsomatic)+R_soma_postsoma);
G_lower(1)=1./(R_half(1)+R_half(2));
G_upper(ncomp-1)=1./(R_half(ncomp-1)+R_half(ncomp));

% Build conductance matrix from main, upper and lower diagonal
G_matrix=diag(G_diagonal, 0)+diag(G_lower, -1)+diag(G_upper, 1); % [mS]

%% CAPACITANCE-CONDUCTANCE MATRIX
```

```
% Construct matrix:
% Own compartment's contribution
AC_diagonal=[1+(dt/C(1))*(1/(R_half(1)+R_half(2)));
    ones(ncomp-2, 1)+(dt./C(2:end-1)).*( ...
        1./(R_half_previous(2:end-1)+R_half(2:end-1)) + ...
        1./(R_half_next(2:end-1)+R_half(2:end-1)) );
    1+(dt/C(end))*(1/(R_half(end-1)+R_half(end)))]; % []
% Contribution from previous compartment
AC_lower=-(dt./C(2:end)).*(1./(circshift(R_half(2:end), 1)+R_half(2:end))); % []
% Contribution from next compartment
AC_upper=-(dt./C(1:end-1)).*(1./(circshift(R_half(1:end-1), -1)+R_half(1:end-1))); % []

% Special treatment for soma and start and end region - bridge soma
% resistance value (set to NaN, replace with previous/next compartment)
AC_diagonal(presomatic_third)=1+(dt./C(presomatic_third)).*(1./(R_half(presomatic_second)+R_half(presomatic_third))+1./(R_presoma_soma+R_half(presomatic_third)));
AC_diagonal(soma_index)=1+(dt./C(soma_index)).*(1./(R_half(presomatic_third)+R_presoma_soma)+1./(R_soma_postsoma+R_half(postsomatic)));
AC_diagonal(postsomatic)=1+(dt./C(postsomatic)).*(1./(R_half(postsomatic)+R_soma_postsoma)+1./(R_half(postsomatic+1)+R_half(postsomatic)));
AC_lower(presomatic_third)=-(dt./C(soma_index)).*(1./(R_presoma_soma+R_half(presomatic_third)));
AC_lower(soma_index)=-(dt./C(postsomatic)).*(1./(R_soma_postsoma+R_half(postsomatic)));
AC_upper(presomatic_third)=-(dt./C(presomatic_third)).*(1./(R_presoma_soma+R_half(presomatic_third)));
AC_upper(soma_index)=-(dt./C(soma_index)).*(1./(R_soma_postsoma+R_half(postsomatic)));
AC_lower(1)=-(dt./C(2)).*(1./(R_half(2)+R_half(1)));
AC_upper(ncomp-1)=-(dt./C(ncomp-1)).*(1./(R_half(ncomp-1)+R_half(ncomp)));

% Build capacitance-conductance matrix from main, upper and lower diagonal
AC_matrix=diag(AC_diagonal,0)+diag(AC_lower,-1)+diag(AC_upper,1);

%% ELECTRODE INFLUENCE & ACTIVATING FUNCTION
% Compute compartment centers [ m ]
centers_x=cumsum(lcomp)-lcomp/2; % x-coordinates
centers_y=zeros(size(centers_x)); % y-coordinates (fiber along x-axis)

```

```
% Vector storing electrode distance to each compartment
diff=[centers_x(:)-elecX, centers_y(:)-elecY];
dist=sqrt(diff(:,1).^2+diff(:,2).^2); % [ m ]
% Find index of compartment closest to electrode
[~, closest_idx]=min(abs(centers_x-elecX));
dist_cm=dist*1e-4; % convert to cm

% Extracellular potential (mV)
Ve=1e-3*(rhoe*Iel)./(4*pi*dist_cm);

% Stimulus current density
iStim=(G_matrix*Ve./A);  % [ A /cm^2]

% Activating function
actfct=G_matrix*Ve./C; % [mV/ms]

%% SOLVE HHM-MODEL
% Initialize the membrane potential and set it to the resting
    potential
V=zeros(ncomp, length(t));
V(:,1)=Vrest; % [mV]

% Membrane Potential without initializing phase
Vm=zeros(ncomp, length(time)); % [mV]

% Initialize gating variables for all compartments over time
m=zeros(ncomp, length(time));
n=zeros(ncomp, length(time));
h=zeros(ncomp, length(time));

% Calculate rate constants at initial potential (resting
    potential)
% m
alpha_M=solve_alpham(V(1), Vrest); % [1/ms]
beta_M=solve_betam(V(1), Vrest); % [1/ms]
% n
alpha_N=solve_alphan(V(1), Vrest); % [1/ms]
beta_N=solve_betan(V(1), Vrest); % [1/ms]
% h
alpha_H=solve_alphah(V(1), Vrest); % [1/ms]
beta_H=solve_betah(V(1), Vrest); % [1/ms]

% Calculate initial value for gating variables
m(:,1)=alpha_M/(alpha_M+beta_M);
n(:,1)=alpha_N/(alpha_N+beta_N);
h(:,1)=alpha_H/(alpha_H+beta_H);

% Additional BE Voltage: improve stability
inclVadd=1; % 1: Yes, 0: No
```

```
Vadd=0.001; % Auxiliary voltage [mV]
s=1; % index for post-stimulus recording

% Loop through time vector
for i = 1:length(t)
    % Align stimulus with time
    if i > del / dt && i <= (del + dur) / dt
        % Use the precomputed iStim vector, which has one value per compartment
        istim = iStim; % vector: ncomp x 1
    else
        istim = zeros(ncomp, 1);
    end

    % Calculate ionic conductances
    gNa(:,i)=gNacomp.*m(:,i).^3.*h(:,i); % [mS/cm^2]
    gK(:,i)=gKcomp.*n(:,i).^4; % [mS/cm^2]
    gL(:,i)=gLcomp; % [mS/cm^2]

    % Use conductances to calculate ionic currents
    I_Na(:,i)=gNa(:,i).*(V(:,i)-E_Na); % [ A /cm^2]
    I_K(:,i)=gK(:,i).*(V(:,i)-E_K); % [ A /cm^2]
    I_L(:,i)=gL(:,i).*(V(:,i)-E_L); % [ A /cm^2]
    % Total ionic current is the sum of sodium, potassium and leak
    % current
    Iion(:,i)=I_Na(:,i)+I_K(:,i)+I_L(:,i); % [ A /cm^2]

    % To improve stability of BE add auxiliary currents (if Vadd is set to
    % 1)
    if inclVadd==1
        I_Naadd(:,i)=gNacomp.*m(:,i).^3.*h(:,i).*(V(:,i)+Vadd-E_Na); % [ A /cm^2]
        I_Kadd(:,i)=gKcomp.*n(:,i).^4.*(V(:,i)+Vadd-E_K); % [ A /cm^2]
        I_Ladd(:,i)=gLcomp.*(V(:,i)+Vadd-E_L); % [ A /cm^2]
        Iionadd(:,i)=(I_Naadd(:,i)-I_Na(:,i)+I_Kadd(:,i)-I_K(:,i)+I_Ladd(:,i)-I_L(:,i))/Vadd; % [( A  /cm^2)/mV]
    else
        Iionadd(:,i)=0;
    end

    % Calculate right side of equation
    b=V(:,i)+(dt./ccomp).*(-Iion(:,i)+Iionadd(:,i).*V(:,i)+istim); %[mV]

    % Add auxiliary currents to other side of equation (main diagonal)
```

```
    AC_matrix(1:1+length(AC_matrix):end)=AC_diagonal+Iionadd(:,i)
        .*(dt ./ ccomp);

    % Solve for V+1 using b and the AC_matrix
    V(:,i+1)=sparse(AC_matrix)\b; % [mV]

    % Get values for time window of interest
    if i>((del/dt)-(pretime/dt))
        Vm(:,s)=V(:,i);
        s=s+1;
    end

    % Get next m, n, h values
    m(:,i+1)=(m(:,i)+k*dt*solve_alpham(V(:,i+1), Vrest))./(1+k*dt
        *(solve_alpham(V(:,i+1), Vrest)+solve_betam(V(:,i+1), Vrest
        )));
    n(:,i+1)=(n(:,i)+k*dt*solve_alphan(V(:,i+1), Vrest))./(1+k*dt
        *(solve_alphan(V(:,i+1), Vrest)+solve_betan(V(:,i+1), Vrest
        )));
    h(:,i+1)=(h(:,i)+k*dt*solve_alphah(V(:,i+1), Vrest))./(1+k*dt
        *(solve_alphah(V(:,i+1), Vrest)+solve_betah(V(:,i+1), Vrest
        )));
end

V(:,end)=[]; % necessary so t and V have same length, not further
    used just for completeness

%% GATING FUNCTIONS
% Sodium channel activation gate: opening rate
function alpha_m=solve_alpham(V, Vrest)
    alpha_m=(2.5-0.1*(V-Vrest))./(exp(2.5-0.1*(V-Vrest))-1);
end

% Sodium channel activation gate: closing rate
function beta_m=solve_betam(V, Vrest)
    beta_m=4*exp((Vrest-V)/18);
end

% Potassium channel activation gate: opening rate
function alpha_n=solve_alphan(V, Vrest)
    alpha_n=(1-0.1*(V-Vrest))./(10*(exp(1-0.1*(V-Vrest))-1));
end

% Potassium channel activation gate: closing rate
function beta_n=solve_betan(V, Vrest)
    beta_n=0.125*exp((Vrest-V)/80);
end

% Sodium channel inactivation gate: opening rate
```

```
function alpha_h=solve_alphah(V, Vrest)
    alpha_h=0.07*exp((Vrest-V)/20);
end

% Sodium channel inactivation gate: closing rate
function beta_h=solve_betah(V, Vrest)
    beta_h=1./(exp(3-0.1*(V-Vrest))+1);
end

end
```

```
function []=minimum_threshold(compartments, compartment_matrix,
    current_type, dur, elecX, elecY)
%% DESCRIPTION OF FUNCTION:
%---------------------------
% FUNCTION:
% This function calculates the threshold current needed to elicit
    an AP at
% the somatic compartment using a binary search algorithm
%
% INPUT:
% compartments: contains label for each compartment
% compartment_matrix: contains parameters length [ m ], capacity
    [ F /cm^2], conductance sodium [mS/cm^2],
% conductance potassium [mS/cm^2], leak conductance [mS/cm^2],
    diameter [ m ]
% current type: 'cathodic' or 'anodic'
% dur: stimulus duration [ms]
% elecX: electrode position along fiber [ m ]
% elecY: electrode position away from fiber [ m ]
%
% OUTPUT:
% minimum threshold current needed for AP to propagate over soma
%---------------------------

%% SET PARAMETERS
threshold_level=-20; %  % Voltage at which AP is considered [mV]
tol=0.01; % Desired level of precision [pA]
max_current=60; % Set current search range, adjust if code does
    not work properly

% Find soma index
soma_index=find(strcmpi(compartments, 'Soma'), 1);
if isempty(soma_index)
    error('Soma compartment not found.');
end

%% DETERMINE CURRENT SIGN
switch lower(current_type)
```

```
    case 'anodic'
        sign_factor=1;
    case 'cathodic'
        sign_factor=-1;
    otherwise
        error('Invalid current_type: use ''anodic'' or ''cathodic''.');
end

% Print header based on current type
fprintf('--- %s Threshold Currents Per Compartment ---\n', upper(current_type));

%% BINARY SEARCH
low=0; % lower bound: lowest current to test
high=max_current; % upper bound: highest current to test

% Binary search until bounds converge to tolerance level
while (high-low)>tol
    % Calculate midpoint current and apply sign factor
    mid=(low+high)/2;
    stim_current=sign_factor*mid;
    % Run extracellular simulation
    [Vm, ~, ~, ~]=HHM_extracellular(compartments, compartment_matrix, stim_current, dur, elecX, elecY);
    % Find maximum membrane voltage
    max_voltage=max(Vm(soma_index, :));

    % Update bounds based on whether AP threshold is reached or not
    if max_voltage>threshold_level
        high=mid;  % Found AP, try smaller current
    else
        low=mid;   % No AP, increase current magnitude
    end
end

% Threshold is approximately the upper bound after convergence
threshold=round(sign_factor*high, 2);
fprintf('Soma threshold current: %.2f  A \n', threshold);


end
```

```
function [] = plotting_ex(compartments, compartment_matrix, Vm, time, dur, closest_idx, actfct, Ve, plot_number)
%% DESCRIPTION OF FUNCTION:
%---------------------------
% FUNCTION:
```

```
% This function visualizes the results of the simulation based on specified
% plot number
%
% INPUT:
% compartments: Labels of compartments
% compartment_matrix: Contains parameters length [ m ], capacity [ F /cm^2], conductance sodium [mS/cm^2],
% conductance potassium [mS/cm^2], leak conductance [mS/cm^2], diameter [ m ]
% Vm: Membrane potential over time [mV]
% time: Corresponding time vector to membrane potential [ms]
% dur: Duration of stimulation [ms]
% closest_idx: Index of closest compartment to electrode position
% actfct: Activating function [mV/ms]
% Ve: Extracellular potential [mV]
% plot number: integer or list of integers specifying which plot is desired
% (1=AP in each compartment, 2=AP in selected compartments, 3=AP propagation along fiber,
% 4=Activating function, 5=Extracellular Potential)
%
% OUTPUT:
% Specified figure
%---------------------------

%% SET PARAMETERS
pretime=0.1; % [ms]
ncomp=size(compartment_matrix, 1); % number of compartments

%% DEFINE SCALE AND OFFSET FOR PLOTTING
scale=7;
lcomp=double(compartment_matrix(:, 1));
lfibre=sum(lcomp)-Vm(end, end)*scale;

% Compute offset for each compartment
offset=zeros(ncomp, 1);
for i=1:ncomp
    if i==1
        offset(i)=lfibre-lcomp(i)/2;
    else
        offset(i)=offset(i-1)-((lcomp(i-1)+lcomp(i))/2);
    end
end

%% ENSURE PLOT NUMBER IS VALID
if isempty(plot_number)
    plot_number=1:4;
elseif ~isvector(plot_number)
```

```
    error('plot_number must be a scalar or a vector.');
end

%% DEFINE BUFFER FOR PLOTTING LIMITS BASED ON PEAK OCCURANCE
[~, idx_max]=max(Vm(:));
[~, max_col]=ind2sub(size(Vm), idx_max);
t_peak=time(max_col);
buffer=1.5;

%% PLOT 1: AP IN EACH COMPARTMENT
if any(plot_number==1)
    figure;
    hold on; box off;
    plot(time, Vm); % plot all compartments
    rectangle('Position', [pretime, -120, dur, 10], 'EdgeColor',
       [0.7 0.7 0.7]); % Stimulating current
    grid on;
    xlim([0, min(t_peak + buffer, time(end))]);
    xlabel('Time [ms]');
    ylabel('Amplitude [mV]');
    title('Extracellular Stimulation: AP of each compartment');
    set(gca, 'FontSize', 14);
end
%% PLOT 2: AP IN SELECTED COMPARTMENTS
if any(plot_number==2)
    compartmentsToPlot=[7,8,9,10,11];
    figure;
    hold on;
    box off;
    % Plot only selected compartments
    for i=1:length(compartmentsToPlot)
        compIdx=compartmentsToPlot(i);
        plot(time, Vm(compIdx, :), 'DisplayName', ['Comp '
           num2str(compIdx)]);
    end
    rectangle('Position', [pretime, -120, dur, 10], 'EdgeColor',
       [0.7 0.7 0.7]); % Stimulating current
    grid on;
    xlabel('Time [ms]');
    ylabel('Amplitude [mV]');
    title('Extracellular Stimulation: AP in selected Compartments
       ');
    set(gca, 'FontSize', 14);
    % Estimate latest AP time across shown compartments
    Vm_selected=Vm(compartmentsToPlot, :);
    [~, idx_max]=max(Vm_selected(:));
    [~, max_col]=ind2sub(size(Vm_selected), idx_max);
    t_peak=time(max_col);
    % Extend x-axis a bit beyond peak
```

```
    buffer=1.5;
    xlim([0, min(t_peak + buffer, time(end))]);
    legend();
end
%% PLOT 3: AP PROPAGATION
if any(plot_number==3)
  figure;
  threshold_level=-20; % Threshold at which AP is considered [mV]
  first_cross_time=inf;
  first_cross_comp=NaN;
  % Find compartment where first AP is initiated
  for c=1:size(Vm, 1)
    Vc=Vm(c, :);
    crossing_idxs=find(Vc(1:end-1)<threshold_level & Vc(2:end)>=
       threshold_level);
    if ~isempty(crossing_idxs)
      t_cross=time(crossing_idxs(1));
      if t_cross<first_cross_time
        first_cross_time=t_cross;
        first_cross_comp=c;
      end
    end
  end
  % Handle case where no AP is triggered and threshold is never
     reached and
  % display results
  if isnan(first_cross_comp)
    fprintf('No compartment ever crossed % g mV      no AP
       detected.\n', threshold_level);
  else
    fprintf('First threshold crossing in compartment: %d (%s)\n',
        first_cross_comp, compartments{first_cross_comp});
  end

  % Plot Vm - different color for compartment with first AP
  for c = 1:size(Vm, 1)
    if ~isnan(first_cross_comp) && c == first_cross_comp
      plot(time, scale*Vm(c, :)+offset(c), 'r', 'LineWidth', 2);
    else
      plot(time, scale*Vm(c, :)+offset(c), 'k', 'LineWidth', 1);
    end
    hold on;
  end

  % Axis label
  soma_index=find(strcmp(compartments, 'Soma'), 1);
  label_shift=0.07*(max(offset) - min(offset));
  yticks([offset(end)-label_shift, offset(soma_index)-label_shift
     , offset(1)-label_shift ]);
```

```
138   yticklabels({'Axon End','Soma','P0'});
139   set(gca, 'TickLabelInterpreter','tex');
140   xlim([0, min(first_cross_time+buffer, time(end))]);
141
142   % Plot Stimulation window of current and position of electrode
143   rectangle('Position',[pretime,-1000,dur,500],'EdgeColor',[.7 .7
        .7]);
144   t_marker=0;
145   [~,tIdx]=min(abs(time-t_marker));
146   y_marker=scale*Vm(closest_idx,tIdx) + offset(closest_idx);
147   plot(t_marker, y_marker, 'ro','MarkerSize',8,'MarkerFaceColor',
        'r',...
148         'DisplayName',sprintf('ElectrodeComp %d',closest_idx));
149   xlabel('Time [ms]');
150   title('Extracellular Stimulation: Propagating AP along fiber');
151   set(gca,'FontSize',14);
152   hold off;
153 end
154
155 %% PLOT 4: ACTIVATING FUNCTION
156 if any(plot_number==4)
157     figure;
158     hold on;
159     % Specify compartments
160     node_indices = [3, 5, 7, 9, 11, 19, 21, 23, 25, 27, 29, 31,
          33, 35, 37, 39]; % NoR
161     soma_index=find(strcmp(compartments, 'Soma'), 1);
162     axon_length=length(actfct);
163     all_indices=1:axon_length;
164     internode_indices=setdiff(all_indices, node_indices); %
          Internodes
165     presomatic=soma_index-[3, 2, 1]; % Presomatic compartments
166     post_idx=soma_index+1; % Postsomatic compartment
167     % Find minimum and maximum value of the activating function
168     ymin = min(actfct);
169     ymax = max(actfct);
170     % Build patches to indicate function of each compartment
171     % Patch for P0 Region
172     h_terminal=patch([0.5 1.5 1.5 0.5], [ymin ymin ymax ymax],
          ...
173                         [1 0.8 0.8], 'FaceAlpha', 0.4, 'EdgeColor',
                              'none');
174     % Patch for presomatic Regions
175     h_presomatic=patch([presomatic(1)-0.5, presomatic(end)+0.5,
          presomatic(end)+0.5, presomatic(1)-0.5], ...
176                           [ymin ymin ymax ymax], [0.9 0.9 1], '
                                FaceAlpha', 0.3, 'EdgeColor', 'none');
177     % Patch for soma
178     h_soma=patch([soma_index-0.5, soma_index+0.5, soma_index+0.5,
```

```
        soma_index-0.5], ...
                    [ymin ymin ymax ymax], [0.6 0.9 1], 'FaceAlpha', 0.5, 'EdgeColor', 'none');
    % Patch for postsomatic region
    h_post=patch([post_idx-0.5, post_idx+0.5, post_idx+0.5, post_idx-0.5], ...
                    [ymin ymin ymax ymax], [0.8 1 1], 'FaceAlpha', 0.4, 'EdgeColor', 'none');
    % Patch for NoRs
    h_node=patch([node_indices(1)-0.5, node_indices(1)+0.5, node_indices(1)+0.5, node_indices(1)-0.5], ...
                    [ymin ymin ymax ymax], [0.4 0.8 0.4], 'FaceAlpha', 0.4, 'EdgeColor', 'none');
    for i=2:length(node_indices)
        idx=node_indices(i);
        patch([idx-0.5, idx+0.5, idx+0.5, idx-0.5], ...
              [ymin ymin ymax ymax], [0.4 0.8 0.4], 'FaceAlpha', 0.4, 'EdgeColor', 'none');
    end
    % Patch for internodes
    first_internode=internode_indices(1);
    h_internode=patch([first_internode-0.5, first_internode+0.5, first_internode+0.5, first_internode-0.5], ...
                        [ymin ymin ymax ymax], [0.9 1 0.9], 'FaceAlpha', 0.2, 'EdgeColor', 'none');
    for i=2:length(internode_indices)
        idx=internode_indices(i);
        patch([idx-0.5, idx+0.5, idx+0.5, idx-0.5], ...
              [ymin ymin ymax ymax], [0.9 1 0.9], 'FaceAlpha', 0.2, 'EdgeColor', 'none');
    end

    % Plot activating function and electrode position
    h_func=plot(1:axon_length, actfct, 'b', 'LineWidth', 2);
    h_elec=xline(closest_idx, 'r--', 'LineWidth', 2, 'Label', 'Electrode', 'LabelOrientation', 'horizontal');
    xlabel('Compartment index');
    ylabel('Activating function [mV/ms]');
    title('Spatial Profile of Activating Function');
    grid on;
    set(gca, 'FontSize', 14);
    legend([h_func, h_elec, h_terminal, h_presomatic, h_soma, h_post, h_node, h_internode], ...
            {'Activating Function', 'Electrode', 'Terminal', 'Presomatic', 'Soma', 'Postsomatic', ...
             'Node of Ranvier', 'Internode'}, 'Location', 'southeast');
    hold off;
end
```

```
%% PLOT 5: EXTRACELLULAR POTENTIAL
if any(plot_number==5)
    figure;
    hold on;
    % Compute vertical padding for y-axis
    padding=0.1*(max(Ve)-min(Ve));
    ymin=min(Ve)-padding;
    ymax=max(Ve)+padding;
    % Specify compartments
    node_indices = [3, 5, 7, 9, 11, 19, 21, 23, 25, 27, 29, 31, 33, 35, 37, 39]; % NoR
    soma_index=find(strcmp(compartments, 'Soma'), 1);
    axon_length=length(actfct);
    all_indices=1:axon_length;
    internode_indices=setdiff(all_indices, node_indices); % Internodes
    presomatic=soma_index-[3, 2, 1]; % Presomatic compartments
    post_idx=soma_index+1; % Postsomatic compartment
    % Build patches to indicate function of each compartment
    % Patch for P0 Region
    h_terminal=patch([0.5 1.5 1.5 0.5], [ymin ymin ymax ymax], ...
                        [1 0.8 0.8], 'FaceAlpha', 0.4, 'EdgeColor', 'none');
    % Patch for presomatic Regions
    h_presomatic=patch([presomatic(1)-0.5, presomatic(end)+0.5, presomatic(end)+0.5, presomatic(1)-0.5], ...
                        [ymin ymin ymax ymax], [0.9 0.9 1], 'FaceAlpha', 0.3, 'EdgeColor', 'none');
    % Patch for soma
    h_soma=patch([soma_index-0.5, soma_index+0.5, soma_index+0.5, soma_index-0.5], ...
                    [ymin ymin ymax ymax], [0.6 0.9 1], 'FaceAlpha', 0.5, 'EdgeColor', 'none');
    % Patch for postsomatic region
    h_post=patch([post_idx-0.5, post_idx+0.5, post_idx+0.5, post_idx-0.5], ...
                    [ymin ymin ymax ymax], [0.8 1 1], 'FaceAlpha', 0.4, 'EdgeColor', 'none');
    % Patch for NoRs
    h_node=patch([node_indices(1)-0.5, node_indices(1)+0.5, node_indices(1)+0.5, node_indices(1)-0.5], ...
                    [ymin ymin ymax ymax], [0.4 0.8 0.4], 'FaceAlpha', 0.4, 'EdgeColor', 'none');
    for i=2:length(node_indices)
        idx=node_indices(i);
        patch([idx-0.5, idx+0.5, idx+0.5, idx-0.5], ...
              [ymin ymin ymax ymax], [0.4 0.8 0.4], 'FaceAlpha',
```

```
                    0.4, 'EdgeColor', 'none');
    end
    % Patch for internodes
    first_internode=internode_indices(1);
    h_internode=patch([first_internode-0.5, first_internode+0.5, first_internode+0.5, first_internode-0.5], ...
                        [ymin ymin ymax ymax], [0.9 1 0.9], 'FaceAlpha', 0.2, 'EdgeColor', 'none');
    for i=2:length(internode_indices)
        idx=internode_indices(i);
        patch([idx-0.5, idx+0.5, idx+0.5, idx-0.5], ...
              [ymin ymin ymax ymax], [0.9 1 0.9], 'FaceAlpha', 0.2, 'EdgeColor', 'none');
    end

    % Plot extracellular potential and electrode position
    h_Ve=plot(1:axon_length, Ve, 'm', 'LineWidth', 2);
    h_elec=xline(closest_idx, 'r--', 'LineWidth', 2, 'Label', 'Electrode', 'LabelOrientation', 'horizontal');
    xlabel('Compartment index');
    ylabel('Extracellular Potential [mV]');
    title('Spatial Profile of Extracellular Potential');
    grid on;
    set(gca, 'FontSize', 14);
    legend([h_Ve, h_elec, h_terminal, h_presomatic, h_soma, h_post, h_node, h_internode], ...
            {'Extracellular Potential (Ve)', 'Electrode', 'Terminal', 'Presomatic', 'Soma', 'Postsomatic', ...
             'Node of Ranvier', 'Internode'}, 'Location', 'best');

    hold off;
end
end
```

References

Arancibia-Cárcamo, I. L., Ford, M. C., Cossell, L., Ishida, K., Tohyama, K., and Attwell, D. (2017). Node of Ranvier length as a potential regulator of myelinated axon conduction speed. *eLife*, 6:e23329.

Arnesen, A. and Osen, K. (1978). The cochlear nerve in the cat: Topography, cochleotopy, and fiber spectrum. *Journal of Comparative Neurology*, 178(4):661–678.

Asaad, R. (2019). Güler and Linaro et al Model in an Investigation of the Neuronal Dynamics using noise Comparative Study. *Academic Journal of Nawroz University*, 8:10.

Ashley, K. and Lui, F. (2023). Physiology, Nerve. *StatsPearls*. https://www.ncbi.nlm.nih.gov/books/NBK551652 (Accessed: 2025-05-17).

Bachmaier, R., Encke, J., Obando-Leitón, M., Hemmert, W., and Bai, S. (2019). Comparison of multi-compartment cable models of human auditory nerve fibers. *Frontiers in Neuroscience*, 13:1173.

Biacabe, B., Chevallier, J. M., Avan, P., and Bonfils, P. (2001). Functional anatomy of auditory brainstem nuclei: application to the anatomical basis of brainstem auditory evoked potentials. *Auris Nasus Larynx*, 28(1):85–94.

Briaire, J. J. and Frijns, J. H. M. (2005). Unraveling the electrically evoked compound action potential. *Hearing Research*, 205(1-2):143–156.

Bucek, F. (2023). Simulation of auditory nerve fiber excitation with prostheses implanted in the scala vestibuli. *reposiTUm*. Diploma Thesis, Technische Universität Wien.

Carricondo, F. and Romero-Gómez, B. (2019). The Cochlear Spiral Ganglion Neurons: The Auditory Portion of the VIII Nerve. . *Anatomical Record*, 302(3):463–471.

Chrysafides, S. M., Bordes, S. J., and Sharma, S. (2024). Physiology, Resting Potential. *StatPearls*. https://www.ncbi.nlm.nih.gov/books/NBK538338/ (Accessed: 2025-05-17).

Dagostin, A. A., Lovell, P. V., Hilscher, M. M., Mello, C. V., and Leão, R. M. (2015). Control of Phasic Firing by a Background Leak Current in Avian Forebrain Auditory Neurons. *Frontiers in Cellular Neuroscience*, 9:471.

Dayan, P. and Abbott, L. F. (2001). Theoretical Neuroscience. Computational and Mathematical Modeling of Neural Systems. https://boulderschool.yale.edu/sites/default/files/files/DayanAbbott.pdf (Accessed: 2025-06-23).

Dewsnup, S. (2022). Anatomy of the Ear and Understanding Hearing. *Happy Ears Hearing*. https://www.happyearshearing.com/anatomy-of-the-ear/ (Accessed: 2025-05-23).

Eshraghi, A. A., Nazarian, R., Telischi, F. F., Rajguru, S. M., Truy, E., and Gupta, C. (2012). The cochlear implant: historical aspects and future prospects. *Anatomical Record*, 295(11):1967–1980.

Faisal, A. A., Selen, L. P. J., and Wolpert, D. M. (2008). Noise in the nervous system. *Nature Reviews Neuroscience*, 9(4):292–303.

Fettiplace, R. and Hackney, C. M. (2006). The sensory and motor roles of auditory hair cells. *Nature Reviews Neuroscience*, 7(1):19–29.

FitzHugh, R. (1961). Impulses and Physiological States in Theoretical Models of Nerve Membrane. *Biophysical Journal*, 1(6):445–466.

Grant, L., Yi, E., and Glowatzki, E. (2010). Two modes of release shape the postsynaptic response at the inner hair cell ribbon synapse. *The Journal of Neuroscience*, 30(12):4210–4220.

He, S., Skidmore, J., Conroy, S., Riggs, W. J., Carter, B. L., and Xie, R. (2022). Neural Adaptation of the Electrically Stimulated Auditory Nerve Is Not Affected by Advanced Age in Postlingually Deafened, Middle-aged, and Elderly Adult Cochlear Implant Users. *Ear and Hearing*, 43(4):1228–1244.

Hille, B. (1940). Ion Channels of Excitable Membranes. *Sunderland, Mass.: Sinauer*. United States. 2001 Edition.

Hochmair-Desoyer, I. J., Hochmair, E. S., Motz, H., and Rattay, F. (1984). A model for the electrostimulation of the nervus acusticus. *Neuroscience*, 13(2):553–562.

Hodgkin, A. L. and Huxley, A. F. (1952a). A quantitative description of membrane current and its application to conduction and excitation in nerve. *The Journal of Physiology*, 117(4):500–544.

Hodgkin, A. L. and Huxley, A. F. (1952b). The components of membrane conductance in the giant axon of Loligo. *The Journal of Physiology*, 116(4):473–496.

Hodgkin, A. L. and Katz, B. (1949). The effect of sodium ions on the electrical activity of giant axon of the squid. *The Journal of Physiology*, 108(1):37–77.

Hudspeth, A. J. (2014). Integrating the active process of hair cells with cochlear function. *Nature Reviews Neuroscience*, 15(9):600–614.

JGraph Ltd. (2005-2023). diagrams.net. *draw.io*. https://www.drawio.com (Accessed: 2025-05-23).

Kole, M. H. P. and Stuart, G. J. (2012). Signal processing in the axon initial segment. *Neuron*, 73(2):235–247.

Leterrier, C. (2016). The Axon Initial Segment, 50 Years Later: A Nexus for Neuronal Organization and Function. *Current Topics in Membranes*, 77:185–233.

Limb, C. J. and Roy, A. T. (2014). Technological, biological, and acoustical constraints to music perception in cochlear implant users. *Hearing Research*, 308:13–26.

Liu, W., Luque, M., Li, H., Schrott-Fischer, A., Glueckert, R., Tylstedt, S., Rajan, G., Ladak, H., Agrawal, S., and Rask-Andersen, H. (2021). Spike Generators and Cell Signaling in the Human Auditory Nerve: An Ultrastructural, Super-Resolution, and Gene Hybridization Study. *Frontiers in Cellular Neuroscience*, 15:642211.

Moore, B. C. J. (2012). An Introduction to the Psychology of Hearing. *Emerald Group Publishing Limited*. United Kingdom, 6th Edition.

Nadol, J. B. (1988). Comparative anatomy of the cochlea and auditory nerve in mammals. *Hearing Research*, 34(3):253–266.

Nayagam, B. A., Muniak, M. A., and Ryugo, D. K. (2011). The spiral ganglion: Connecting the peripheral and central auditory systems. *Hearing Research*, 278(1–2):2–20.

Negm, M. H. and Bruce, I. C. (2014). The Effects of HCN and KLT Ion Channels on Adaptation and Refractoriness in a Stochastic Auditory Nerve Model. *IEEE Transactions on Biomedical Engineering*, 61(11):2749–2759.

Ota, C. Y. and Kimura, R. S. (1980). Ultrastructural study of the human spiral ganglion. *Acta Oto-Laryngologica*, 89(1-2):53–62.

Panganiban, C. H., Barth, J. L., Tan, J., Noble, K. V., McClaskey, C. M., Howard, B. A., Jafri, S. H., Dias, J. W., Harris, K. C., and Lang, H. (2022). Two distinct types of nodes of Ranvier support auditory nerve function in the mouse cochlea. *Glia*, 70(4):768–791.

Peter, M. S., Warnecke, A., and Staecker, H. (2022). A Window of Opportunity: Perilymph Sampling from the Round Window Membrane Can Advance Inner Ear Diagnostics and Therapeutics. *Journal of Clinical Medicine*, 11(2):316.

Pickles, J. O. (2015). Handbook of Clinical Neurology. Chapter 1 - Auditory Pathways: Anatomy and Physiology. *Elsevier*, 129:3–25.

Potrusil, T., Heshmat, A., Sajedi, S., Wenger, C., Johnson-Chacko, L., Glueckert, R., Schrott-Fischer, A., and Rattay, F. (2020). Finite element analysis and three-dimensional reconstruction of tonotopically aligned human auditory fiber pathways: A computational environment for modeling electrical stimulation by a cochlear implant based on micro-CT. *Hearing Research*, 393:108001.

Raghavan, M., Fee, D., and Barkhaus, P. E. (2019). Handbook of Clinical Neurology. Chapter 1 - Generation and propagation of the action potential. *Elsevier*, 160:3–22.

Rattay, F. (1986). Analysis of models for external stimulation of axons. *IEEE Transactions on Biomedical Engineering*, 33(10):974–977.

Rattay, F. (1990). Electrical Nerve Stimulation. Theory, Experiments and Applications. *Springer-Verlag Wien GmbH*. Austria. 1990 Edition.

Rattay, F. (1999). The basic mechanism for the electrical stimulation of the nervous system. *Neuroscience*, 89(2):335–346.

Rattay, F. and Danner, S. M. (2014). Peak I of the human auditory brainstem response results from the somatic regions of type I spiral ganglion cells: evidence from computer modeling. *Hearing Research*, 315:67–79.

Rattay, F., Greenberg, R. J., and Resatz, S. (2002). Handbook of Neuroprosthetic Methods. Neuron modeling. *CRC Press LLC*, pages 39–71.

Rattay, F., Lutter, P., and Felix, H. (2001). A model of the electrically excited human cochlear neuron: I. Contribution of neural substructures to the generation and propagation of spikes. *Hearing Research*, 153(1-2):43–63.

Rattay, F., Potrusil, T., Wenger, C., Wise, A. K., Glueckert, R., and Schrott-Fischer, A. (2013). Impact of Morphometry, Myelinization and Synaptic Current Strength on Spike Conduction in Human and Cat Spiral Ganglion Neurons. *PLOS ONE*, 8(11):e79256.

Rattay, F. and Tanzer, T. (2022). Impact of electrode position on the dynamic range of a human auditory nerve fiber. *Journal of Neural Engineering*, 19(1).

Schiebler, H. T. and Korf, H.-W. (2007). *Anatomie*. Germany. 10th Edition.

Sheikh, A., Bint-e-Zainab, Shabbir, K., and Imtiaz, A. (2022). Auditory System - Function and Disorders. Structure and Physiology of Human Ear Involved in Hearing. https://www.intechopen.com/chapters/82266 (Accessed 2025-05-22).

Smit, J., Hanekom, T., and Hanekom, J. (2008). Predicting action potential characteristics of human auditory nerve fibres through modification of the Hodgkin–Huxley equations. *South African Journal of Science*, 104(7-8):284–292.

Smit, J. E., Hanekom, T., Van Wieringen, A., Wouters, J., and Hanekom, J. J. (2010). Threshold predictions of different pulse shapes using a human auditory nerve fibre model containing persistent sodium and slow potassium currents. *Hearing Research*, 269(1-2):12–22.

Spoendlin, H. and Schrott, A. (1988). The spiral ganglion and the innervation of the human organ of Corti. *Acta Oto-Laryngologica*, 105(5–6):403–410.

Swenson, R. (2017). Conn's Translational Neuroscience. Chapter 8 - The Vestibular System. *Academic Press*, pages 167–183.

Tsay, D. and Yuste, R. (2002). Role of dendritic spines in action potential backpropagation: a numerical simulation study. *Journal of Neurophysiology*, 88(5):2834–2845.

Vlajkovic, S. M. and Thorne, P. R. (2022). Purinergic Signalling in the Cochlea. *International Journal of Molecular Sciences*, 23(23):14874.

Weiss, G. (1901). Sur la possibilité de rendre sensibles les variations de la résistance des métaux conducteurs au moyen des courants alternatifs très rapides. *Archives Italiennes de Biologie*, 35:413–445.

Zeng, F.-G., Rebscher, S., Harrison, W., Sun, X., and Feng, H. (2008). Cochlear Implants: System Design, Integration and Evaluation. *IEEE Reviews in Biomedical Engineering*, 1:115–142.

Zhou, N., Kraft, C. T., Colesa, D. J., and Pfingst, B. E. (2015). Integration of Pulse Trains in Humans and Guinea Pigs with Cochlear Implants. *Journal of the Association for Research in Otolaryngology*, 16(4):523–534.